Investigation of Replication Fork Progression and Re-replication Fork Instability at the Drosophila Follicle Cell Amplicons

by

Jessica L. Alexander

B.S. Biochemistry, 2010
Rochester Institute of Technology
Rochester, NY

Submitted to the Department of Biology
in Partial Fulfilment of the Requirements for the Degree of

Doctor of Philosophy in Biology

at the

Massachusetts Institute of Technology
Cambridge, MA

June 2016

Signature of Author: _____
Department of Biology
May 9, 2016

Certified by: _____
Terry L. Orr-Weaver
Professor of Biology
Thesis Supervisor

Accepted by:_____
Michael Hemann
Associate Professor of Biology
Co-Chair, Biology Graduate Committee

Investigation of Replication Fork Progression and Re-replication Fork Instability at the Drosophila Follicle Cell Amplicons

by
Jessica L. Alexander
Submitted to the Department of Biology on May 20, 2016
in Partial Fulfilment of the Requirements for the Degree of Doctor of Philosophy in Biology

Abstract

The Drosophila follicle cell amplicons are a well-established model system of origin firing, and have been extensively used to investigate the cis and trans-acting elements that govern origin regulation in metazoan development. Precisely timed origin initiation from defined genomic locations also has made the amplicons a powerful model system to delineate control of replication fork progression. We utilized this system to survey fork progression across diverse genomic positions from amplicons generated at ectopic genomic positions. Comparative genome hybridization (CGH) analysis reveals fork progression varies with the position of insertion, indicating fork movement is influenced by sequence, chromatin and/or chromosome architecture. Additionally, we have developed a slope analysis tool to measure changes in fork progression between different amplicons, as well as within a single amplified site. Together the CGH survey and slope analysis can be used to discover positions that are inhibitory to fork progression and delineate intrinsic sources of fork stalling across the genome. Furthermore, we utilized the amplicons to investigate the consequences of re-replication on fork stability. We find that double-strand breaks (DSBs) are generated at positions of active replication forks, supporting the model that head-to-tail collisions between adjacent replication forks generate DSBs during re-replication. A single fork collision and collapse event would block all subsequent forks, suggesting efficient break repair is required for continued fork movement at the amplicons. To define the pathways responsible for maintaining re-replication fork elongation, we developed the half-maximum distance analysis to measure global fork progression at each site of re-replication in the absence of various DNA damage response (DDR) and repair components. We find that fork progression is reduced in various DDR mutants, suggesting the DNA damage response is essential to maintain overall fork movement during re-replication. We also have begun to define the mechanisms of DSB repair during re-replication, and find the preferred pathway is influenced by repair efficiency and amplicon position. Our analysis thus establishes the Drosophila follicle cell amplicons as a re-replication model system and suggests that DSB repair pathway choice during re-replication is governed by genomic position, reaction kinetics and repair pathway competition.

Thesis Supervisor: Terry L. Orr-Weaver
Title: Professor of Biology

Dedicated to my family
Jeffrey, Becky and Kristen Alexander

And to my best friend
Matt Thoman

Acknowledgments

Thank to my advisor Terry Orr-Weaver for her mentorship and support throughout my time in the lab. When I first joined Terry's lab, the idea of pursuing a novel scientific question was both exciting and daunting, and I often felt I was not capable of leading my own research project. However, through Terry's patient guidance I not only learned how to approach scientific problems, but also how to be confident in my own ideas. This confidence was in large part through Terry's emphasis on writing and presentation. Although often stressful at the time, I'm now extremely grateful that I was able to take charge of writing my own paper and to have had so many opportunities to present my research. I'm also grateful for the collaborative research environment that Terry fosters in her lab. I've always respected Terry's philosophy that each student and postdoc should have complete ownership of their research project, yet at the same time has established an environment that encourages us to be intellectually involved in all projects going on in the lab. This balance is not commonly encountered in science, and is one attribute that makes Terry's lab such a great place to work and grow intellectually.

I also want to thank my committee members Steve Bell and Adam Martin who both served on my committee from the beginning of my graduate work. Their advice and input was instrumental in the direction of my project, and I am very grateful for their continued interest in my research. I also want to thank Steve for allowing me to be a part of his lab's weekly meetings and journal clubs. Especially valuable were the 'Super Journal Clubs'; I think it's safe to say that I passed my preliminary exam largely from what I learned at the Bell lab SJC sessions.

Thank you to all the current and previous Orr-Weaver lab members who I've worked with. Each of you has contributed to my growth as a scientist and helped with my project in some way, from fly genetics to PCR woes, data analysis and life advice. I owe a great deal of my success in grad school to Jared Nordman, whose mentorship was instrumental for the development of my project. Thank you to Bory Petrova, Masatoshi Hara, Jessie Von Stetina, Iva Kronja and Emir Aviles Pagan who not only were always helpful in the lab, but also are a wonderful group of friends. I want to especially thank Brain Hua and Belinda Pinto, whose friendship has helped me through the many ups-and-down of grad school.

Grad school has been a rewarding yet challenging time, and I am immensely grateful to all my friends and family who supported me throughout this process, but also reminded me to step back and enjoy life. A special thank you to Amanda Bathalon Pouliot, Rachel Hewes, Phyllis Wall, Allie Smith Desjardins and Kerie Ridlon Larochelle for your many years of friendship, for all the fun you've made me have, and for keeping me grounded during these grad school years. Thank you to my sister and oldest friend, Kristen Alexander. Your monthly visits to Boston during my time in grad school are memories I will always cherish. Thank you for always believing that I'm "wicked smaht" especially when I didn't feel smart at all. Above all, thank you for reminding me of where I come from and the person I want to be.

Thank you to my parents Jeffrey and Becky Alexander. You have always pushed me to be my best possible self, and have instilled in me the drive I needed to get through grad school. I've always been inspired by your work ethic and determination through adversity, and aspire to live by your example. Thank you for always believing in me, and for your endless love and support.

Thank you to my best friend and boyfriend Matt Thoman who has been by my side through this entire ride. Your love, support and friendship has kept me going through grad school and other difficult times. I still consider convincing you to go out with me in the 9^{th} grade to be of my greatest accomplishments; little did I know then that you would shape the person I grew up to be. Thank you for choosing to spend your life with me.

TABLE OF CONTENTS

Chapter One:
Introduction

Complete and accurate duplication of DNA at each S-phase is required to maintain genome integrity between cell divisions. This is accomplished by exquisite control of the DNA replication program at the level of origin firing and coordination with replication fork progression. Genome stability requires that fork elongation is complete across every chromosome. However, not all genomic positions are replicated equally. Both DNA damage and intrinsic properties of the chromosome can slow or prevent passage of the replication fork. Failure to alleviate these blockades can lead to incomplete genome duplication, resulting in chromosome breakage, fusions and rearrangements.

Many of the components that constitute the replication fork are well-defined, and recent proteomics analyses have cataloged fork components during normal elongation as well as stress conditions. Increasing evidence suggests that replication forks recruit repair components even during unstressed replication, suggesting this system is well poised to respond to fork impediments. Despite this, fork collapse and resulting DNA damage are observed under a variety of conditions that block fork elongation. Although significant advances have been made, the mechanisms that maintain fork stability and repair damaged forks are still under investigation. This chapter summarizes the structure of the replication fork, as well as known sources of fork instability and the mechanisms employed to repair damage generated by fork collapse.

Assembly & Structure of the Eukaryotic Replication Fork

In G1 of the cell cycle, origins of replication are bound by the pre-Replication Complex (pre-RC). This complex includes the Origin Recognition Complex (ORC), which directly binds to the DNA (Bell & Stillman 1992), Cdc6, Cdt1 and the Mcm2-7 complex (Bell & Dutta 2002). Cdt1 recruits Mcm2-7 to ORC and Cdc6 bound origins, and *in vitro* studies show that both Cdc6

and Cdt1 quickly disassociate once Mcm2-7 is stably loaded (Ticau *et al.* 2015). The Mcm2-7 complex is sequentially loaded as a head-to-head double-hexamer onto the double-stranded DNA (dsDNA) origin to facilitate bi-directional fork movement (Evrin *et al.* 2009, Remus *et al.* 2009, Gambus *et al.* 2011, Ticau *et al.* 2015). Once assembled, the origin is said to be licensed.

Replication origin activation in S-phase requires sequential activity of DDK (Dbf4-dependent kinase) and S-phase CDK to recruit the helicase components and other regulatory factors that facilitate unwinding and form the replisome (Heller *et al.* 2011). DDK and CDK phosphorylation events lead to the recruitment of Cdc45 and the GINS complex (Sld5, Pif1, Pif2 and Pif3), respectively, which together with Mcm2-7 comprise the CMG helicase that unwinds the double-stranded DNA for replication (Gambus *et al.* 2006, Moyer *et al.* 2006, Pacek *et al.* 2006, Heller *et al.* 2011). Assembly of the helicase is also dependent on the regulatory components Sld2, Sld3, Sld7 and Dbp11 in budding yeast and TopBP1/Mus101, RecQL4/RecQ4 and Treslin/Ticrr in higher eukaryotes; together with the CMG and Polε, these components comprise the pre-Initiation Complex (pre-IC) (Tanaka and Araki 2013).

Another essential replication factor is Mcm10; however its role in origin activation remains controversial. Some studies show that Mcm10 is not essential for CMG assembly, but is required for DNA unwinding at the origin (van Deurson *et al.* 2012, Kanke *et al.* 2012, Watse *et al.* 2012). However, recent studies show that Mcm10 directly binds to Mcm2-7 (Douglas and Diffley 2016) and facilitates separation of the Mcm2-7 double-hexamer (Quan *et al.* 2015). Additionally, Mcm10 was shown to promote association of Cdc45 and GINS with Mcm2-7 in early S-phase, suggesting it may coordinate helicase assembly and activation (Perez-Arnaiz *et al.* 2016).

Assembly of the pre-IC and origin melting is accompanied by activation of the CMG

helicase and polymerase recruitment. Helicase activation requires that the Mcm2-7 complex transition from encircling double-stranded DNA (dsDNA) as part of the pre-RC (Evrin *et al.* 2009, Remus *et al.* 2009) to single-stranded DNA (ssDNA) as part of the replication fork (Fu *et al.* 2011). The CMG helicase translocates along the leading strand, supporting a model in which the DNA is unwound by steric exclusion from the Mcm2-7 central channel (Fu *et al.* 2011). The exposed ssDNA on the lagging strand is coated by RPA (Adachi & Laemmli 1992, 1994). This allows Polα-primase to associate (Tanaka & Nasmyth 1998, Mimura *et al.* 2000, Walter and Newport 2000) and synthesize 8-15 nucleotide long RNA primers (Conway & Lehman 1982 [1], [2]).

Replacement of Polα-primase by Polδ is mediated by PCNA loading (Johnson & O'Donnell 2005). PCNA binds to Polδ and Polε and enhances their processivity by preventing diffusion away from the replication fork (Tan *et al.* 1986, Prelich *et al.* 1987, Lee *et al.* 1991, Maga & Hübscher 1995, Einolf & Guengerich 2000). The chemistry of nucleotide synthesis necessitates that nucleic acids are synthesized in the 5' to 3' direction. Therefore, whereas the leading strand is continuously replicated, the lagging strand is replicated piecemeal in 100-400 nucleotide units called Okazaki fragments that are then ligated together (Okazaki *et al.* 1968, Johnson & O'Donnell 2005). Polε replicates the leading strand (Pursell *et al.* 2007), and Polδ is recruited after origin unwinding to replicate the lagging strand (Nick McElhinny *et al.* 2008). Replication of the leading and lagging strands are coordinated with helicase unwinding in a large protein complex called the replisome; together the replicating DNA and replisome constitute the replication fork (Fig. 1) (Johnson & O'Donnell 2005).

Figure 1. Summary of the Eukaryotic DNA Replication Fork

Cdc45, Mcm2-7 and GINS complex comprise the CMG helicase that unwinds the double-stranded DNA. Leading strand synthesis is shown on top and is accomplished by Polε. Lagging strand synthesis is depicted below. Polα-primase synthesizes 8-15 nucleotide long RNA primers along the lagging strand. Synthesis of the lagging strand is performed by Polδ. PCNA binds to Polδ and Polε to enhance processivity. The nucleosome remodelers FACT and ASF1 bind to Mcm2-7 to coordinate removal of nucleosomes with the oncoming replication fork. ASF1 also cooperates with CAF-1 to deposit new H3-H4 tetramer behind the elongating fork. (Illustration by Steven Lee/graphiko.com).

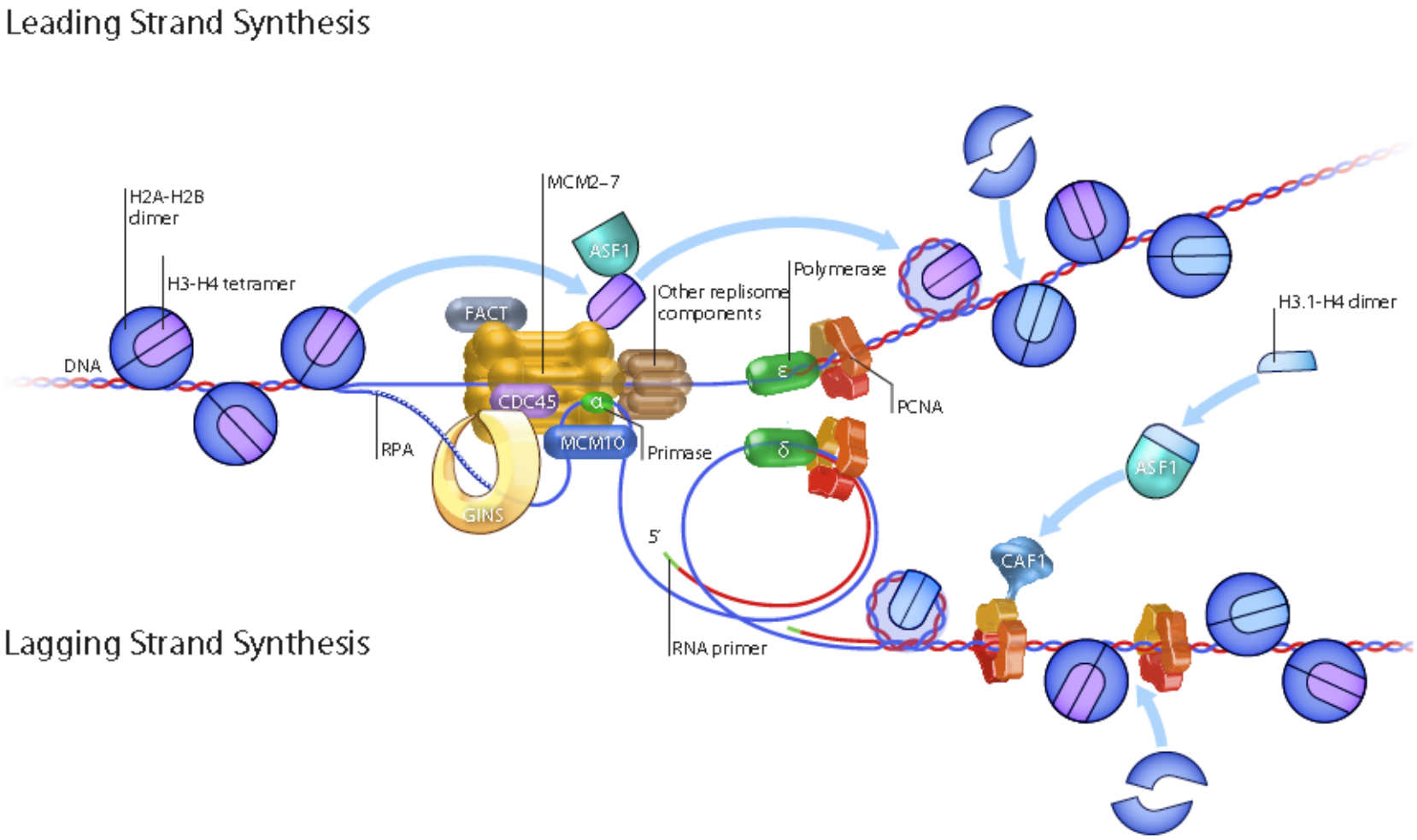
Leading Strand Synthesis
H2A-H2B dimer
H3-H4 tetramer
DNA
RPA
MCM2–7
ASF1
FACT
Other replisome components
Polymerase
CDC45
α
MCM10
Primase
GINS
ε
PCNA
δ
5'
RNA primer
H3.1-H4 dimer
ASF1
CAF1
Lagging Strand Synthesis

Fork progression must also be coordinated with disassembly of nucleosomes ahead of the fork and re-establishment of nucleosomes and the chromatin state on newly synthesized DNA. Nucleosome deposition is coordinated with fork elongation by interactions between histone chaperones and fork components (Shibahara & Stillman 1999, Moggs *et al.* 2000, Groth *et al.* 2007, Huang *et al.* 2015). The CAF-1 chaperone binds PCNA and deposits newly synthesized H3-H4 tetramers (Smith & Stillman 1989, Shibahara & Stillman 1999, Moggs *et al.* 2000, Winkler *et al.* 2012). Transport of new H3-H4 dimers to CAF-1 at the fork involves several chaperones, including ASF1, which directly binds CAF-1 and H3-H4 dimers (Mello *et al.* 2002, English *et al*. 2006, Natsume *et al.* 2007). ASF1 also interacts with the Mcm2-7 helicase via an H3-H4 bridge (Groth *et al.* 2007, Jasencakova *et al.* 2010, Huang *et al.* 2015), and it can deposit H3 variants as well as canonical H3 (Huang *et al.* 2015). ASF1 binds histones with modifications associated with parental and newly synthesized H3, suggesting it may evict old histones ahead of the fork as well as bring in new ones (Groth *et al.* 2007, Jasencakova *et al.* 2010). The histone chaperone FACT binds to Mcm2-7 (Gambus *et al.* 2006, Tan *et al.* 2006), as well as Polα (Wittmeyer & Formosa 1997); this chaperone is involved in nucleosome remodeling and displaces H2A-H2B dimers from nucleosomes ahead of the replication fork (Winkler *et al.* 2011, Tsunaka *et al.* 2016). Numerous other chaperones also are involved in building nucleosomes, as well as re-establishment of chromatin marks on newly synthesized histones (Alabert & Groth 2012).

In the past five years, several methodologies have been developed for the capture of active replication forks and assessment of associated protein components (Sirbu *et al.* 2011, Kliszczak *et al.* 2011, Lopez-Contreras *et al.* 2013, Sirbu *et al.* 2013, Alabert *et al.* 2014). Isolation of proteins bound to nascent DNA (iPOND) and DNA-mediated chromatin pulldown (DM-ChP)

use the thymidine analog EdU and click chemistry (Salic & Mitchison 2008) to pulldown DNA fragments into which EdU is incorporated (Sirbu *et al.* 2011, Kliszczak *et al.* 2011). Short pulses of EdU followed by fixation allows selective pulldown of components at active replication forks (Sirbu *et al.* 2011, Lopez-Contreras *et al.* 2013, Sirbu *et al.* 2013). An EdU pulse followed by a thymidine chase resulted in pulldown of mature chromatin marks and the responsible remodelers (Sirbu *et al.* 2011, Lopez-Contreras *et al.* 2013). Additionally, iPOND analysis of forks in the presence of HU detected known checkpoint proteins at stalled forks (Sirbu *et al.* 2011, Sirbu *et al.* 2013). When fork collapse is induced by long HU exposure or ATR knockdown, high levels of double-strand break (DSB) repair components are pulled down (Sirbu *et al.* 2011, Sirbu *et al.* 2013). A similar approach termed nascent chromatin capture (NCC) incorporates biotin-dUTP rather than EdU into replicating DNA (Alabert *et al.* 2014). Combining these techniques with mass spectrometry methods has allowed for proteomics analysis of active, stalled and collapsed replication forks as well as chromatin maturation (Kliszczak *et al.* 2011, Lopez-Contreras *et al.* 2013, Sirbu *et al.* 2013, Alabert *et al.* 2014). One of many interesting findings of these experiments is that several checkpoint and repair proteins travel with undamaged replication forks (Sirbu *et al.* 2011, Sirbu *et al.* 2013, Alabert *et al.* 2014). These results suggest that forks are poised to deal with stalling throughout S-phase. This property may be essential as forks proceed through difficult-to-replicate regions of the genome, and for timely response to DNA damage and exogenous fork stress.

Impediments to Replication Fork Progression

Once replication forks are established, there are numerous challenges that the forks may face before replication is completed. DNA damage such as interstrand crosslinks cannot be unwound,

and protein-DNA crosslinks form barriers to the CMG helicase (Fu *et al.* 2011); these lesions require specialized pathways to repair and/or bypass (Duxin *et al.* 2014, Zhang *et al.* 2015). Other forms of damage, such as UV and MMS-induced damage, block replication and cause uncoupling of the CMG helicase and polymerases (Byun *et al.* 2005), similarly to chemical inhibition of polymerase activity by aphidicolin (Walter and Newport 2000). Additionally, the dNTP and histone supply must be coordinated with fork elongation for proper S-phase progression and fork stability (Bonner *et al.* 1988, Nelson *et al.* 2002, Mantiero *et al.* 2011, Poli *et al.* 2012, Mejlvang *et al.* 2014). It has been shown that disruption of the origin activation timing program leads to dNTP depletion, causing slowed fork elongation, fork stalling and checkpoint activation (Mantiero *et al.* 2011, Poli *et al.* 2012). These studies highlight the importance of the replication program in coordinating fork elongation with a steady supply of raw materials for DNA synthesis.

It has been widely observed that specific regions of the genome are particularly prone to damage in the presence of replication stress, indicating endogenous characteristics of the DNA sequence and chromatin structure can be problematic to fork progression; these regions are termed fragile sites. Fragile sites are formally defined as positions of constriction or breakage on metaphase chromosomes after exposure to replication stress (Glover *et al.* 1984), and can be sub-divided into rare (RFCs) and common fragile sites (CFSs). CFSs are positions that exhibit fragility across most individuals of a population, and the frequency of breakage is referred to as CFS expression (Debatisse *et al.* 2012). It is thought that CFSs are inherently difficult to replicate, as CFS expression is seen when the ATR checkpoint is inhibited in the absence of exogenous stress (Casper *et al.* 2002). Similarly, replication slow zones (RSZs) in yeast are prone to fork stalling and DNA breaks in the absence of the ATR homolog Mec1 (Cha &

Kleckner 2002). However, increased stalling fork stalling is not observed across all metazoan CFSs (Palumbo *et al.* 2010, Letessier *et al.* 2011). Instead, there is a collection of characteristics that are common but not universal among CFSs: slow fork progression and/or frequent fork stalling, actively transcribed genes during replication, late replication timing and lack of replication origins (Debatisse *et al.* 2012, Ozeri-Galai *et al.* 2012).

Various forms of repetitive DNA can form DNA secondary structures in the single stranded DNA formed on the lagging strand during replication, which blocks the replication fork (Mirkin & Mirkin 2007). Slow replicating CFSs contain AT-dinucleotide repeats (Reid *et al.* 2000, Zlotorynski *et al.* 2003, Mitsui *et al.* 2010), which exhibit hyper flexibility and can form DNA secondary structures at AT-dinucleotide repeats (Mirkin & Mirkin 2007). Replication forks frequently stall at these AT repeats and lead to DNA breaks in the absence of replication stress, and stalling is enhanced in the presence of aphidicolin (Zhang & Freudenreich 2007, Shah *et al.* 2010, Ozeri-Galai *et al.* 2011). Direct tandem repeats (DTR) are a well-documented source of inherited chromosome fragility and are the source of RFCs. It has been shown that various trinucleotide repeats cause fork pausing and reversal at these secondary structures, and pausing events frequently correspond to break formation (Follonier *et al.* 2013, Liu *et al.* 2013, Gerhardt *et al.* 2014). One extensively studied example is G-quadruplexes (G4's), highly stable secondary structures that form at stretches of G-rich DNA. G4's have been implicated in regulating gene expression (Maizels and Gray 2013) and origin selection (Besnard *et al.* 2012, Hoshina *et al.* 2013, Valton *et al.* 2014) in metazoan cells, yet paradoxically pose a threat to genome stability by blocking replication forks. Replication across G4's requires specialized helicases such as FANCJ (London *et al.* 2008, Wu *et al.* 2008, Schwab *et al.* 2013) and Pif1 (Sanders 2010, Paeschke *et al.* 2011, Sabouri *et al.* 2014).

Fragile sites are prevalent in Drosophila endocycling tissues. The endocycle is a cell cycle variant composed of consecutive S and G-phases in the absence of mitosis, resulting in increased cell ploidy (Spradling & Orr-Weaver 1987). Replication of heterochromatin is actively repressed during the endocycle (Spradling & Orr-Weaver 1987). This reduces the copy number of heterochromatic sequences compared the overall cell ploidy, and is known as under-replication. Certain euchromatic regions are also under-replicated during the endocycle in a tissue-specific manner (Nordman *et al.* 2011, Sher *et al.* 2012). The DNA damage marker γH2Av is present throughout under-replicated sites of salivary gland chromosomes (Fig. 2A), indicating there is persistent double-strand break formation at these sites (Andreyeva *et al.* 2008, Nordman *et al.* 2014). Additionally, the observation that γH2Av is present across entire under-replicated domains rather than at the borders indicates that replication forks are not completely blocked, but destabilized as they progress through these regions (Nordman *et al.* 2014).

Under-replication is dependent on Suppressor of Under-Replication (SuUR), and *SuUR* mutants both restore copy number and alleviate DNA damage (Fig. 2A) (Belyaeva *et al.* 1998, Andreyeva *et al.* 2008, Nordman *et al.* 2011, Sher *et al.* 2012, Nordman *et al.* 2014). Although euchromatic under-replicated regions are tissue-specific, loss of *SuUR* uniformly restores replication across all tissues and positions (Nordman *et al.* 2011). Fork progression during follicle cell amplification is also regulated by SuUR (Sher *et al.* 2012, Nordman *et al.* 2014). Gene amplification occurs at six loci in the follicle cells by repeated origin activation, and generates a gradient of amplified DNA visible by comparative genome hybridization analysis (Fig. 2B). Fork movement is enhanced at the amplicons by about 30% in *SuUR* mutants, whereas *SuUR* overexpression nearly halves the distances fork traverse (Fig. 2B) (Nordman *et al.* 2014).

Figure 2. SuUR is a Developmentally Regulated to Destabilize Replication Forks

(A) CGH and γH2Av ChIP-seq in Drosophila salivary glands (top) Underreplicated regions exhibit extensive DNA damage that is dependent on SuUR-mediated fork instability. Copy number is restored and γH2Av reduced at underreplicated sites in a *SuUR* mutant. Salivary gland DNA was hybridized with diploid embryonic DNA to microarrays. ChIP-seq peaks were called by MACS2.

(B) CGH at *DAFC-66D* in wild-type and *SuUR* mutants. Fork progression at follicle cell amplicons is enhanced in the absence of *SuUR* (middle) and inhibited in *SuUR* overexpression lines (bottom). DNA from stage 13 egg chambers was competitively hybridized with diploid embryonic DNA to microarrays with approximately one probe every 125bp. The log2 ratio of stage 13 DNA to embryonic DNA is plotted on the y-axis.

(Adapted from Nordman *et al.* 2014)

A

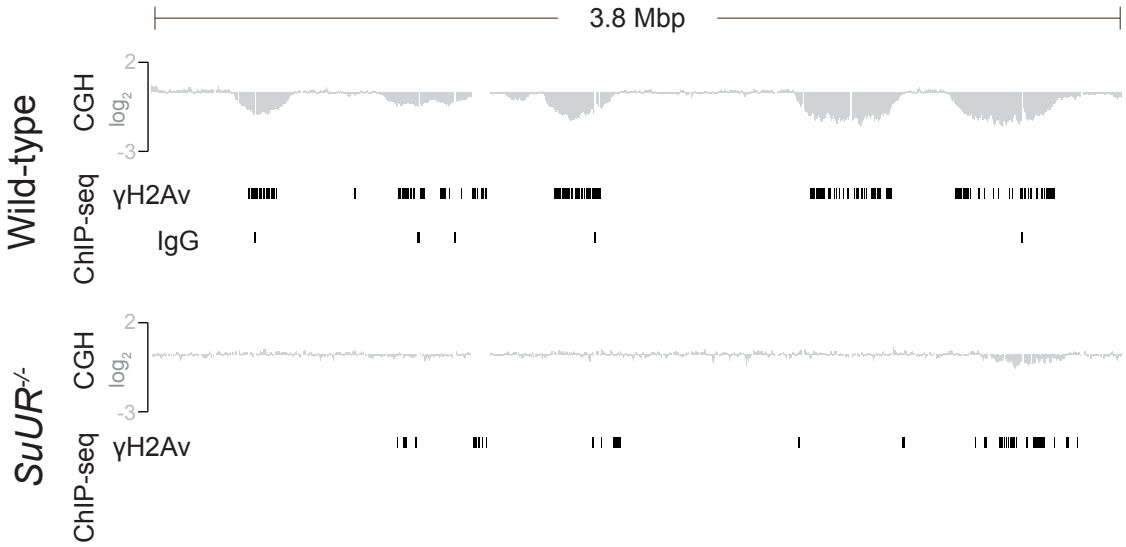
3.8 Mbp
Wild-type
CGH
log2
2
-3
ChIP-seq
γH2Av
IgG
SuUR-/-
CGH
log2
2
-3
ChIP-seq
γH2Av

B *DAFC-66D*

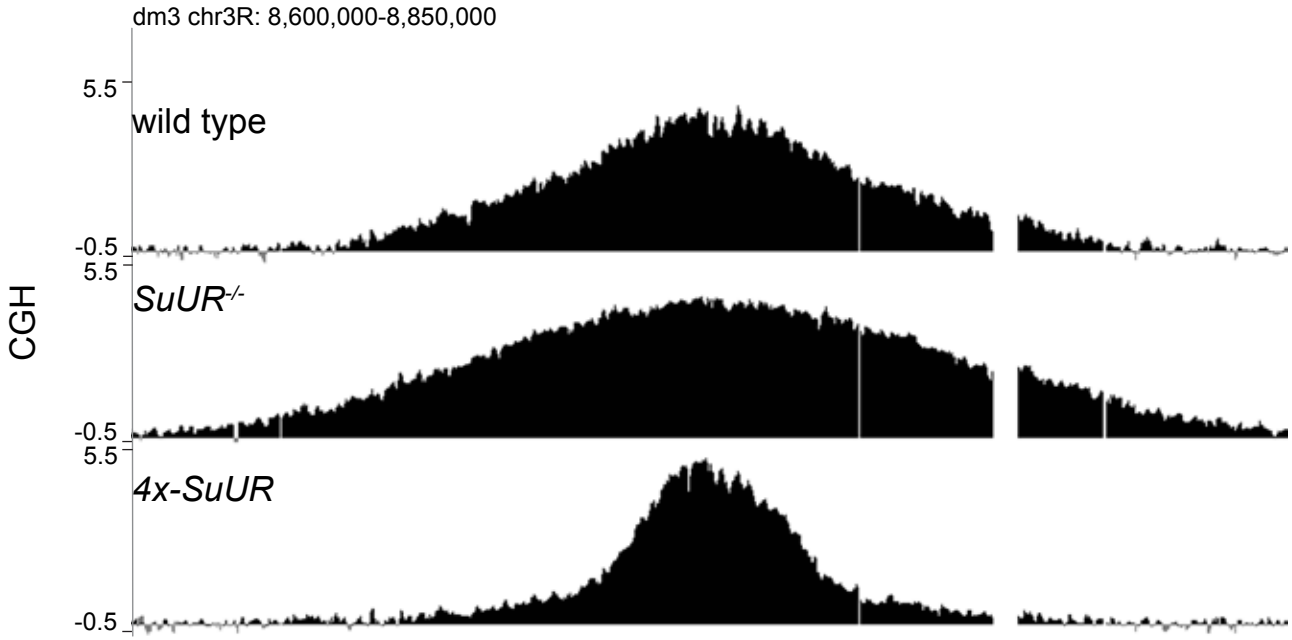
dm3 chr3R: 8,600,000-8,850,000
CGH
5.5
wild type
-0.5
5.5
SuUR-/-
-0.5
5.5
4x-SuUR
-0.5

SuUR is localized to under-replicated regions of salivary gland polytene chromosome spreads (Andreyeva *et al.* 2008) and associated with repressive chromatin in Drosophila cell culture (Filion *et al.* 2010), suggesting SuUR may block fork progression by promoting a repressive chromatin state. However, more recent evidence shows that SuUR binds the CMG helicase component Cdc45 and travels with elongating forks during follicle cell amplification (Nordman *et al.* 2014). These results suggest SuUR destabilizes forks rather than acting as a replication barrier (Nordman *et al.* 2014). Although full-length *SuUR* has no known human homologs, the N-terminus is homologous to the SWI/SNF family ATPase/helicase domain (Makunin *et al.* 2002). However, residues essential for ATP binding and hydrolysis are not conserved. It therefore remains an intriguing possibility that catalytically-dead SWI/SNF homologs could function in other organisms to developmentally regulate fork progression.

Repair of Stalled & Collapsed Replication Forks

Obstructions to replication fork progression cause fork stalling and increase the likelihood of fork collapse and breakage. Stalled forks can resume replication once the barrier or fork stress is alleviated. Replication fork stalling can lead to uncoupling of the CMG helicase and DNA polymerases (Walter and Newport 2000, Byun *et al.* 2005). Uncoupling results in extended RPA tracks on exposed ssDNA and initiates a checkpoint response (Zou & Elledge 2003, Byun *et al.* 2005). ATR binds to the RPA-coated ssDNA via its binding partner ATRIP (Zou & Elledge 2003). TopBP1 (Mus101 in Drosophila, Dbp11 in yeast) signaling from stalled forks recruits the Rad9 – Rad1 – Hus1 (9-1-1) complex (Yan & Michael 2009), and interaction with Rad9 facilitates activation of ATR by TopBP1 (Kumagai *et al.* 2006, Delacroix *et al.* 2007, Lee *et al.* 2007). iPOND and NCC experiments showed that TopBP1 travels with elongating forks in the

absence of fork stress (Sirbu *et al.* 2013, Alabert *et al.* 2014), poising it as a first responder to replication stress. ATR activation leads to phosphorylation of several substrates in the DNA damage response, including Chk1 (Liu *et al.* 2000, Zou *et al.* 2002); activated Chk1 then prevents initiation of origins nearby stressed replication forks (Ge & Blow 2010). Loss of ATR activity in cells exposed to hydroxyurea (HU) was shown to reduce the enrichment of replisome components on replicating DNA, suggesting the ATR checkpoint stabilizes the fork during replication stress (Cobb *et al.* 2003). However, more recent studies reveal the replisome is maintained on DNA in the absence of the ATR checkpoint (De Piccoli *et al.* 2012). The authors find that the GINS subunit Psf1 is phosphorylated by ATR in response to HU, and suggest the checkpoint functions to regulate replisome function rather than stability (De Piccoli *et al.* 2012).

If stalling is prolonged, the replication machinery can disassemble in a process known as fork collapse. EM studies in yeast found that HU treatment in the absence of Rad53/Chk2 leads to the accumulation of ssDNA at replication forks and reversed forks (Sogo *et al.* 2002). These reversed forks are known as 'chicken-foot' structures. Fork reversal was long thought to be the result of failed checkpoint response to fork stalling. However, a recent study in human cell culture demonstrated that fork reversal is a common response to various replication perturbations when the checkpoint is intact (Zellweger *et al.* 2015). Fork reversal also is observed at trinucleotide repeats (Follonier *et al.* 2013), suggesting chicken-foot structures can form during unperturbed replication at hard-to-replicate sequences. Formation of reversed forks is dependent on PARP-1 regulation of the RECQ1 helicase, as well as Rad51 (Zellweger *et al.* 2015). Other papers have also demonstrated a role for Rad51 and other homologous recombination (HR) components in fork stabilization independent of DSB repair (Lomonosov *et al.* 2003, Petermann *et al.* 2010, Pathania *et al.* 2011, Schlacher *et al.* 2011, Gonzalez-Prieto *et al.* 2013, Hashimoto *et*

al. 2015). Additionally, proteomic studies of active replication forks found Rad51, BRCA1 and BRCA2, among other repair components, are bound to replication forks in the absence of fork stalling or collapse (Sirbu *et al.* 2011, Sirbu *et al.* 2013, Alabert *et al.* 2014).

When forks cannot be repaired, collapse generates single-sided double-strand breaks (DSB) that require the DSB repair response. Several components are recruited to the break site upon DSB formation. Mre11-Rad50-Nbs1 (MRN, MRX in yeast) binds to DSBs and recruits ATM (Lee & Paull 2005). Inactive ATM forms a dimer; recruitment to DSBs leads to autophosphorylation and dimer dissociation, activating the kinase activity of the two monomers (Bakkenist & Kastan 2003). Upon activation, ATM phosphorylates multiple DSB response targets including Chk2 and H2AX (Rogakou *et al.* 1998, Ahn *et al.* 2000, Matsuoka *et al.* 2000). The histone variant H2AX (H2A in yeast, H2Av in Drosophila) is phosphorylated in response to DSB formation up to 50kb on either side of the break in yeast and several megabases in mammalian cells (Rogakou *et al.* 1998, Madigan *et al.* 2002, Schroff *et al.* 2004, Iacovoni *et al.* 2010). The phosphorylated histone is known as γH2AX and serves as a docking platform for DSB repair proteins (Celeste *et al.* 2002, Celeste *et al.* 2003, Ward *et al.* 2003).

The cell has multiple pathways to repair DSBs, and pathway decision is ultimately determined by end resection of the break. Both the phase of the cell cycle and levels of accessory proteins influence whether nucleases have access to the DSB, thus dictating the repair pathway winner. During S-phase, when replication forks are actively elongating daughter DNA strands, S-phase CDK activity promotes break resection (Aylon *et al.* 2004, Ferreira & Cooper 2004, Ira *et al.* 2004, Bennardo *et al.* 2008, Yun & Hiom 2009, Chen *et al.* 2011, Tomimatsu *et al.* 2014). CDK promotes activity of the exonuclease CtIP, and with MRN mediates limited resection of the DSB ends exposing 3' ssDNA overhangs (Bennardo *et al.* 2008, Yun & Hiom 2009). Extensive

break resection also is mediated by CDK activity via EXO1 (Chen *et al.* 2011, Tomimatsu *et al.* 2014). In addition to CDK regulation, resection is dictated by competition between BRCA1 and 53BP1 for access to the DSB. Both BRCA1 and 53BP1 are concentrated at DSBs by γH2AX (Celeste *et al.* 2003, Ward *et al.* 2003), but they also antagonize each other's recruitment (Escribano-Díaz *et al.* 2013). BRCA1 forms a complex with CtIP during S and G2 and promotes DSB resection (Yu & Chen 2004, Yun & Hiom 2009, Escribano-Díaz *et al.* 2013). However, during G1/G0 of the cell cycle 53BP1 prevents BRCA1 and CtIP access to DSBs and thus blocks resection-mediated repair (Escribano-Díaz *et al.* 2013). It therefore seems that the antagonistic relationship between 53BP1 and BRCA1 helps to integrate cell cycle regulation of DSB repair pathway choice.

Limited resection by MRN and CtIP commits the break to homologous recombination (HR) or alternative end joining (alt-EJ) repair pathways (Yun & Hiom 2009, Truong *et al.* 2013). More extensive resection by EXO is required for HR repair (Yun & Hiom 2009, Truong *et al.* 2013). During HR repair, BRCA2 mediates the recruitment Rad51 and facilitates the replacement of RPA with Rad51 filaments (Yuan *et al.* 1999, Moynahan *et al.* 2000, Jensen *et al.* 2010, Liu *et al.* 2010). Rad51 then mediates the search for homologous sequences and strand invasion (McIlwraith *et al.* 2000), using the homologous strand as a template for repair (Fig. 3).

One subtype of HR is break-induced replication (BIR), in which one end of a broken chromosome copies a homologous template to the end of the chromosome. The first evidence for BIR in eukaryotes came from experiments in *S. cerevisiae*, showing that 35% of DSBs were repaired in the absence of Rad51 (Malkova *et al.* 1996). Surviving cells did not show evidence for traditional HR, but rather became homozygous for markers between the breakpoint and closest telomere (Malkova *et al.* 1996). These repair products supported a mechanism by which

Figure 3. Pathways of Double-Strand Break Repair

Resection of the DSB commits repair to homologous recombination (HR) or alternative end joining (alt-EJ) repair pathways. (left) Alt-EJ by microhomology-mediated end joining (MMEJ) requires Pol θ align or template short microhomologies, generating deletions and insertions. The ends are then ligated together by the LigaseIII/XRCC1 complex. (middle) HR repair requires BRCA2 to recruit Rad51 and facilitates filament formation along the resected DNA. Rad51 filaments search for homologous sequences and initiate strand invasion to restore the exact sequence to the break site. (right) Resection is blocked in nonhomologous end joining (NHEJ) by Ku70-80 binding. The Ku70-80 heterodimer recruits the DNA-PKcs and together this complex brings the broken DNA ends together. The XRCC4-DNA Ligase IV complex is recruited and catalyzes DSB ligation. (Illustration by Steven Lee/graphiko.com).

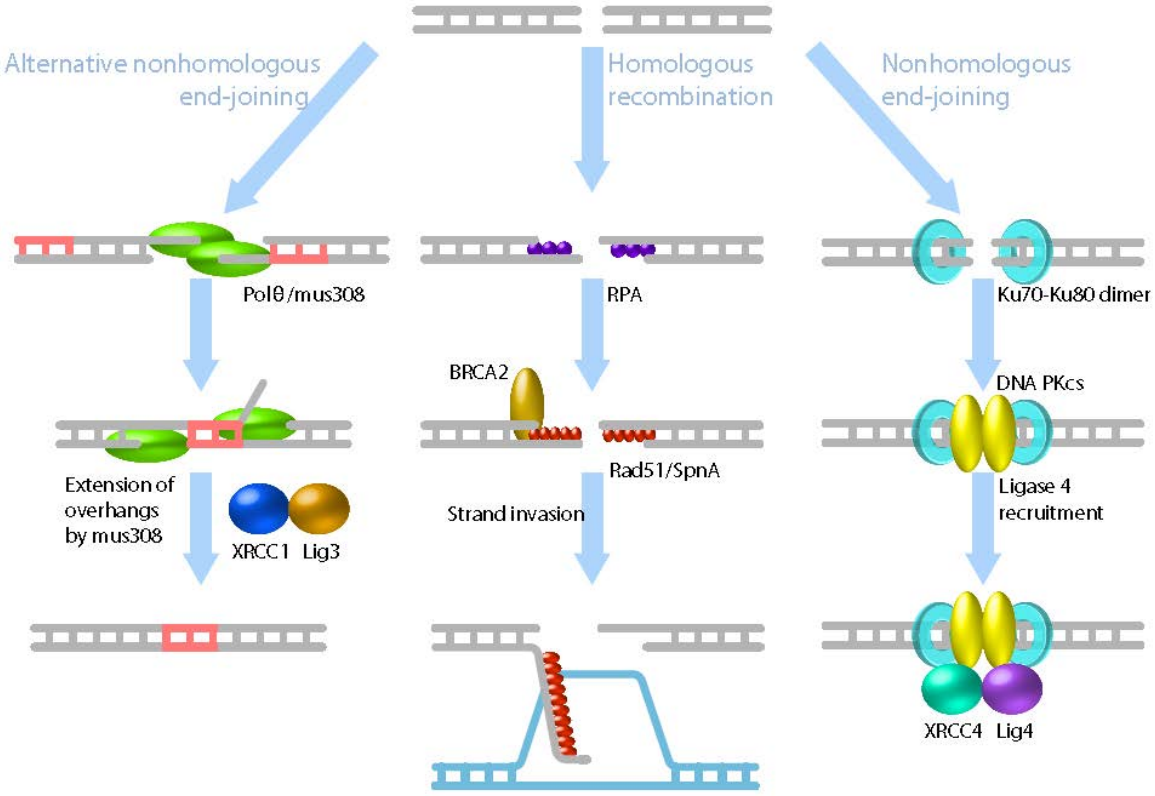
Alternative nonhomologous end-joining
Homologous recombination
Nonhomologous end-joining
Polθ/mus308
RPA
Ku70-Ku80 dimer
BRCA2
DNA PKcs
Extension of overhangs by mus308
XRCC1 Lig3
Rad51/SpnA
Strand invasion
Ligase 4 recruitment
XRCC4 Lig4

one end of the DSB is repaired via strand invasion of the homologous template followed by replication up to 100 kb to the end of the chromosome (Malkova *et al.* 1996). Later studies provided evidence for distinct Rad51-dependent and independent pathways (Signon *et al.* 2001, Davis & Symington 2004), of which the Rad51-dependent pathway is much more efficient (Davis & Symington 2004, Malkova *et al.* 2005). BIR is only preferred over HR repair when one side of the break shares homology with the repair template (Malkova *et al.* 2005).

BIR in *S. cerevisiae* also requires many of the components present at S-phase replication forks, consistent with the hypothesis that BIR establishes new processive forks for repair. Using PCR to monitor repair products, it was found that temperature-sensitive mutants in Cdt1, Mcm2-7, Cdc45, GINS, Dpb11, Sld3, Mcm10, Polα and Polδ all reduce the efficiency of BIR at the restrictive temperature (Lydeard *et al.* 2007, 2010). Absence of PCNA and the clamp loader RFC also eliminate BIR (Wilson *et al.* 2013). Although Polε is not required for initiation of BIR, it is necessary for processive replication (Lydeard *et al.* 2007). BIR also requires the DDK subunit Cdc7 (Lydeard *et al.* 2010); DDK activity recruits Cdc45 and Sld3 to replication origins in G1 (Heller *et al.* 2011, Deegan *et al.* 2016), and therefore may have a similar role in recruiting these fork components during BIR. Interestingly, BIR repair products appear at the same frequency in the permissive and restrictive temperatures in ORC and Cdc6 temperature-sensitive mutants (Lydeard *et al.* 2010). Together, these results support the hypothesis that BIR establishes processive replication forks in the absence of an origin. In addition to canonical fork requirements, the appearance of BIR repair products also depends on the nonessential Polδ subunit Pol32 (Lydeard *et al.* 2007), and the Pif1 helicase is required for long-range synthesis during BIR (Saini *et al.* 2013, Wilson *et al.* 2013, Vasianovich *et al.* 2014).

BIR also was demonstrated in human cell lines under conditions of replication stress,

suggesting it was used to repair collapsed replication forks (Costantino *et al.* 2014). The authors also found that BIR generated duplications and rearrangements. A model for the generation of copy number variations proposed a form of BIR that relies on microhomology annealing, termed microhomology-mediated BIR (MMBIR), in repair of collapsed replication forks (Hastings *et al.* 2009). MMEJ was later described in budding yeast, and was shown to generate complex chromosome rearrangements (Sakofsky *et al.* 2015). Indeed, complex rearrangements and copy number variations consistent with BIR and MMBIR are observed across human cancers and other genomic diseases (Hastings *et al.* 2009).

If only limited resection of the break occurs, alt-EJ can be used to repair the break (Yun & Hiom 2009, Truong *et al.* 2013). One form of alt-EJ is microhomology-mediated end joining (MMEJ), which joins together microhomologies exposed by resection. The broken ends are efficiently ligated together by Ligase III with its binding partner XRCC1 (Fig. 3) (Liang *et al.* 2008, Sharma *et al.* 2015, Lu *et al.* 2016), but Ligase I can partially compensate for loss of Ligase III in MMEJ repair (Lu *et al.* 2016). MMEJ requires DNA Polymerase θ (Pol θ), encoded by *mus308* in Drosophila (Chan *et al.* 2010, Kent *et al.* 2015, Mateos-Gomez *et al.* 2015). Pol θ binds to ssDNA on both ends of a DSB and aligns short 4-10bp microhomology sequences (Fig. 3) (Chan *et al.* 2010, Kent *et al.* 2015). Microhomologies also can be generated by Pol θ, resulting in insertions templated from sequences outside the break site (Chan *et al.* 2010, Yu & McVey 2010, Hogg *et al.* 2012, Kent *et al.* 2015). MMEJ a highly error prone pathway, generating deletions and insertions at the break site from microhomology alignment and extension (Chan *et al.* 2010, Yu & McVey 2010, Hogg *et al.* 2012, Kent *et al.* 2015, Mateos-Gomez *et al.* 2015).

Nonhomologous end joining (NHEJ) repair directly joins the two broken ends of a DSB,

often leading to small deletions (Jeggo 1998). The first step in the pathway is Ku70-80 binding to blunt DNA ends (Fig. 3) (Dvir *et al.* 1992, Yoo & Dynan 1999, Walker *et al.* 2001). In vertebrates, Ku70-80 recruits the DNA-dependent protein kinase catalytic subunit (DNA-PKcs) to form the DNA-dependent protein kinase (DNA-PK) (Dvir *et al.* 1992, Gottlieb & Jackson 1993). Ku70-80 binding and DNA-PK activity prevents resection of the DSB (Pierce *et al.* 2001), thus blocking other repair pathways. Binding of the DSB ends by Ku70-80 and DNA-PKcs also is required to bring the broken DNA ends in close proximity (Graham *et al.* 2016). Ku binding recruits the XRCC4-DNA Ligase IV complex (Nick McElhinny *et al.* 2000) which together with XL4 and DNA-PK activity promotes close association of the two broken ends (Graham *et al.* 2016). Ligase IV then catalyzes ligation of the DSB ends, and this reaction is enhanced by XRCC4 (Fig. 3) (Grawunder *et al.* 1997). NHEJ is active throughout the cell cycle, but competition from resection-mediated pathways during S and G2 make it more prevalent during G1.

Re-replication: How origin deregulation impairs fork integrity

Replication initiation is tightly regulated with the cell cycle to ensure each origin fires only once per cell cycle (Bell & Dutta 2002). In budding yeast, CDK activity prevents re-replication by inhibiting multiple components of the pre-RC at several levels of regulation. Phosphorylation of Orc2 and Orc6 by CDK prevents pre-RC formation (Nguyen *et al.* 2001, Wilmes *et al.* 2004). CDK phosphorylation events inhibit *Cdc6* transcription (Moll *et al.* 1991); direct phosphorylation of Cdc6 promotes ubiquitination by SCF thus leading to its degradation by the proteasome from late G1 to S-phase (Drury *et al.* 1997, Drury *et al.* 2000), and then in mitosis prevents Cdc6 from loading Mcm2-7 (Mimura *et al.* 2004). Finally, CDK phosphorylation

exports Cdt1 and Mcm2-7 from the nucleus (Labib *et al.* 1999, Nguyen *et al.* 2001, Tanaka & Diffley 2002, Liku *et al.* 2005). CDK activity also prevents re-replication in metazoans by targeting multiple pre-RC components, although the mechanisms differ between model organisms. One common and major regulator of pre-RC activity is Geminin, which binds to and sequesters Cdt1 to prevent Mcm2-7 from being loaded at origins (Wohlschlegel *et al.* 2000, Quinn *et al.* 2001, Tada *et al.* 2001, Cook *et al.* 2004). Depletion of Geminin is sufficient to induce re-replication in Drosophila and human cell culture experiments (Mihaylov *et al.* 2002, Melixetian *et al.* 2004, Zhu *et al.* 2004, Zhu & Dutta 2006, Ding & MacAlpine 2010). Overexpression of its target Cdt1 in human cells and Drosophila (Vaziri *et al.* 2003, Thomer *et al.* 2004) and addition of recombinant Cdt1 to Xenopus cell extract also causes re-replication (Arias & Walter 2005, Li & Blow 2005, Maiorano *et al.* 2005, Davidson *et al.* 2006).

Origin re-firing in a single S-phase activates the DNA damage checkpoint (Mihaylov *et al.* 2002, Vaziri *et al.* 2003, Melixetian *et al.* 2004, Zhu *et al.* 2004, Archambault *et al.* 2005, Green & Li 2005, Li & Blow 2005, Davidson *et al.* 2006, Neelsen *et al.* 2013), generates DSBs (Green & Li 2005, Davidson *et al.* 2006, Zhu & Dutta 2006, Finn & Li 2013, Neelsen *et al.* 2013) and causes DNA fragmentation (Melixetian *et al.* 2004, Green & Li 2005, Davidson *et al.* 2006, Neelsen *et al.* 2013). Re-replication forks exhibit inhibited elongation and only progress 30-35kb from the origin (Ngyuen *et al.* 2001). Consistent with this observation, re-replication doesn't result in full replication of the genome and generates cells with ploidies between incremental doubling values (Melixetian *et al.* 2004, Zhu *et al.* 2004, Green & Li 2005, Tanny *et al.* 2006, Ding & MacAlpine 2010). If the DNA damage checkpoint is blocked, cells enter mitosis with partially re-replicated DNA, resulting in cells with sub-G1 ploidy (Mihaylov *et al.* 2002) and chromosome breaks and fusions (Melixetian *et al.* 2004). Origin re-firing within repetitive

sequences leads to copy number expansions (Green *et al.* 2010, Finn & Li 2013), and re-replication near centromeres increases the rate of aneuploidy (Hanlon & Li 2015). These types of chromosomal aberrations are common across numerous human cancers (Abbas & Dutta 2013). Additionally, Cdt1 overexpression drives oncogenic transformation in cell culture and tumor formation in mouse models, and it is observed in various human cancers cell lines (Arenstonand *et al.* 2002, Karakaidos *et al.* 2004, Xouri *et al.* 2004, Seo *et al.* 2005). Together these observations strongly suggest that the same mechanisms used to artificially induce re-replication in the laboratory, as well as the consequences for genome instability, are physiologically relevant to cancer progression.

DSBs and chromosome fragmentation generated during re-replication are consistent with predicted products of head-to-tail collisions between adjacent replication forks (Fig. 4) (Davidson *et al.* 2006). This is supported by the observation that broken DNA fragments are generated around an origin after re-replication is induced (Finn & Li 2013). The pattern of repeat expansion during re-replication also is consistent with a forks-chasing-forks model of DSB formation (Green *et al.* 2010, Finn & Li 2013). Such collisions require that re-replication forks can progress faster along the newly synthesized DNA and thus catch-up with the forks in front (Davidson *et al.* 2006). Indeed, nascent DNA is in an immature chromatin state for up to 20 minutes after replication that is more susceptible to nuclease degradation (Hildebrand & Walters 1976). Immature chromatin behind the first replication fork could thus be easier to disassemble as the re-replication forks arrive.

Other data suggest that DSBs formed by re-replication occur in the absence of fork collisions. RNAi depletion of *Emi1* in human cells, an APC/C inhibitor that prevents Geminin degradation during S and G2 (Machida & Dutta 2007), generates ssDNA gaps along the DNA

Figure 4. The fork collision model of DSB generation by re-replication

Collisions between back-to-back replisomes (green) would generate a double-strand break (DSB) behind the second replication fork (arrow). (A) A single origin re-initiation event could lead to DSB formation at a collision site. (B) Multiple origin re-initiations would increase the frequency of fork collisions and thus the number DSBs formed. Fork collisions are expected to be stochastic, and may occur at only a subset of forks as shown here.

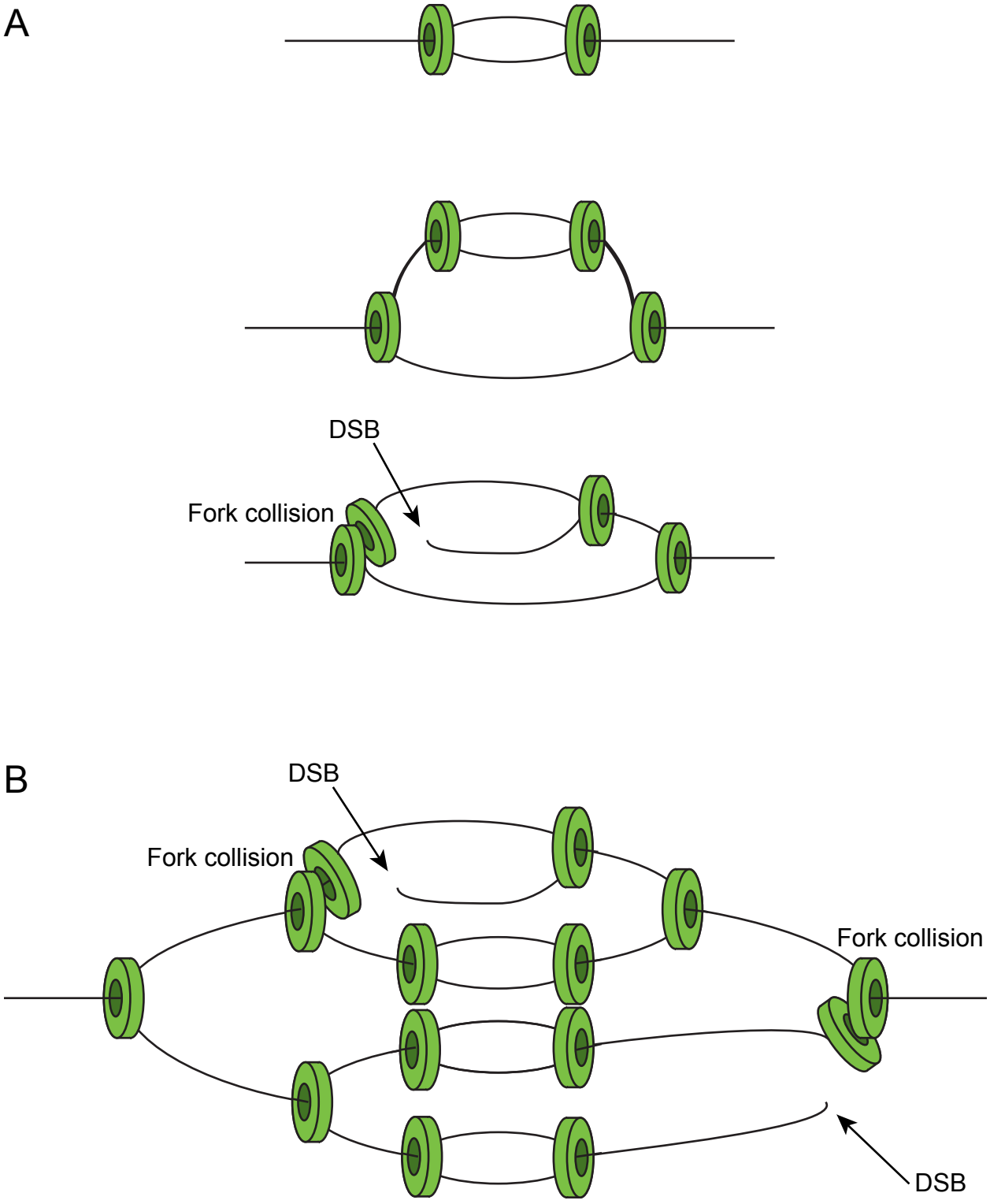
A
DSB
Fork collision
B
DSB
Fork collision
Fork collision
DSB

before detectable re-replication occurs (Neelson *et al.* 2013). The authors propose that de-regulated origin firing leads to unrepaired gaps in the first round of replication, which causes fork collapse and DNA fragmentation when re-replication forks meet these gaps on the template strand. Gaps also were reported when recombinant Cdt1 was added to *Xenopus* extracts, however the appearance of gaps in relation to the onset of re-replication was not reported (Neelsen *et al.* 2013). It is therefore possible that the cause of DSBs during re-replication is dependent on the mechanism and timing of origin deregulation.

The generation of DSBs during re-replication poses the question of how these breaks are repaired. In Drosophila and human cell culture, Rad51 foci form after Geminin depletion (Melixetian *et al.* 2004, Zhu & Dutta 2006), suggesting the HR repair pathway is activated to repair broken forks. Another study in human cell culture reported 53BP1 foci appear overlapping with γH2AX when re-replication is induced, suggesting NHEJ repair (Neelson *et al.* 2013). However, these studies only report on markers of one repair pathway and do not test whether there is a preferred mechanism of repair. In two human cell culture lines, knockdown of the HR components Rad51, BRCA1 and CtIP reduced cell proliferation when Cdt1 was overexpressed, whereas knockdown of the NHEJ components Ku70 and XRCC4 had no effect (Truong *et al.* 2014). Interestingly, knockdown of the MMEJ component Lig3 also reduced proliferation, although to a lesser extent than HR factors (Truong *et al.* 2014). Using GFP reporter constructs for HR and MMEJ repair after re-replication, the authors find the percent of GFP positive cells increases upon Cdt1 overexpression; this frequency is not altered by knockdown of Ku70 or XRCC4, suggesting NHEJ does not compete for repair in these cells (Truong *et al.* 2014).

In *S. cerevisiae*, HR pathway mutants *rad52* and *rad59* are synthetically lethal in re-replicating strains, as are the three components of the MRX complex *mre11*, *rad50* and

xrs1(Archambault *et al.* 2005). In budding yeast, the MRX complex is involved in both NHEJ and HR repair (D'Amours & Jackson 2002); however, mutations in the NHEJ components *yku70*, *yku80* and *dnl4* (*lig4*) are viable in re-replicating strains, suggesting MRX is functioning in HR repair during re-replication (Archambault *et al.* 2005). Repeat expansion after re-replication in *S. cerevisiae* occurs via single-strand annealing (SSA) repair and is genetically dependent on *rad52*, *rad1* and *msh3*, but not *rad51* or *dnl4* (Green 2010, Finn 2013). The frequency of re-replication induced aneuploidy is halved in *rad52* mutants, and tripled in *dnl4* mutants; these results demonstrate that both the HR and NHEJ pathways are active and compete to repair DSBs generated by re-replication (Hanlon & Li 2015).

Studies from multiple model systems suggest a variety of pathways can be used to repair DSBs generated during re-replication. Resection-dependent pathways including HR, SSA and MMEJ are the most commonly observed, consistent with re-replication occurring in S and G2 phase of the cell cycle when resection is most efficient (see previous section). However, signatures of NHEJ repair are also reported (Neelson *et al.* 2013, Hanlon & Li 2015). Therefore, as with general DSBs, pathway choice for repair of re-replication DSBs could be the result of pathway competition influenced by the cell cycle phase and exonuclease access to the break site.

Modeling Fork Progression & Re-replication during Drosophila Follicle Cell Amplification

The follicle cells of *Drosophila melanogaster* undergo re-replication from defined origins as a developmental strategy to enhance gene expression. The follicle cells are somatic cells that form a single-cell epithelial layer around the nurse cells and oocyte. Together, these three cell types make up the egg chamber. One of the primary functions of the follicle cells is to produce and secrete large quantities of eggshell proteins, which is accomplished in just a few hours

(Spradling & Mahowald 1979, Waring & Mahowald 1979). To meet protein production demands the follicle cells increase the copy number of eggshell protein genes by repeated activation of adjacent replication origins (Spradling & Mahowald 1980). Gene amplification occurs at six loci in the follicle cells, termed *Drosophila Amplicons in Follicle Cells* (*DAFCs*) (Claycomb *et al.* 2004, Kim *et al.* 2011). The *DAFCs* have specific replication origins that utilize the same machinery as in canonical S-phase (Landis 1997 *et al.*, Landis & Tower 1999, Henderson *et al.* 2000, Whittaker *et al.* 2000, Schwed *et al.* 2002). Bidirectional fork movement away from the origin produces a gradient of amplified DNA spanning approximately 100kb at each *DAFC* (Fig. 5) (Claycomb *et al.* 2004, Kim *et al.* 2011). Electron microscopy studies demonstrated that re-replicated DNA is maintained in the chromosome, forming an onion-skin structure (Osheim *et al.* 1988). Amplification occurs after follicle cell proliferation has ceased, and therefore onion-skin structures do not pose a threat to future divisions.

Drosophila egg chambers are divided into 14 developmental stages based on their distinct morphologies, each of which lasts for a defined period of time. This enables isolation of the follicle cells at specific times in development by ovary dissection. Over the course of egg chamber development, the follicle cells undergo two major transitions into alternative cell cycles. In stages 1-6 they proliferate via the canonical cell cycle. At stage 7 the follicle cells stop dividing, but enter the endocycle and increase their genome ploidy from 2C to 16C. In stage 10A the follicle cells cease whole genome replication, and at stage 10B initiate amplification synchronously throughout all the follicle cells of a given egg chamber (Calvi *et al.* 1998).

The precise timing and location of origin firing at the *DAFCs* enables us to isolate replication forks at specific points after origin initiation and track their progression in real-time (Claycomb *et al.* 2002, Park *et al.* 2007). Replication forks can be directly visualized by

Figure 5. CGH Profiles of the *Drosophila Follicle Cell Amplicons*

CGH of the *DAFCs* in the wild-type strain OrR. DNA from stage 13 egg chambers was competitively hybridized with diploid embryonic DNA to microarrays with approximately one probe every 125bp. Chromosomal position is plotted on the x-axis, the log2 ratio of stage 13 DNA to embryonic DNA is plotted on the y-axis.

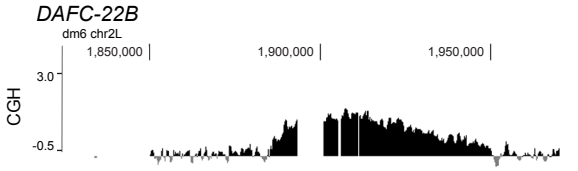
DAFC-22B
dm6 chr2L
1,850,000
1,900,000
1,950,000
3.0
CGH
-0.5

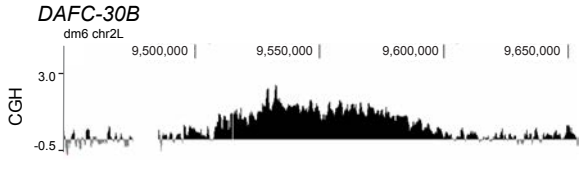
DAFC-30B
dm6 chr2L
9,500,000
9,550,000
9,600,000
9,650,000
3.0
CGH
-0.5

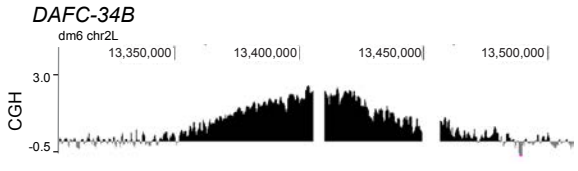
DAFC-34B
dm6 chr2L
13,350,000
13,400,000
13,450,000
13,500,000
3.0
CGH
-0.5

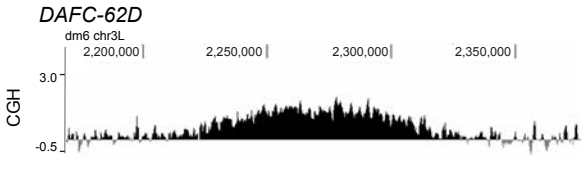
DAFC-62D
dm6 chr3L
2,200,000
2,250,000
2,300,000
2,350,000
3.0
CGH
-0.5

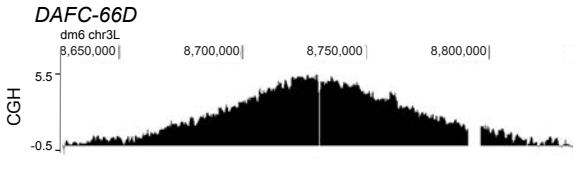
DAFC-66D
dm6 chr3L
8,650,000
8,700,000
8,750,000
8,800,000
5.5
CGH
-0.5

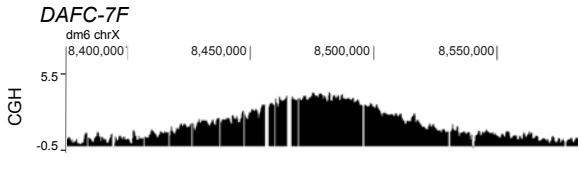
DAFC-7F
dm6 chrX
8,400,000
8,450,000
8,500,000
8,550,000
5.5
CGH
-0.5

introducing a nucleotide analogue (Calvi *et al.* 1998, Claycomb *et al.* 2002), providing the necessary resolution to measure the distance between forks and observe events occurring at sites of active replication. Measurements of fork progression in BrdU-labelled follicle cells revealed that forks move more slowly during amplification than in endocycling or S-phase (Claycomb *et al.* 2002), consistent with other re-replication systems (Ngyuen *et al.* 2001). Fork progression also can be measured by comparative genome hybridization (CGH), which provides a detailed view of the gradient of amplification at each *DAFC* (Claycomb *et al.* 2004, Kim *et al.* 2011). The shape of the CGH gradient is reflective of replication fork progression, making it a powerful tool to pick out positions of altered fork progression and compare fork elongation between different genetic backgrounds.

Summary

Here I present work utilizing the Drosophila amplification system to study fork progression across diverse chromosome positions and understand mechanisms of fork instability and repair during re-replication. Taking advantage of the amplification gradients generated by the *DAFCs*, we have measured fork progression by CGH at different genomic positions from ectopic amplicon origins. We have developed two analyses to quantify fork progression for comparison across different positions and genetic backgrounds: slope analysis and half-maximum distance. The slope analysis will enable the discovery of sequence and chromatin motifs that alter fork elongation. The half-maximum distance was used to dissect pathways that maintain fork stability during re-replication. We show that like other re-replication systems, the *DAFCs* generate DSBs. We find that these breaks are located at active re-replication forks, supporting the fork collision model of DSB generation during re-replication (Fig. 4) (Davidson *et al.* 2006). Additionally, we

present evidence that the DNA damage response maintains fork progression during re-replication. Our results also indicate multiple pathways can repair re-replication DSBs, and the contribution of each pathway to productive fork progression is influenced by repair kinetics and restrictions from the developmental timeline.

References

Abbas, T., Keaton, M.A., Dutta, A. (2013). Genomic instability in cancer. Cold Spring Harb. Perspect. Biol. *5*, a012914.

Adachi, Y., Laemmli, U.K. (1992). Identification of nuclear pre-replication centers poised for DNA synthesis in Xenopus egg extracts: immunolocalization study of replication protein A. J. Cell Biol. *119*, 1-15.

Adachi, Y., Laemmli, U.K. (1994). Study of the cell cycle-dependent assembly of the DNA pre-replication centres in Xenopus egg extracts. EMBO J. *13*, 4153-4164.

Ahn, J.Y., Schwarz, J.K., Piwnica-Worms, H., and Canman, C.E. (2000). Threonine 68 phosphorylation by ataxia telangiectasia mutated is required for efficient activation of Chk2 in response to ionizing radiation. Cancer Res. *60*, 5934–5936.

Alabert, C., Groth, A. (2012). Chromatin replication and epigenome maintenance. Nat. Rev. Mol. Cell Biol. *13*, 153-167.

Alabert, C., Bukowski-Wills, J.C., Lee, S.B., Kustatscher, G., Nakamura, K., de Lima Alves, F., Menard, P., Mejlvang, J., Rappsilber, J., Groth, A. (2014). Nascent chromatin capture proteomics determines chromatin dynamics during DNA replication and identifies unknown fork components. Nat. Cell Biol. *16*, 281-293.

Andreyeva, E.N., Kolesnikova, T.D., Belyaeva, E.S., Glaser, R.L., Zhimulev, I.F. (2008). Local DNA underreplication correlates with accumulation of phosphorylated H2Av in the *Drosophila melanogaster* polytene chromosomes. Chromosome Res. *16*, 851-862.

Aylon, Y., Liefshitz, B., Kupiec, M. (2004). The CDK regulates repair of double-strand breaks by homologous recombination during the cell cycle. EMBO J. *23*, 4868–4875.

Archambault. V., Ikui, A.E., Drapkin, B.J., Cross, F.R. (2005). Disruption of mechanisms that prevent re-replication triggers a DNA damage response. Mol. Cell. Biol. *25*, 6707–6721.

Arentson, E., Faloon, P., Seo, J., Moon, E., Studts, J.M., Fremont, D.H. Choi., K. (2002). Oncogenic potential of the DNA replication licensing protein CDT1. Oncogene *21*, 1150–1158.

Arias, E.E., Walter, J.C. (2005). Replication-dependent destruction of Cdt1 limits DNA replication to a single round per cell cycle in *Xenopus* egg extracts. Genes Dev. *19*, 114–126.

Bakkenist, C.J., and Kastan, M.B. (2003). DNA damage activates ATM through intermolecular autophosphorylation and dimer dissociation. Nature *421*, 499–506.

Bell, S.P., Stillman, B. (1992). ATP-dependent recognition of eukaryotic origins of DNA replication by a multiprotein complex. Nature *357*, 128-134.

Bell, S.P., Dutta, A. (2002). DNA Replication in Eukaryotic Cells. Annu. Rev. Biochem. *71*, 333–374.

Belyaeva, E.S., Zhimulev, I.F., Volkova, E.I., Alekseyenko, A.A., Moshkin, Y.M., Koryakov, D.E. (1998). Su(UR)ES: a gene suppressing DNA underreplication in intercalary and pericentric heterochromatin of *Drosophila melanogaster* polytene chromosomes. Proc. Natl. Acad. Sci. USA *95*, 7532-7537.

Bennardo, N., Cheng, A., Huang, N., Stark, J.M. (2008) Alternative-NHEJ is a mechanistically distinct pathway of mammalian chromosome break repair. PLoS Genet. *4*, e1000110.

Besnard, E., Babled, A., Lapasset, L., Milhavet, O., Parrinello, H., Dantec, C., Marin, J.M., Lemaitre, J.M. (2012). Unraveling cell type-specific and reprogrammable human replication origin signatures associated with G-quadruplex consensus motifs. Nat. Struct. Mol. Biol. *19*, 837-844.

Bonner, W.M., Wu, R.S., Panusz, H.T., Muneses, C. (1988). Kinetics of accumulation and depletion of soluble newly synthesized histone in the reciprocal regulation of histone and DNA synthesis. Biochemistry. *27*, 6542–6550.

Byun, T.S., Pacek, M., Yee, M., Walter, J.C., Cimprich, K.A. (2005). Functional uncoupling of MCM helicase and DNA polymerase activities activates the ATR-dependent checkpoint. Genes Dev. *19*, 1040-1052.

Calvi, B. R., Lilly, M.A., Spradling, A.C. (1998). Cell cycle control of chorion gene amplification. Genes Dev. *12*, 734-744.

Casper, A.M., Nghiem, P., Arlt, M.F., Glover, T.W. (2002). ATR regulates fragile site stability. Cell *11*, 779-789.

Celeste, A., Petersen, S., Romanienko, P.J., Fernandez-Capetillo, O., Chen, H.T., Sedelnikova, O.A., Reina-San-Martin, B., Coppola, V., Meffre, E., Difilippantonio, M.J., Redon, C., Pilch, D.R., Olaru, A., Eckhaus, M., Camerini-Otero, R.D., Tessarollo, L., Livak, F., Manova, K., Bonner, W.M., Nussenzweig, M.C., Nussenzweig, A. (2002). Genomic instability in mice lacking histone H2AX. Science *296*, 922-927.

Celeste, A., Fernandez-Capetillo, O., Kruhlak, M.J., Pilch, D.R., Staudt, D.W., Lee, A., Bonner, R.F., Bonner, W.M., Nussenzweig, A. (2003). Histone H2AX phosphorylation is dispensable for the initial recognition of DNA breaks. Nat. Cell Biol. *5*, 675–679.

Cha, R.S., Kleckner, N. (2002). ATR homolog Mec1 promotes fork progression, thus averting breaks in replication slow zones. Science *297*, 602–606.

Chan, S.H., Yu, A.M., McVey, M. (2010). Dual roles for DNA polymerase theta in alternative end-joining repair of double-strand breaks in Drosophila. PLoS Genet. *6*, e1001005.

Chen, X. Niu, H., Chung, W.H., Zhu, Z., Papusha, A., Shim, E.Y., Lee, S.E., Sung, P., Ira, G. (2011). Cell cycle regulation of DNA double-strand break end resection by Cdk1-dependent Dna2 phosphorylation. Nat. Struct. Mol. Biol. *18*, 1015–1019.

Claycomb, J.M., MacAlpine, D.M., Evans, J.G., Bell, S.P., Orr-Weaver, T.L. (2002). Visualization of replication initiation and elongation in *Drosophila*. J. Cell Biol. *159*, 225-236.

Claycomb, J.M., Benasutti, M., Bosco, G., Fenger, D.D., Orr-Weaver, T.L. (2004). Gene amplification as a developmental strategy: isolation of two developmental amplicons in *Drosophila*. Dev. Cell *6*, 145-155.

Cobb, J.A., Bjergbaek, L., Shimada, K., Frei, C., Gasser, S.M. (2003). DNA polymerase stabilization at stalled replication forks requires Mec1 and the RecQ helicase Sgs1. EMBO J. *22*, 4325-4336.

Conaway, R.C., Lehman, I.R. [1] (1982). A DNA primase activity associated with DNA polymerase alpha from *Drosophila melanogaster* embryos. Proc. Natl. Acad. Sci. USA. *79*, 2523-2527.

Conaway, R.C., Lehman, I.R. [2] (1982). Synthesis by the DNA primase of *Drosophila melanogaster* of a primer with a unique chain length. Proc. Natl. Acad. Sci. USA. *79*, 4585-4588.

Cook, J.G., Chasse, D.A., Nevins, J.R. (2004). The regulated association of Cdt1 with minichromosome maintenance proteins and Cdc6 in mammalian cells. J. Biol. Chem. *279*, 9625–9633.

Costantino, L., Sotiriou, S.K., Rantala, J.K., Magin, S., Mladenov, E., Helleday, T., Haber, J.E., Iliakis, G., Kallioniemi, O.P., Halazonetis, T.D. (2014). Break-induced replication repair of damaged forks induces genomic duplications in human cells. Science *343*, 88-91.

D'Amours, D., Jackson, S.P. (2002). The Mre11 complex: at the crossroads of DNA repair and checkpoint signaling. Nat. Rev. Mol. Cell Biol. *3*, 317-327.

Davidson, I.F., Anatoily, L., Blow, J.J. (2006). Deregulated replication licensing causes DNA fragmentation consistent with head-to-tail fork collision. Mol. Cell *24*, 433-443.

Davis, A.P., Symington, L.S. (2004). Replication in Yeast RAD51-Dependent Break-Induced Replication in Yeast. Mol. Cell. Biol. *6*, 2344-2351.

Debatisse, M., Le Tallec, B., Letessier, A., Dutrillaux, B., Brison, O. (2012). Common fragile sites: mechanisms of instability revisited. Trends Genet. *28*, 22-32.

Deegan, T.D., Yeeles, J.T., Diffley, J.F. (2016). Phosphopeptide binding by Sld3 links Dbf4-dependent kinase to MCM replicative helicase activation. EMBO J. *35*, 961-973.

Delacroix, S., Wagner, J.M., Kobayashi, M., Yamamoto, K., Karnitz, L.M. (2007). The Rad9-Hus1-Rad1 (9-1-1) clamp activates checkpoint signaling via TopBP1. Genes Dev. *21*, 1472 – 1477.

De Piccoli, G., Katou, Y., Itoh, T., Nakato, R., Shirahige, K., Labib, K. (2012). Replisome stability at defective DNA replication forks is independent of S phase checkpoint kinases. Mol. Cell. *45*, 696-704.

Ding, Q., MacAlpine, D.M. (2010). Preferential re-replication of *Drosophila* heterochromatin in the absence of geminin. PLoS Genet. 6, e1001112.

Douglas, M.E., Diffley J.F. (2016). Recruitment of Mcm10 to Sites of Replication Initiation Requires Direct Binding to the Minichromosome Maintenance (MCM) Complex. J. Biol. Chem. *291*, 5879-5888.

Drury, L.S., Perkins, G., and Diffley, J.F. (1997). The Cdc4/34/53 pathway targets Cdc6p for proteolysis in budding yeast. EMBO J. *16*, 5966–5976.

Drury LS, Perkins G, Diffley JFX. (2000). The cyclin-dependent kinase Cdc28p regulates distinct modes of Cdc6p proteolysis during the budding yeast cell cycle. Curr. Biol. *10*, 231–240.

Duxin, J.P., Dewar, J.M., Yardimci, H., Walter, J.C. (2014). Repair of a DNA-protein crosslink by replication-coupled proteolysis. Cell *159*, 346-357.

Dvir, A., Peterson, S.R., Knuth, M.W., Lu, H., Dynan,W.S. (1992). Ku autoantigen is the regulatory component of a template-associated protein kinase that phosphorylates RNA polymerase II. Proc. Natl Acad. Sci. USA *89*, 11920-11924.

Einolf, H.J., Guengerich, F.P. (2000). Kinetic analysis of nucleotide incorporation by mammalian DNA polymerase delta. J. Biol. Chem. *275*, 16316-16322.

English, C.M., Adkins, M.W., Carson, J.J., Churchill, M.E., Tyler, J.K. (2006). Structural basis for the histone chaperone activity of Asf1. Cell *127*, 495-508.
Escribano-Díaz, C., Orthwein, A., Fradet-Turcotte, A., Xing, M., Young, J.T., Tkáč, J., Cook, M.A., Rosebrock, A.P., Munro, M., Canny, M.D., Xu, D., Durocher, D. (2013). A cell cycle-dependent regulatory circuit composed of 53BP1-RIF1 and BRCA1-CtIP controls DNA repair pathway choice. Mol. Cell. *49*, 872-883.
Evrin, C., Clarke, P., Zech, J., Lurz, R., Sun, J., Uhle, S., Li, H., Stillman, B., Speck, C. (2009). A double-hexameric MCM2–7complex is loaded onto origin DNA during licensing of eukaryotic DNA replication. Proc. Natl. Acad. Sci. USA *106*, 20240–20245.
Ferreira, M.G., Cooper, J.P. (2004). Two modes of DNA double-strand break repair are reciprocally regulated through the fission yeast cell cycle. Genes Dev. *18*, 2249–2254.
Filion, G.J., Bemmel, J.G.van, Braunschweig, U., Talhout, W., Kind, J., Ward, L.D., Brugman, W., Castro, I.J. de, Kerkhoven, R.M., Bussemaker, H.J., van Steensel, B. (2010). Systematic Protein Location Mapping Reveals Five Principal Chromatin Types in *Drosophila* Cells. Cell *143*, 212-224.
Finn, K., Li, J.J. (2013). Single-stranded annealing induced by re-initiation of replication origins provides a novel and efficient mechanism for generating copy number expansion via non-allelic homologous recombination. PLoS Genet. *9*, e1003192.
Follonier, C., Oehler, J., Herrador, R., Lopes, M. (2013). Friedreich's ataxia-associated GAA repeats induce replication-fork reversal and unusual molecular junctions. Nat. Struct. Mol. Biol. *20*, 486-94.
Fu, Y.V., Yardimci, H., Long, D.T., Guainazzi, A., Bermudez, V.P., Hurwitz, J., van Oijen, A., Schärer, O.D., Walter, J.C. (2011). Selective Bypass of a Lagging Strand Roadblock by the Eukaryotic Replicative DNA Helicase. Cell *146*, 931-941.
Gambus, A., Jones, R.C., Sanchez-Diaz, A., Kanemaki, M., van Deursen, F., Edmondson, R.D., Labib, K. (2006). GINS maintains association of Cdc45 with MCM in replisome progression complexes at eukaryotic DNA replication forks. Nat. Cell Biol. *8*, 358–366.
Gambus, A., Khoudoli, G.A., Jones, R.C., Blow, J.J. (2011). MCM2–7 form double hexamers at licensed origins in Xenopus egg extract. J. Biol. Chem. *286*, 11855–11864.
Ge, X.Q. and Blow, J.J. (2010). Chk1 inhibits replication factory activation but allows dormant origin firing in existing factories. J. Cell Biol. *191*, 1285-1297.
Gerhardt, J., Tomishima, M.J., Zaninovic, N., Colak, D., Yan, Z., Zhan, Q., Rosenwaks, Z., Jaffrey, S.R., Schildkraut, C.L. (2014). The DNA replication program is altered at the FMR1 locus in fragile X embryonic stem cells. Mol. Cell *53*, 19-31.
Glover, T.W., Berger C., Coyle J., Echo B. (1984). DNA polymerase alpha inhibition by aphidicolin induces gaps and breaks at common fragile sites in human chromosomes. Hum. Genet. *67*, 136–142.
Gonzalez-Prieto, R., Munoz-Cabello, A.M., Cabello-Lobato, M.J., Prado, F. (2013). Rad51 replication fork recruitment is required for DNA damage tolerance. EMBO J. *32*, 1307-1321.
Gottlieb, T.M., Jackson, S.P. (1993). The DNA-dependent protein kinase: requirement for DNA ends and association with Ku antigen. Cell *72*, 131-142.
Graham, T.G., Walter, J.C., Loparo, J.J. (2016). Two-Stage Synapsis of DNA Ends during Non-homologous End Joining. Mol. Cell. *61*, 850-858.

Grawunder, U., Wilm, M., Wu, X., Kulesza, P., Wilson, T.E., Mann, M., Lieber, M.R. (1997). Activity of DNA ligase IV stimulated by complex formation with XRCC4 protein in mammalian cells. Nature *388*, 492–495.

Green, B. M., and Li. J.J. (2005). Loss of rereplication control in *Saccharomyces cerevisiae* results in extensive DNA damage. Mol. Biol. Cell *16*, 421-432.

Green, B.M., Finn, K.J., Li, J.J. (2010). Loss of DNA replication control is a potent inducer of gene amplification. Science *329*, 943–946.

Groth, A., Corpet, A., Cook, A.J., Roche, D., Bartek, J., Lukas, J., Almouzni, G. (2007). Regulation of replication fork progression through histone supply and demand. Science *318*, 1928–1931.

Hanlon, S.L., Li, J.J. (2015). Re-replication of a centromere induces chromosomal instability and aneuploidy. PLoS Genet. *4*, e1005039.

Hashimoto, Y., Puddu, F., Costanzo, V. (2012). RAD51- and MRE11-dependent reassembly of uncoupled CMG helicase complex at collapsed replication forks. Nat. Struct. Mol. Biol. *19*, 17-24.

Hastings, P.J., Ira G., Lupski, J.R. (2009). A microhomology-mediated break-induced replication model for the origin of human copy number variation. PLoS Genet. *5*, e1000327.

Heller, R.C., Kang, S., Lam, W.M., Chen, S., Chan, C.S., Bell, S.P. (2011). Eukaryotic origin-dependent DNA replication in vitro reveals sequential action of DDK and S-CDK kinases. Cell *146*, 80–91.

Henderson, D.S., Wiegand U.K., Norman D.G., Glover D.M. (2000) Mutual correction of faulty PCNA subunits in temperature-sensitive lethal *mus209* mutants of *Drosophila melanogaster*. Genetics *154*, 1721–1733.

Hildebrand, C.E., Walters, R.A. (1976). Rapid assembly of newly synthesized DNA into chromatin subunits prior to joining to small DNA replication intermediates. Biochem. Biophys. Res. Commun. *73*, 157–163.

Hogg, M., Sauer-Eriksson, A.E., Johansson, E. (2012). Promiscuous DNA synthesis by human DNA polymerase theta. Nucleic Acids Res. *40*, 2611–2622.

Hoshina, S., Yura, K., Teranishi, H., Kiyasu, N., Tominaga, A., Kadoma, H., Nakatsuka, A., Kunichika, T., Obuse, C., Waga, S. (2013). Human origin recognition complex binds preferentially to G-quadruplex-preferable RNA and single-stranded DNA. J. Biol. Chem. 288, 30161-30171.

Huang, H., Strømme, C.B., Saredi, G., Hödl, M., Strandsby, A., González-Aguilera, C., Chen, S., Groth, A., Patel, D.J. (2015). A unique binding mode enables MCM2 to chaperone histones H3-H4 at replication forks. Nat. Struct. Mol. Biol. *22*, 618-626.

Iacovoni, J.S., Caron, P., Lassadi, I., Nicolas, E., Massip, L., Trouche, D., Legube, G. (2010). High-resolution profiling of gammaH2AX around DNA double strand breaks in the mammalian genome. EMBO J. *29*, 1446-1457.

Ira, G., Pellicioli, A., Balijja, A., Wang, X., Fiorani, S., Carotenuto, W., Liberi, G., Bressan, D., Wan, L., Hollingsworth, N.M., Haber, J.E., Foiani, M.. DNA end resection, homologous recombination and DNA damage checkpoint activation require CDK1. Nature *431*, 1011–1017.

Jeggo, P.A. (1998). Identification of genes involved in repair of DNA double-strand breaks in mammalian cells. Radiat. Res. *150*, S80–S91.

Jensen, R.B., Carreira, A., Kowalczykowski, S.C. (2010). Purified human BRCA2 stimulates RAD51-mediated recombination. Nature *467*, 678–683.

Johnson, A., O'Donnell, M. (2005). Cellular DNA Replicases: Components and Dynamics at the Replication Fork. Annu. Rev. Biochem. *74*, 283–315.

Kanke, M., Kodama, Y., Takahashi, T.S., Nakagawa, T., Masukata, H. (2012). Mcm10 plays an essential role in origin DNA unwinding after loading of the CMG components. EMBO J. *31*, 2182–2194.

Karakaidos, P., Taraviras, S., Vassiliou, L.V., Zacharatos, P., Kastrinakis, N.G., Kougiou, D., Kouloukoussa, M., Nishitani, H., Papavassiliou, A.G., Lygerou, Z., Gorgoulis, V.G. (2004). Over- expression of the replication licensing regulators hCdt1 and hCdc6 characterizes a subset of non-small-cell lung carcinomas: Synergistic effect with mutant p53 on tumor growth and chromosomal instability - Evidence of E2F-1 transcriptional control over hCdt1. Am. J. Pathol. *165*, 1351–1365.

Kent, T., Chandramouly, G., McDevitt, S.M., Ozdemir, A.Y., Pomerantz, R.T. (2015). Mechanism of microhomology-mediated end-joining promoted by human DNA polymerase θ. Nat. Struct. Mol. Biol. *22*, 230-237.

Kim, J.C., Nordman, J., Xie, F., Kashevsky, H., Eng, T., Li, S., MacAlpine, D.M., Orr-Weaver, T.L. (2011). Integrative analysis of gene amplification in *Drosophila* follicle cells: parameters of origin activation and repression. Genes Dev. *25*, 1384-1398.

Kliszczak, A.E., Rainey, M.D., Harhen, B., Boisvert, F.M., Santocanale, C. (2011). DNA mediated chromatin pull-down for the study of chromatin replication. Sci. Rep. *1*, 95.

Kumagai, A. , Lee, J., Yoo, H.Y., Dunphy, W.G. (2006). TopBP1 activates the ATR-ATRIP complex. Cell *124*, 943 – 955.

Labib, K., Diffley, J.F., Kearsey, S.E. (1999). G1-phase and B-type cyclins exclude the DNA replication factor Mcm4 from the nucleus. Nat. Cell Biol. *1*, 415–422.

Landis, G., Richard, K., Spradling, A.C., Tower, J. (1997). The *k43* gene, required for chorion gene amplification and diploid cell chromosome replication, encodes the *Drosophila* homolog of yeast origin recognition complex subunit 2. Proc. Natl. Acad. Sci. USA *94*, 3888-3892.

Landis, G., Tower, J. (1999) The *Drosophila chiffon* gene is required for chorion gene amplification, and is related to the yeast dbf4 regulator of DNA replication and cell cycle. Development *126*, 4281–4293.

Lee, S.H., Pan, Z.Q., Kwong, A.D., Burgers, P.M., Hurwitz, J. (1991). Synthesis of DNA by DNA polymerase epsilon in vitro. J. Biol. Chem. *266*, 22707-22717.

Lee, J.H., Paull, T.T. (2005). ATM activation by DNA double-strand breaks through the Mre11-Rad50-Nbs1 complex. Science *308*, 551-554.

Lee, J., Kumagai, A., Dunphy, W.G. (2007). The Rad9-Hus1-Rad1 check- point clamp regulates interaction of TopBP1 with ATR. J. Biol. Chem. *282*, 28036 – 28044.

Letessier, A. Millot, G.A., Koundrioukoff, S., Lachagès, A.M., Vogt, N., Hansen, R.S., Malfoy, B., Brison, O., Debatisse, M. (2011). Cell-type-specific replication initiation programs set fragility of the FRA3B fragile site. Nature *470*, 120–123.

Li, A., Blow, J.J. (2005). Cdt1 downregulation by proteolysis and geminin inhibition prevents DNA re-replication in *Xenopus*. EMBO J. *24*, 395–404.

Liang, L., Deng, L., Nguyen, S.C., Zhao, X., Maulion, C.D., Shao, C., Tischfield, J.A. (2008). Human DNA ligases I and III, but not ligase IV, are required for microhomology-mediated end joining of DNA double-strand breaks. Nucleic Acids Res. *36*, 3297-310.

Liku, M.E., Nguyen, V.Q., Rosales, A.W., Irie, K., Li, J.J. (2005). CDK phosphorylation of a novel NLS-NES module distributed between two subunits of the Mcm2-7 complex prevents chromosomal rereplication. Mol. Biol. Cell *16*, 5026–5039.

Liu, Q., Guntuku, S., Cui, X.S., Matsuoka, S., Cortez, D., Tamai, K., Luo, G., Carattini-Rivera, S., DeMayo, F., Bradley, A., Donehower, L.A., Elledge, S.J. (2000). Chk1 is an essential kinase that is regulated by Atr and required for the G(2)/M DNA damage checkpoint. Genes Dev. *14*, 1448-1459.

Liu, J., Doty, T., Gibson, B., Heyer, W.D. (2010). Human BRCA2 protein promotes RAD51 filament formation on RPA-covered single-stranded DNA. Nat. Struct. Mol. Biol. *17*, 1260-1262.

Liu, G., Chen, X., Leffak, M. (2013). Oligodeoxynucleotide binding to (CTG) · (CAG) microsatellite repeats inhibits replication fork stalling, hairpin formation, and genome instability. Mol. Cell. Biol. *33*, 571-581.

Lomonosov, M., Anand, S., Sangrithi, M., Davies, R., Venkitaraman, A.R. (2003). Stabilization of stalled DNA replication forks by the BRCA2 breast cancer susceptibility protein. Genes Dev. *17*, 3017-3022.

London, T.B., Barber, L.J., Mosedale, G., Kelly, G.P., Balasubramanian, S., Hickson, I.D., Boulton, S.J., Hiom, K. (2008). FANCJ is a structure-specific DNA helicase associated with the maintenance of genomic G/C tracts. J. Biol. Chem. *283*, 36132–36139.

Lopez-Contreras, A.J., Ruppen, I., Nieto-Soler, M., Murga, M., Rodriguez-Acebes, S., Remeseiro, S., Rodrigo-Perez, S., Rojas, A.M., Mendez, J., Muñoz, J., Fernandez-Capetillo, O. (2013). A Proteomic Characterization of Factors Enriched at Nascent DNA Molecules. Cell Rep. *3*, 1105-1116.

Lu, G., Duan, J., Shu, S., Wang, X., Gao, L., Guo, J., Zhang, Y. (2016). Ligase I and ligase III mediate the DNA double-strand break ligation in alternative end-joining. Proc. Natl. Acad. Sci. USA. *113*, 1256-1260.

Lydeard, J.R., Jain, S., Yamaguchi, M., Haber, J.E. (2007). Break-induced replication and telomerase-independent telomere maintenance require Pol32. Nature *448*, 820-823.

Lydeard, J.R., Lipkin-Moore, Z., Sheu, Y., Stillman, B., Burgers, P.M., Haber, J.E. (2010). Break-induced replication requires all essential DNA replication factors except those specific for pre-RC assembly. Genes Dev. *24*, 1133-1144.

Machida, Y.J., Dutta, A. (2007). The APC/C inhibitor, Emi1, is essential for prevention of rereplication. Genes Dev. *21*, 184–194.

Madigan, A.P., Chotkowski, H.L., Glaser, R.L. (2002). DNA double-strand break-induced phosphorylation of *Drosophila* histone variant H2Av helps prevent radiation-induced apoptosis. Nucleic Acids Res. *30*, 3698-3705.

Maga, G., Hübscher, U. (1995). DNA polymerase epsilon interacts with proliferating cell nuclear antigen in primer recognition and elongation. Biochemistry *34*, 891-901.

Maiorano, D., Krasinska, L., Lutzmann, M., Mechali, M. (2005). Recombinant Cdt1 induces rereplication of G2 nuclei in *Xenopus* egg extracts. Curr. Biol. *15*, 146–153.

Maizels, N., Gray, L.T. (2013). The G4 genome. PLoS Genet. *9*, e1003468.

Makunin, I.V., Volkova, E.I., Belyaeva, E.S., Nabirochkina, E.N., Pirrotta, V., Zhimulev, I.F. (2002). The *Drosophila* suppressor of underreplication protein binds to late-replicating regions of polytene chromosomes. Genetics *160*, 1023-1034.

Malkova, A., Ivanov, E.L., Haber, J.E. (1996). Double-strand break repair in the absence of RAD51 in yeast: a possible role for break-induced DNA replication. Proc. Natl. Acad. Sci. USA *93*, 7131-7136.

Malkova, A., Naylor, M.L., Yamaguchi, M., Ira, G., Haber, J.E. (2005). RAD51-Dependent Break-Induced Replication Differs in Kinetics and Checkpoint Responses from RAD51-Mediated Gene Conversion. Mol. Cell. Biol. *25*, 933-944.

Mantiero, D., Mackenzie, A., Donaldson, A., Zegerman, P. (2011). Limiting replication initiation factors execute the temporal programme of origin firing in budding yeast. EMBO J. 30, 4805-4814.

Mateos-Gomez, P.A., Gong, F., Nair, N., Miller, K.M., Lazzerini-Denchi, E., Sfeir, A. (2015). Mammalian polymerase θ promotes alternative NHEJ and suppresses recombination. Nature *518*, 254-257.

Matsuoka, S., Rotman, G., Ogawa, A., Shiloh, Y., Tamai, K., Elledge, S.J. (2000). Ataxia telangiectasia-mutated phosphorylates Chk2 in vivo and in vitro. Proc. Natl. Acad. Sci. USA. *97*, 10389-10394.

McIlwraith, M.J., Van Dyck, E., Masson, J.Y., Stasiak, A.Z., Stasiak, A., West, S.C. (2000). Reconstitution of the strand invasion step of double-strand break repair using human Rad51 Rad52 and RPA proteins. J. Mol. Biol. *304*, 151-164.

Melixetian, M., Ballabeni, A., Masiero, L., Gasparini, P., Zamponi, R., Bartek, J., Lukas, J., Helin, K., (2004). Loss of Geminin induces rereplication in the presence of functional p53. J. Cell Biol. *165*, 473-482.

Mejlvang, J., Feng, Y., Alabert, C., Neelsen, K.J., Jasencakova, Z., Zhao, X., Lees, M., Sandelin, A., Pasero, P., Lopes, M., Groth, A. (2014). New histone supply regulates replication fork speed and PCNA unloading. J. Cell. Biol. *204*, 29-43.

Mello, J.A., Silljé, H.H., Roche, D.M., Kirschner, D.B., Nigg, E.A., Almouzni, G. (2002). Human Asf1 and CAF-1 interact and synergize in a repair-coupled nucleosome assembly pathway. EMBO Rep. *3*, 329-34.

Mihaylov, I.S., Kondo, T., Jones, L., Ryzhikov, S., Tanaka, J., Zheng, J., Higa, L. A., Minamino, N., Cooley, L., Zhang, H. (2002). Control of DNA replication and chromosome ploidy by Geminin and Cyclin A. Mol. Cell. Biol. *22*, 1868-1880.

Mimura, S., Masuda, T., Matsui, T., Takisawa, H. (2000). Central role for cdc45 in establishing an initiation complex of DNA replication in Xenopus egg extracts. Genes Cells. *5*, 439-452.

Mimura, S., Seki, T., Tanaka, S., and Diffley, J.F. (2004). Phosphorylation-dependent binding of mitotic cyclins to Cdc6 contributes to DNA replication control. Nature *431*, 1118– 1123.

Mirkin, E.V., Mirkin, S.M. (2007). Replication fork stalling at natural impediments. Microbiol. Mol. Biol. Rev. *71*, 13-35.

Mitsui, J., Takahashi, Y., Goto, J., Tomiyama, H., Ishikawa, S., Yoshino, H., Minami, N., Smith, D.I., Lesage, S., Aburatani, H., Nishino, I., Brice, A., Hattori, N., Tsuji, S. (2010). Mechanisms of genomic instabilities underlying two common fragile-site-associated loci, PARK2 and DMD, in germ cell and cancer cell lines. Am. J. Hum. Genet. *87*, 75–89.

Moggs, J.G., Grandi, P., Quivy, J.P., Jónsson, Z.O., Hübscher, U., Becker, P.B., Almouzni, G. (2000). A CAF-1-PCNA-mediated chromatin assembly pathway triggered by sensing DNA damage. Mol. Cell. Biol. *20*, 1206-1218.

Moll, T., Tebb, G., Surana, U., Robitsch, H., Nasmyth, K. (1991). The role of phosphorylation and the CDC28 protein kinase in cell cycle-regulated nuclear import of the *S. cerevisiae* transcription factor SWI5. Cell *66*, 743–758.

Moynahan, M.E., Pierce, A.J., Jasin, M. (2001). BRCA2 is required for homology-directed repair of chromosomal breaks. Mol. Cell 7, 263-272.
Moyer, S.E., Lewis, P.W., Botchan, M.R. (2006). Isolation of the Cdc45/Mcm2-7/GINS (CMG) complex, a candidate for the eukaryotic DNA replication fork helicase. Proc. Natl. Acad. Sci. USA *103*, 10236-10241.
Natsume, R., Eitoku, M., Akai, Y., Sano, N., Horikoshi, M., Senda, T. (2007). Structure and function of the histone chaperone CIA/ASF1 complexed with histones H3 and H4. Nature *446*, 338–341.
Neelsen, K.J., Zanini, I.M.Y., Mijic, S., Herrador, R., Zellweger, R., Chaudhuri, A.R., Creavin, K.D., Blow, J.J., Lopes, M. (2013). Deregulated origin licensing leads to chromosomal breaks by rereplication of a gapped DNA template. Genes Dev. *27*, 2537-2542.
Nelson, D.M., Ye, X., Hall, C., Santos, H., Ma, T., Kao, G.D., Yen, T.J., Harper, J.W., Adams, P.D. (2002). Coupling of DNA synthesis and histone synthesis in S phase independent of cyclin/cdk2 activity. Mol. Cell. Biol. *22*, 7459–7472.
Nguyen, V.Q., Co, C., Li, J.J. (2001). Cyclin-dependent kinases prevent DNA re-replication through multiple mechanisms. Nature *411*, 1068-1073.
Nick McElhinny, S.A., Snowden, C.M., McCarville, J., Ramsden, D.A. (2000). Ku recruits the XRCC4-ligase IV complex to DNA ends. Mol. Cell Biol. *20*, 2996-3003.
Nick McElhinny, S.A., Gordenin, D.A., Stith, C.M., Burgers, P.M., Kunkel, T.A. (2008). Division of labor at the eukaryotic replication fork. Mol. Cell. *30*, 137-144.
Nordman, J., Li, S., Eng, T., MacAlpine, D., Orr-Weaver, T.L. (2011). Developmental control of the DNA replication and transcription programs. Genome Res. *21*, 175–181.
Nordman, J.T., Kozhevnikova, E.N., Verrijzer, C.P., Pindyurin, A.V., Andreyeva, E.N., Shloma, V.V., Zhimulev, I.F., Orr-Weaver, T.L. (2014). DNA copy-number control through inhibition of replication fork progression. Cell Rep. *9*, 841-849.
Okazaki, R., Okazaki, T., Sakabe, K., Sugimoto, K., Sugino, A. (1968). Mechanism of DNA chain growth. I. Possible discontinuity and unusual secondary structure of newly synthesized chains. Proc. Natl. Acad. Sci. USA. *59*, 598-605.
Osheim, Y.N., Miller, O.L., Beyer, A.L. (1988). Visualization of *Drosophila melanogaster* chorion genes undergoing amplification. Mol. Cell. Biol. *8*, 2811-2821.
Ozeri-Galai, E., Lebofsky, R., Rahat, A., Bester, A.C., Bensimon, A., Kerem, B. (2011). Failure of origin activation in response to fork stalling leads to chromosomal instability at fragile sites. Mol. Cell *43*, 122–131.
Ozeri-Galai, E., Bester, A.C., Kerem, B. (2012). The complex basis underlying common fragile site instability in cancer. Trends Genet. *26*, 295-302.
Pacek, M., Tutter, A.V., Kubota, Y., Takisawa, H., Walter, J.C. (2006). Localization of MCM2-7, Cdc45, and GINS to the site of DNA unwinding during eukaryotic DNA replication. Mol. Cell *21*, 581-587.
Paeschke, K., Capra, J.A., Zakian, V.A. (2011). DNA replication through G-quadruplex motifs is promoted by the *Saccharomyces cerevisiae* Pif1 DNA helicase. Cell *145*, 678-691.
Palumbo, E., Matricardi, L., Tosoni, E., Bensimon, A., Russo, A. (2010). Replication dynamics at common fragile site FRA6E. Chromosoma *119*, 575–587.
Park, E.A., MacAlpine, D. M., Orr-Weaver, T.L. (2007). *Drosophila* follicle cell amplicons as models for metazoan DNA replication: a *cyclinE* mutant exhibits increased replication fork elongation. Proc. Natl. Acad. Sci. USA *104*, 16739-16746.

Pathania, S., Nguyen, J., Hill, S.J., Scully, R., Adelmant, G.O., Marto, J.A., Feunteun, J., Livingston, D.M. (2011). BRCA1 is required for postreplication repair after UV-induced DNA damage. Mol. Cell *44*, 235-251.

Pierce, A.J., Hu, P., Han, M., Ellis, N., Jasin, M. (2001). Ku DNA end- binding protein modulates homologous repair of double-strand breaks in mammalian cells. Genes Dev. *15*, 3237–3242.

Petermann, E., Lui, M., Issaeva, N., Schultz, N., Helleday, T. (2010). Hydroxyurea-Stalled Replication Forks Become Progressively Inactivated and Require Two Different RAD51-Mediated Pathways for Restart and Repair. Mol. Cell *37*, 492-502.

Perez-Arnaiz, P., Bruck, I., Kaplan, D. L. (2016). Mcm10 coordinates the timely assembly and activation of the replication fork helicase. Nucl. Acids Res. *44*, 315-329.

Poli, J., Tsaponina, O., Crabbé, L., Keszthelyi, A., Pantesco, V., Chabes, A., Lengronne, A., Pasero, P. (2012). dNTP pools determine fork progression and origin usage under replication stress. EMBO J. 31, 883-894.

Prelich, G., Tan, C.K., Kostura, M., Mathews, M.B., So, A.G., Downey, K.M., Stillman, B. (1987). Functional identity of proliferating cell nuclear antigen and a DNA polymerase-delta auxiliary protein. Nature *326*, 517-520.

Pursell, Z.F., Isoz, I., Lundström, E.B., Johansson, E., Kunkel, T.A. (2007). Yeast DNA polymerase epsilon participates in leading-strand DNA replication. Science *317*, 127-130.

Quan, Y., Xia, Y., Liu, L., Cui, J., Li, Z., Cao, Q., Chen, X.S., Campbell, J.L., Lou, H. (2015). Cell-Cycle-Regulated Interaction between Mcm10 and Double Hexameric Mcm2-7 Is Required for Helicase Splitting and Activation during S Phase. Cell Rep. *13*, 2576-2586.

Quinn, L.M., Herr, A., McGarry, T.J., Richardson, H. (2001). The *Drosophila* Geminin homolog: roles for Geminin in limiting DNA replication, in anaphase and in neurogenesis. Genes Dev. *15*, 2741-2754.

Rogakou, E.P., Pilch, D.R., Orr, A.H., Ivanova, V.S., Bonner, W.M. (1998). DNA double-stranded breaks induce histone H2AX phosphorylation on serine 139. J. Biol. Chem. *273*, 5858-5868.

Ried, K., Finnis, M., Hobson, L., Mangelsdorf, M., Dayan, S., Nancarrow, J.K., Woollatt, E., Kremmidiotis, G., Gardner, A., Venter, D., Baker, E., Richards, R.I. (2000). Common chromosomal fragile site FRA16D sequence: identification of the FOR gene spanning FRA16D and homozygous deletions and translocation breakpoints in cancer cells. Hum. Mol. Genet. *9*, 1651–1663.

Remus, D., Beuron, F., Tolun, G., Griffith, J.D., Morris, E.P., Diffley, J.F. (2009). Concerted loading of Mcm2–7 double hexamers around DNA during DNA replication origin licensing. Cell *139*, 719–730.

Sabouri, N., Capra, J.A., Zakian, V.A. (2014). The essential *Schizosaccharomyces pombe* Pfh1 DNA helicase promotes fork movement past G-quadruplex motifs to prevent DNA damage. BMC Biol. *12*, 101.

Saini, N., Ramakrishnan, S., Elango, R., Ayyar, S., Zhang, Y., Deem, A., Ira, G., Haber, J.E., Lobachev, K.S., Malkova, A. (2013). Migrating bubble during break-induced replication drives conservative DNA synthesis. Nature *502*, 389-392.

Sakofsky, C. J., Ayyar, S., Deem, A.K., Chung, W.H., Ira, G., Malkova, A. (2015). Translesion Polymerases Drive Microhomology-Mediated Break-Induced Replication Leading to Complex Chromosomal Rearrangements. Mol. Cell *60*, 860-872.

Salic, A., Mitchison, T.J. (2008). A chemical method for fast and sensitive detection of DNA synthesis in vivo. Proc. Natl. Acad. Sci. USA *105*, 2415–2420.

Sanders, C.M. (2010). Human Pif1 helicase is a G-quadruplex DNA-binding protein with G-quadruplex DNA-unwinding activity. Biochem. J. *430*, 119–128.

Schroff, R., Arbel-Eden, A., Pilch, D., Ira, G., Bonner, W. M., Petrini, J. H., Haber, J. E., Lichten, M. (2004). Distribution and dynamics of chromatin modification induced by a defined DNA double-strand break. Curr. Biol. 14, 1703-1711.

Schwab, R.A., Nieminuszczy, J., Shin-Ya, K., Niedzwiedz, W. (2013). FANCJ couples replication past natural fork barriers with maintenance of chromatin structure. J. Cell. Biol. *201*, 33-48.

Schwed, G. May, N., Pechersky, Y., Calvi, B.R. (2002) *Drosophila* minichromosome maintenance 6 is required for chorion gene amplification and genomic replication. Mol. Biol. Cell 13, 607–620.

Seo, J., Chung, Y.S., Sharma, G.G., Moon, E., Burack, W.R., Pandita, T.K., Choi, K. (2005). Cdt1 transgenic mice develop lymphoblastic lymphoma in the absence of p53. Oncogene *24*, 8176–8186.

Shah, S.N., Opresko, P.L., Meng, X., Lee, M.Y., Eckert, K.A. (2010). DNA structure and the Werner protein modulate human DNA polymerase delta-dependent replication dynamics within the common fragile site FRA16D. Nucl. Acids Res. *38*, 1149–1162.

Sharma, S., Javadekar, S.M., Pandey, M., Srivastava, M., Kumari. R., Raghavan, S.C. (2015). Homology and enzymatic requirements of microhomology-dependent alternative end joining. Cell Death Dis. *6*, e1697.

Sher, N., Bell, G.W., Li, S., Nordman, J., Eng, T., Eaton, M.L., Macalpine, D.M., Orr-Weaver, T.L. (2012). Developmental control of gene copy number by repression of replication initiation and fork progression. Genome Res. *22*, 64-75.

Shibahara, K., Stillman, B. (1999). Replication-dependent marking of DNA by PCNA facilitates CAF-1-coupled inheritance of chromatin. Cell *96*, 575-585.

Signon, L., Malkova, A., Naylor, M.L., Klein, H., Haber, J.E. (2001). Genetic Requirements for *RAD51* - and *RAD54* -Independent Break-Induced Replication Repair of a Chromosomal Double-Strand Break. Mol. Biol. Cell *21*, 2048-2056.

Sirbu, B.M., Couch, F.B., Feigerle, J.T., Bhaskara, S., Hiebert, S.W., Cortez, D. (2011). Analysis of protein dynamics at active, stalled, and collapsed replication forks. Genes Dev. *25*, 1320-1327.

Sirbu, B.M., McDonald, W.H., Dungrawala, H., Badu-Nkansah, A., Kavanaugh, G.M., Chen, Y., Tabb, D.L., Cortez, D. (2013). Identification of Proteins at Active, Stalled, and Collapsed Replication Forks Using Isolation of Proteins on Nascent DNA (iPOND) Coupled with Mass Spectrometry. J. Biol. Chem. *288*, 31458-31467.

Smith, S., Stillman, B. (1989). Purification and characterization of CAF-I, a human cell factor required for chromatin assembly during DNA replication in vitro. Cell 58, 15-25.

Sogo, J.M., Lopes, M., Foiani, M. (2002). Fork Reversal and ssDNA Accumulation at Stalled Replication Forks Owing to Checkpoint Defects. Science *297*, 599-602.

Spradling, A.C., Mahowald, A.P. (1979). Drosophila bearing the *ocelliless* mutation underproduce two major chorion proteins both of which map near this gene. Cell *16*, 609-616.

Spradling, A.C., Mahowald, A.P. (1980). Amplification of genes for chorion proteins during oogenesis in *Drosophila melanogaster*. Proc. Natl. Acad. Sci. USA *77*, 1096-1100.

Spradling, A.C., Orr-Weaver, T.L. (1987). Regulation of DNA Replication During *Drosophila* Development. Ann. Rev. Genet. *21*, 373-403.

Tada, S., Li, A., Maiorano, D., Mechali, M., Blow, J.J. (2001). Repression of origin assembly in metaphase depends on inhibition of RLF-B/Cdt1 by geminin. Nat. Cell Biol. *3*, 107– 113.

Tan, C.K., Castillo, C., So, A.G., Downey, K.M. (1986). An auxiliary protein for DNA polymerase-delta from fetal calf thymus. J. Biol. Chem. 261, 12310-12316.

Tan, B.C., Chien, C.T., Hirose, S., Lee, S.C. (2006). Functional cooperation between FACT and MCM helicase facilitates initiation of chromatin DNA replication. EMBO J. *25*, 3975–3985.

Tanaka, T., Nasmyth, K. (1998). Association of RPA with chromosomal replication origins requires an Mcm protein, and is regulated by Rad53, and cyclin- and Dbf4-dependent kinases. EMBO J. *17*, 5182-5191.

Tanaka, S., Diffley, J.F. (2002). Interdependent nuclear accumulation of budding yeast Cdt1 and Mcm2–7 during G1 phase. Nat. Cell Biol. *4*, 198–207.

Tanaka, S., Araki, H. (2013). Helicase Activation and Establishment of Replication Forks at Chromosomal Origins of Replication. Cold Spring Harb. Perspect. Biol. *5*, a010371.

Tanny, R.E., MacAlpine, D.M., Blitzblau, H.G., Bell, S.P. (2006). Genome-wide analysis of re-replication reveals inhibitory controls that target multiple stages of replication initiation. Mol. Biol. Cell *17*, 2415-2423.

Thomer, M., May, N.R., Aggarwal, B.D., Kwok, G., Calvi, B.R. (2004). *Drosophila double-parked* is sufficient to induce re-replication during development and is regulated by cyclin E/CDK2. Development *131*, 4807-4818.

Ticau, S., Friedman, L.J., Ivica, N.A., Gelles, J., Bell, S.P. (2015). Single-Molecule Studies of Origin Licensing Reveal Mechanisms Ensuring Bidirectional Helicase Loading. Cell *16*, 513-525.

Tomimatsu, N. et al. (2014) Phosphorylation of EXO1 by CDKs 1 and 2 regulates DNA end resection and repair pathway choice. Nat. Commun. *5*, 3561.

Truong, L.N., Li, Y., Shi, L.Z., Hwang, P.Y., He, J., Wang, H., Razavian, N., Berns, M.W., Wu X. (2013). Microhomology-mediated End Joining and Homologous Recombination share the initial end resection step to repair DNA double-strand breaks in mammalian cells. Proc. Natl. Acad. Sci. USA *110*, 7720-7725.

Truong, L.N., Li, Y., Sun, E., Ang, K., Hwang, P.Y.H., Wu, X. (2014). Homologous recombination is a primary pathway to repair DNA double-strand breaks generated during DNA rereplication. J. Biol. Chem. *289*, 28910-28923.

Tsunaka, Y., Fujiwara, Y., Oyama, T., Hirose, S., Morikawa, K. (2016). Integrated molecular mechanism directing nucleosome reorganization by human FACT. Genes Dev. *30*, 673-686.

Valton, A.L., Hassan-Zadeh, V., Lema, I., Boggetto, N., Alberti, P., Saintomé, C., Riou, J.F., Prioleau, M.N. (2014). G4 motifs affect origin positioning and efficiency in two vertebrate replicators. EMBO J. *33*, 732-746.

van Deursen, F., Sengupta, S., De Piccoli, G., Sanchez-Diaz, A., Labib, K. (2012). Mcm10 associates with the loaded DNA helicase at replication origins and defines a novel step in its activation. EMBO J. *31*, 2195-206.

Vasianovich, Y., Harrington, L.A., Makovets, S. (2014). Break-Induced Replication Requires DNA Damage-Induced Phosphorylation of Pif1 and Leads to Telomere Lengthening. PLoS Genet. *10*, e1004679.

Vaziri, C., Saxena, S., Jeon, Y., Lee, C., Murata, K., Machida, Y., Wagle, N., Hwang, D.S., Dutta, A. (2003). A p53-dependent checkpoint pathway prevents rereplication. Mol. Cell *11*, 997–1008.

Walker, J.R., Corpina, R.A., Goldberg, J. (2001). Structure of the Ku heterodimer bound to DNA and its implications for double-strand break repair. Nature *412*, 607-614.

Walter, J., Newport, J. (2000). Initiation of eukaryotic DNA replication: Origin unwinding and sequential chromatin association of Cdc45, RPA, and DNA polymerase α. Mol. Cell *5*, 617–627.

Ward, M,, Minn, K., Jorda, K.G., Chen, J. (2003). Accumulation of checkpoint protein 53BP1 at DNA breaks involves its binding to phosphorylated histone H2AX. J. Biol. Chem. *278*, 19579-19582.

Waring, G.L., Mahowald, A.P. (1979). Identification and Time of Synthesis of Chorion Proteins in *Drosophila melanogaster*. Cell *16*, 599-607.

Watase, G., Takisawa, H., Kanemaki, M.T. (2012). Mcm10 plays a role in functioning of the eukaryotic replicative DNA helicase, Cdc45-Mcm-GINS. Curr. Biol. *22*, 343–349.

Whittaker, A.J. Royzman, I., Orr-Weaver, T.L. (2000) *Drosophila* double parked: a conserved, essential replication protein that colocalizes with the origin recognition complex and links DNA replication with mitosis and the downregulation of S phase transcripts. Genes Dev. *14*, 1765–1776.

Wittmeyer, J., Formosa, T. The *Saccharomyces cerevisiae* DNA polymerase α catalytic subunit interacts with Cdc68/Spt16 and with Pob3, a protein similar to an HMG1‐like protein. (1997). Mol. Cell. Biol. *17*, 4178–4190.

Wilmes, G.M., Archambault, V., Austin, R.J., Jacobson, M.D., Bell, S.P., Cross, F.R. (2004). Interaction of the S-phase cyclin Clb5 with an "RXL" docking sequence in the initiator protein Orc6 provides an origin-localized replication control switch. Genes Dev. *18*, 981–991.

Wilson, M.A., Kwon, Y., Xu, Y., Chung, W.H., Chi, P., Niu, H., Mayle, R., Chen, X., Malkova, A., Sung, P., Ira, G. (2013). Pif1 helicase and Polδ promote recombination-coupled DNA synthesis via bubble migration. Nature *502*, 393-396.

Winkler, D.D., Muthurajan, U.M., Hieb, A.R., Luger, K. (2011). Histone chaperone FACT coordinates nucleosome interaction through multiple synergistic binding events. J. Biol. Chem. 286, 41883–41892.

Winkler, D.D., Zhou, H., Dar, M.A., Zhang, Z., Luger, K. (2012). Yeast CAF-1 assembles histone (H3-H4)2 tetramers prior to DNA deposition. Nucleic Acids Res. *40*, 10139-10149.

Wohlschlegel, J.A., Dwyer, B.T., Dhar, S.K., Cvetic, C., Walter, J.C., and Dutta, A. (2000). Inhibition of eukaryotic DNA replication by Geminin binding to Cdt1. Science *290*, 2309–2312.

Wu, Y., Shin-Ya, K., Brosh, R.M. (2008). FANCJ helicase defective in Fanconi anemia and breast cancer unwinds G-quadruplex DNA to defend genomic stability. Mol. Cell. Biol. *28*, 4116–4128.

Xouri, G., Lygerou, Z., Nishitani, H., Pachnis, V., Nurse, P., Taraviras, S. (2004). Cdt1 and geminin are down-regulated upon cell cycle exit and are over-expressed in cancer-derived cell lines. Eur. J. Biochem. *271*, 3368–3378.

Yan, S. & Michael, W.M.. (2009). TopBP1 and DNA polymerase α-mediated recruitment of the 9-1-1 complex to stalled replication forks. J. Cell Biol. *184*, 793-804.

Yoo, S., Dynan, W,S. (1999). Geometry of a complex formed by double strand break repair proteins at a single DNA end: recruitment of DNA-PKcs induces inward translocation of Ku protein. Nucleic Acids Res. *27*, 4679-4686.

Yu, X., Chen, J. (2004). DNA damage-induced cell cycle checkpoint control requires CtIP, a phosphorylation-dependent binding partner of BRCA1 C-terminal domains. Mol. Cell. Biol. *24*, 9478–9486.

Yu, A.M., McVey, M. (2010). Synthesis-dependent microhomology-mediated end joining accounts for multiple types of repair junctions. Nucl. Acids Res. *38*, 5706-5717.

Yuan, S.S., Lee, S.Y., Chen, G., Song, M., Tomlinson, G.E., Lee, E.Y. (1999). RCA2 is required for ionizing radiation-induced assembly of Rad51 complex in vivo. Cancer Res. *59*, 3547-3551.

Yun, M.H., Hiom, K. (2009) CtIP-BRCA1 modulates the choice of DNA double-strand-break repair pathway throughout the cell cycle. Nature *459*, 460–463.

Zellweger, R., Dalcher, D., Mutreja, K., Berti, M., Schmid, J.A., Herrador, R., Vindigni, A., Lopes, M. (2015). Rad51-mediated replication fork reversal is a global response to genotoxic treatments in human cells. J. Cell Biol. *208*, 563-579.

Zhang, H., Freudenreich, C.H. (2007). An AT-rich sequence in human common fragile site FRA16D causes fork stalling and chromosome breakage in *S. cerevisiae*. Mol. Cell *27*, 367–379.

Zhang, J., Dewar, J.M., Budzowska, M., Motnenko, A., Cohn, M.A., Walter, J.C. (2015). DNA interstrand cross-link repair requires replication-fork convergence. Nat. Struct. Mol. Biol. *22*, 242-247.

Zhu, W., Chen, Y., Dutta, A. (2004). Rereplication by depletion of Geminin is seen regardless of p53 status and activates a G2/M checkpoint. Mol. Cell. Biol. *16*, 7140-7150.

Zhu, W., Dutta, A. (2006). An ATR- and BRCA1-mediated Fanconi anemia pathway is required for activating the G2/M checkpoint and DNA damage repair upon rereplication. Mol. Cell. Biol. *26*, 4601-4611.

Zlotorynski, E., Rahat, A., Skaug, J., Ben-Porat, N., Ozeri, E., Hershberg, R., Levi, A., Scherer, S.W., Margalit, H., Kerem, B. (2003). Molecular basis for expression of common and rare fragile sites. Mol. Cell. Biol. *23*, 7143-51.

Zou, L., Cortez, D., Elledge, S.J. (2002). Regulation of ATR substrate selection by Rad17-dependent loading of Rad9 complexes onto chromatin. Genes Dev. *16*, 198-208.

Zou, L. & Ellege, S. (2003). Sensing DNA damage through ATRIP recognition of RPA-ssDNA complexes. Science *300*, 1542-1548.

Chapter Two:
Methods for Discovering Positions of Differential Fork Progression

Jessica L. Alexander[1,2], George Bell[1], Terry L. Orr-Weaver[1,2]

[1]Whitehead Institute for Biomedical Research, 9 Cambridge Center, Cambridge, MA 02142, USA
[2]Department of Biology, Massachusetts Institute of Technology, 77 Massachusetts Ave., 68-132, Cambridge, MA 02139, USA

George Bell developed the slope analysis and provided bioinformatics support for CGH
Jessica L. Alexander did all other experiments and analysis

Abstract

Replication fork progression must be tightly monitored to ensure complete duplication of the genome. However, certain sequence and chromatin features are problematic to fork elongation, creating regions that are prone to fork pausing and collapse. Here we utilize the *Drosophila Amplicon in Follicle Cells (DAFCs)* to track fork progression and identify genomic regions that impede fork progression. Using Comparative Genome Hybridization (CGH) analysis, we surveyed fork progression across diverse genomic positions from *P*-element-derived ectopic *DAFCs*. This analysis revealed that the size and shape of the amplification gradients are influenced by the position of insertion, suggesting some sites harbor sequence and/or chromatin motifs that promote fork instability. An inversion within *DAFC-7F*, known as the *ocelliless* mutation, moves the replication origin to an adjacent cytological position and generates an ectopic amplicon. CGH reveals fork progression is altered on either side of the inversion breakpoint, demonstrating both repressed and enhanced fork progression from the origin. Repressed fork movement across the inverted *DAFC-7F* region indicates inhibition is not at the sequence level. To systematically define changes in fork progression, we have developed an analysis to discover and calculate distinct slopes along the amplification gradients generated from CGH analysis. Pairing this slope analysis with our collection of CGH data will create a platform to investigate aspects of the sequence, chromatin and chromosome structure that promote fork instability.

Introduction

Replication fork stability is essential to ensure complete genome duplication at each S-phase. Incomplete replication causes DNA damage resulting in either cell death or chromosomal aberrations (Ozeri-Galai *et al.* 2012, Abbass & Dutta 2013, Nordman & Orr-Weaver 2015). However, specific regions are highly susceptible to fork stalling and DNA breaks, especially in the presence of replication stress, revealing fork progression is not equal throughout the genome. These difficult-to-replicate regions are observed as positions of constriction or breakage on metaphase chromosomes after exposure to replication stress, and are referred to as fragile sites (Glover *et al.* 1984). Common fragile sites (CFSs) are positions that exhibit fragility across the population and the frequency of fragility is termed CFS expression (Debatisse *et al.* 2012). There are a variety of features associated with CFS expression including slow fork progression and/or frequent fork stalling, active transcription during S-phase, late replication timing and lack of 'back-up' or dormant replication origins (Debatisse *et al.* 2012, Ozeri-Galai *et al.* 2012). Although not all CFSs exhibit fork pausing rates above the rest of the genome (Palumbo *et al.* 2010, Letessier *et al.* 2011), others undergo extensive fork stalling even in the absence of replication stress and are reliant on the ATR checkpoint to prevent CFS expression (Casper *et al.* 2002, Zhang & Freudenreich 2007, Shah *et al.* 2010, Ozeri-Galai *et al.* 2011).

Fragility is also a feature of repetitive DNA, which can form secondary structures that block the replication fork (Mirkin & Mirkin 2007). Frequent fork stalling is observed at both di- and trinucleotide repeats, which leads to breaks when aggravated by exogenous fork stress (Zhang & Freudenreich 2007, Shah *et al.* 2010, Ozeri-Galai *et al.* 2011, Follonier *et al.* 2013, Liu *et al.* 2013, Gerhardt *et al.* 2014). Repetitive stretches of G-rich DNA can form highly stable G-quadruplexes (G4's). Although G4's appear to play important roles in gene expression and

metazoan origin selection (Besnard *et al.* 2012, Hoshina *et al.* 2013, Maizels and Gray 2013, Valton *et al.* 2014), these structures block replication forks and require specialized helicases including FANCJ and Pif1 to maintain fork stability (London *et al.* 2008, Wu *et al.* 2008, Sanders 2010, Paeschke *et al.* 2011, Schwab *et al.* 2013, Sabouri *et al.* 2014).

Fragile sites are generated in Drosophila endocycling cells by a phenomenon termed under-replication. During the endocycle, replication is repressed across heterochromatic sequences and tissue-specific euchromatic positions, resulting in reduced copy number at these sites compared to total cell ploidy (Spradling & Orr-Weaver 1987, Nordman *et al.* 2011, Sher *et al.* 2012). The DNA damage marker γH2Av is present throughout under-replicated sites of salivary gland chromosomes, highlighting the fragility and wide-spread fork instability throughout these regions (Andreyeva *et al.* 2008, Nordman *et al.* 2014).

Under-replication is dependent on Suppressor of Under-Replication (SuUR). *SuUR* mutants both restore copy number and alleviate DNA damage uniformly across all positions of under-replication in all tissues analyzed (Belyaeva *et al.* 1998, Andreyeva *et al.* 2008, Nordman *et al.* 2011, Sher *et al.* 2012, Nordman *et al.* 2014). Additionally, SuUR is recruited to active forks and regulates their progression during follicle cell amplification (Sher *et al.* 2012, Nordman *et al.* 2014). Forks advance about 30% further in *SuUR* mutants, whereas *SuUR* overexpression cuts fork progression nearly by nearly 50% (Nordman *et al.* 2014). The SuUR N-terminus exhibits homology to the SWI/SNF family ATPase/helicase domain, but residues essential for ATP binding and hydrolysis are not conserved (Makunin *et al.* 2002). This leaves the question of whether catalytically-dead SWI/SNF homologs have evolved across the animal kingdom to developmentally regulate fork stability.

The follicle cells of *Drosophila melanogaster* are an ideal system to study metazoan DNA

replication that is under tight developmental control. These are somatic cells of the ovary that secrete large quantities of eggshell proteins in just a few hours. To meet protein production demands the follicle cells increase the copy number of eggshell protein genes by repeated activation of adjacent replication origins (Spradling & Mahowald 1980). Gene amplification occurs at six loci in the follicle cells, termed *Drosophila Amplicons in Follicle Cells* (*DAFCs*). The *DAFCs* have specific replication origins that utilize the same machinery as in canonical S-phase (Claycomb & Orr-Weaver 2005). Bidirectional fork movement away from the origin produces a gradient of amplified DNA spanning approximately 100kb at each *DAFC* (Claycomb & Orr-Weaver 2005).

Drosophila egg chambers are divided into developmental stages based on their distinct morphologies, each of which lasts for a defined period of time. This enables isolation of the follicle cells at specific times in development by ovary dissection. Origin firing at the *DAFCs* begins at a specific stage in development, stage 10B, across all follicle cells of a given egg chamber in the absence of genome-wide replication (Calvi *et al.* 1998). The precise timing and location of origin firing enables us to isolate replication forks at specific points after origin initiation and track their progression in real-time (Claycomb *et al.* 2002, Park *et al.* 2007).

Here we utilize ectopic amplicons derived from *P*-element insertion and inversion of *DAFCs* sequences to model fork progression at various chromosome positions. We find that fork progression does vary with genomic position, and even identical sequences exhibit altered fork movement when placed at ectopic sites. Additionally, we developed a slope analysis tool that discovers breakpoints along the CGH gradients in order to systematically define positions of altered fork progression.

Results

A Survey of Replication Fork Progression at Diverse Genomic Positions

Follicle cell amplicons were previously generated at ectopic sites by *P*-element insertion of the *DAFC-66D* region encompassing the amplification control element (*ACE3*) and the origin of replication (*oriβ*) (deCicco & Spradling 1984, Orr-Weaver & Spradling 1986, Orr-Weaver *et al.* 1989, Carminati *et al.* 1992). The *ACE3* sequence element is sufficient to induce amplification with the same tissue and developmental specificity as the endogenous locus (Carminati *et al.* 1992). Each ectopic amplicon line was named for the transgene construct used for *P*-element transformation, and multiple insertions of the same transgene were sequentially numbered. For example, lines $A_{48}O_{28}$-8 and $A_{10}O_{31}$-1 were generated from different transgenes, while lines $A_{10}O_{31}$-1 and $A_{10}O_{31}$-13 were generated from the same transgene inserted at different ectopic sites. All transgenes contain the *rosy* gene for a selectable marker. The R7.7 and $A_{48}O_{28}$ transgenes were generated from a 7.7kb fragment of *DAFC-66D* that includes *ACE3*, *oriβ*, and the chorion genes *s18*, *s15* and *s19* (Orr-Weaver & Spradling 1986, Orr-Weaver *et al.* 1989). S6.9 has a 3.8kb fragment of *DAFC-66D* containing *ACE3*, *oriβ*, *s18* and *s15* with the *E. coli lacZ* gene fused to the 3' untranslated region of *s15* (deCicco & Spradling 1984). The $A_{48}O_{28}$ transgene is a derivative of R7.7 with the *E. coli lacZ* gene fused to the 3' untranslated region of *s18* (Orr-Weaver & Spradling 1986). The M9 construct contains a tandem array of nine 440bp fragments of ACE3 (Carminati *et al.* 1992).

Previous studies found that the number of origin firings is heavily influenced by the position of insertion (Orr-Weaver & Spradling 1986, Orr-Weaver *et al.* 1989, Carminati *et al.* 1992); however the extent of replication fork movement was not assessed at different insertion sites. To investigate how these replication forks progress through ectopic chromatin, we analyzed the

amplification gradients of several *DAFC-66D* transgenes inserted at various positions by Comparative genome hybridization (CGH). CGH allows us to visualize global replication fork progression across each of the *DAFCs*. Follicle cell DNA is labeled and competitively hybridized to an array containing probes covering the Drosophila genome or specific positions of interest. The DNA copy number is measured over chromosomal position, providing a detailed view of the gradient of amplification at each *DAFC* (Claycomb *et al.* 2004, Kim *et al.* 2011). The shape of this gradient is reflective of replication fork progression. Uninhibited forks can traverse longer distances before the next origin firing and allows forks to spread out from one another; this results in a gradual decrease in copy number on the CGH gradient. Conversely, if progression is impeded then adjacent forks pile up as origin firing continues. This generates back-to-back forks in close proximity, resulting in a rapid decrease in copy number over short distances. CGH analysis is therefore a powerful tool to find sites of altered replication fork progression.

CGH analysis revealed that fork progression, like origin firing, varies with the position of insertion (Fig. 1). However, it is important to note that the size of the gradients is not correlated with copy number at the origin. We compared the gradients to endogenous *DAFC-66D*; this amplicon covers an approximately 150kb region, and copy number decreases symmetrically within the first 30kb on either side of the origin (Fig. 1, top). There are three major variations in fork progression: 1) Symmetric fork progression to approximately 50kb from either side of the center, as seen for M9, $A_{48}O_{28}$-2 and $A_{48}O_{28}$-8. Although these gradients are smaller than *DAFC-66D*, they are comparable to the other endogenous *DAFCs* (Kim *et al.* 2011); 2) Reduced total fork progression, in which the gradient only spans 50-70kb, in lines $A_{10}O_{31}$-1 and -13. This is smaller than any of the endogenous sites, revealing these insertion positions are restrictive to fork progression; 3) Asymmetric fork progression, where copy number decreases more rapidly

Figure 1. Amplification profiles of ectopic *DAFC-66D* transgenes

CGH of endogenous *DAFC-66D* in *OrR*. DNA from stage 13 egg chambers was competitively hybridized with diploid embryonic DNA to microarrays containing probes for select genome regions spaced approximately every 125bp (top). CGH of *DAFC-66D* transgenes inserted at various ectopic locations. DNA from stage 16C follicle cells or stage 13 egg chambers was competitively hybridized to microarrays containing probes for most of the genome spaced approximately every 250bp. DNA from two different transgene lines were competitively hybridized to a single array. Gradients in gray were used as the control DNA in the CGH analysis making the actual CGH values negative. All gradients are displayed as positive to allow for direct comparison between transgenes. Chromosomal position is plotted on the x-axis, the log2 ratio of DNA copy number is plotted on the y-axis. Blank spaces in the gradients are genomic regions for which there are no probes on the CGH array.

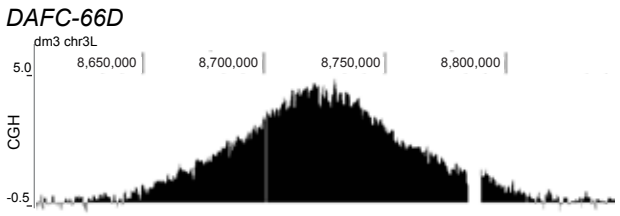
DAFC-66D
dm3 chr3L
5.0
8,650,000
8,700,000
8,750,000
8,800,000
CGH
-0.5

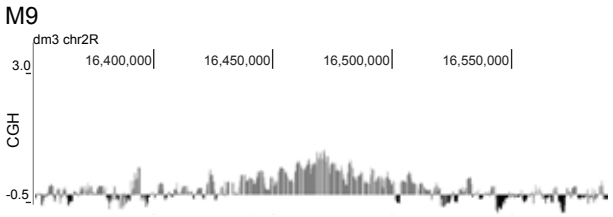
M9
dm3 chr2R
3.0
16,400,000
16,450,000
16,500,000
16,550,000
CGH
-0.5

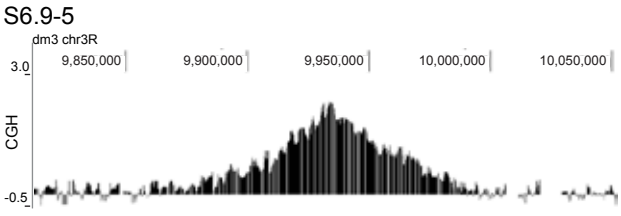
S6.9-5
dm3 chr3R
3.0
9,850,000
9,900,000
9,950,000
10,000,000
10,050,000
CGH
-0.5

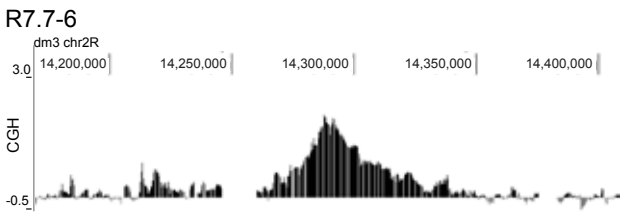
R7.7-6
dm3 chr2R
3.0
14,200,000
14,250,000
14,300,000
14,350,000
14,400,000
CGH
-0.5

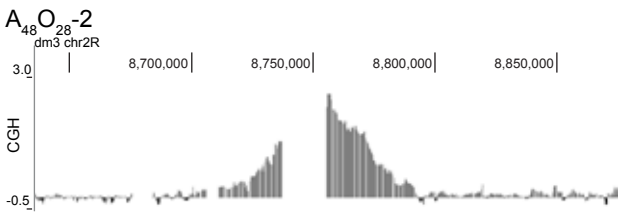
A48O28-2
dm3 chr2R
3.0
8,700,000
8,750,000
8,800,000
8,850,000
CGH
-0.5

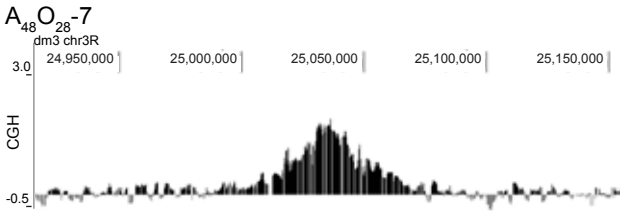
A48O28-7
dm3 chr3R
3.0
24,950,000
25,000,000
25,050,000
25,100,000
25,150,000
CGH
-0.5

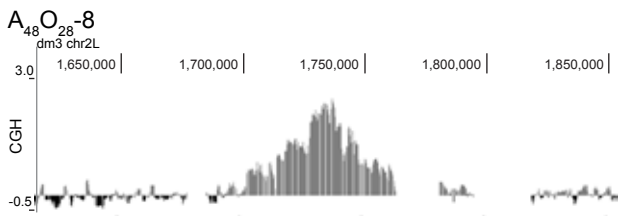
A48O28-8
dm3 chr2L
3.0
1,650,000
1,700,000
1,750,000
1,800,000
1,850,000
CGH
-0.5

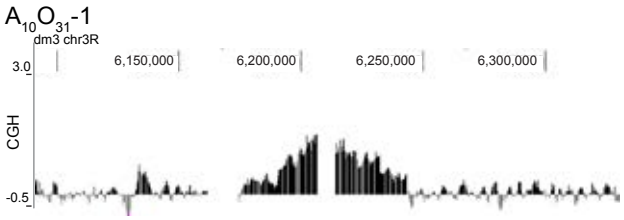
A10O31-1
dm3 chr3R
3.0
6,150,000
6,200,000
6,250,000
6,300,000
CGH
-0.5

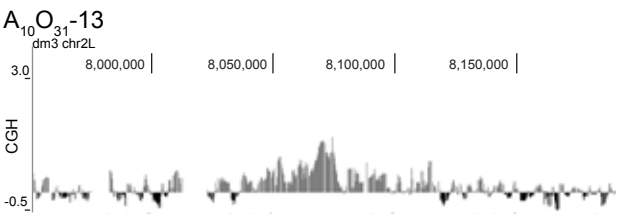
A10O31-13
dm3 chr2L
3.0
8,000,000
8,050,000
8,100,000
8,150,000
CGH
-0.5

on one side of the gradient than the other. The most striking asymmetry is observed in R7.7-6, in which copy number drops off sharply to the left while steadily decreasing to the right. Some asymmetry is also visible in S6.9-5, $A_{48}O_{28}$-7 and $A_{10}O_{31}$-1.

Collectively, our survey of ectopic amplification gradients has discovered regions that are restrictive to fork progression. These results suggest that there are sequence, structural and/or chromatin features inhibit fork movement. Additionally, ectopic amplicons that exhibit asymmetrical fork progression reveal that localized sequence or chromatin motifs can slow fork progression directly adjacent to a site that is permissible to fork elongation.

Characterization of the Amplicon Inversion *ocelliless*

A unique ectopic amplicon was generated by an inversion in *DAFC-7F*, known as *ocelliless*. This inversion was first characterized as female-sterile due to impaired amplification at *DAFC-7F* (Spradling & Mahowald 1981). The approximate breakpoints of the inversion were mapped to *DAFC-7F* and the adjacent cytological position *8A* (Spradling & Mahowald 1979, 1981). Southern blotting indicated amplification was abolished at endogenous *DAFC-7F* sequences that were not disrupted by the inversion, but strikingly the endogenous *8A* region adjacent to the breakpoint now underwent amplification (Spradling & Mahowald 1981). This inversion thus generates an ectopic amplicon independently of *P*-element insertion. Amplification levels were measured across a portion of the *ocelliless* amplicon (Spradling & Mahowald 1981) revealing copy number gradually decreases on either side of the origin, as is observed at the endogenous *DAFCs*. However, copy number was not measured to the end of the amplification gradient and thus the extent of fork progression into the *8A* region is unknown.

We first mapped the exact inversion coordinates by sequencing across the approximate

breakpoints and found the inverted sequence spans just over 152kb from chrX: 8,370,443 within *DAFC-7F* to chrX: 8,522,653 from region *8A*. No sequence was recovered from the approximately 1kb regions chrX: 8,369,604 - 8,370,442 or chrX: 8,522,654 - 8,524,024, indicating these regions were deleted during repair of the inverted DNA fragment. (All coordinates are from the dm3 Drosophila genome annotation).

To measure fork progression across the *ocelliless* amplicon, CGH was done with the above inversion coordinates included in the analysis. We found that fork movement is altered on both sides of the gradient. Forks moving into the *8A* region reach nearly 100kb distance from the origin, revealing the first example of enhanced fork progression at an ectopic site (Fig. 2A). Conversely, the left side of the *ocelliless* amplification gradient, which contains sequences that undergo amplification up to 50kb from the origin at the endogenous *DAFC-7F*, exhibits reduced fork progression to approximately 25kb in the context of the inversion (Fig. 2A). qPCR revealed that although the level of amplification is reduced in the inversion, the developmental timing of origin firing is maintained (Fig. 2B). These results are consistent with previous Southern blot analysis (Spradling & Mahowald 1980) and confirm that the gradient size is not the result of delayed origin initiation. Therefore fork movement into the *DAFC-7F* side of the inversion is decreased independently of the primary sequence.

Previous genome-wide mapping of the Origin Recognition Complex (ORC) in 16C follicle cells showed that ORC binds the *DAFCs* in 10-30kb domains around the amplification peaks (Kim *et al.* 2011). We mapped the ORC binding sites in *ocelliless* follicle cells by ChIP-seq to test if ORC is also recruited to the inversion over a large binding domain. The inversion coordinates revealed that the ORC binding domain at *DAFC-7F* mapped in wild-type *OrR* (Kim *et al.* 2011) is moved to the *8A* region in *ocelliless*; this is consistent with our CGH results and

Figure 2. Characterization of amplification and fork progression at the *DAFC-7F* inversion *ocelliless*

(A) Amplification gradient and ORC2 binding profile of *ocelliless*. (top) CGH of *OrR* at *DAFC-7F* is shown with ORC2 ChIP-chip peaks below (Kim *et al.* 2011). (bottom) CGH of *ocelliless* inversion with ORC2 ChIP-seq peaks below. Inversion breakpoints are shown as red lines with the exact coordinates written above. DNA from stage 13 egg chambers was competitively hybridized with diploid embryonic DNA to microarrays with approximately one probe every 250bp. Chromosomal position is plotted on the x-axis, the log2 ratio of DNA copy number is plotted on the y-axis. MACS was used for ChIP peak-calling with $p \leq$ 1E-5.

(B) Amplification timing at was measured at the peak of amplification in *ocelliless* and *OrR*. Both profiles correspond to the same origin sequence, which is moved to *8A* in *ocelliless*. Copy number is relative to the nonamplified *polalpha* locus in stage 1-8 egg chambers. Error bars are standard error of three technical replicates.

(C) Amplification gradient of *ocelliless* (top) and *ocelliless; SuUR* (bottom). CGH scale is shown on the left. DNA from stage 13 egg chambers was competitively hybridized with diploid embryonic DNA to microarrays with approximately one probe every 250bp. Chromosomal position is plotted on the x-axis, the log2 ratio of DNA copy number is plotted on the y-axis.

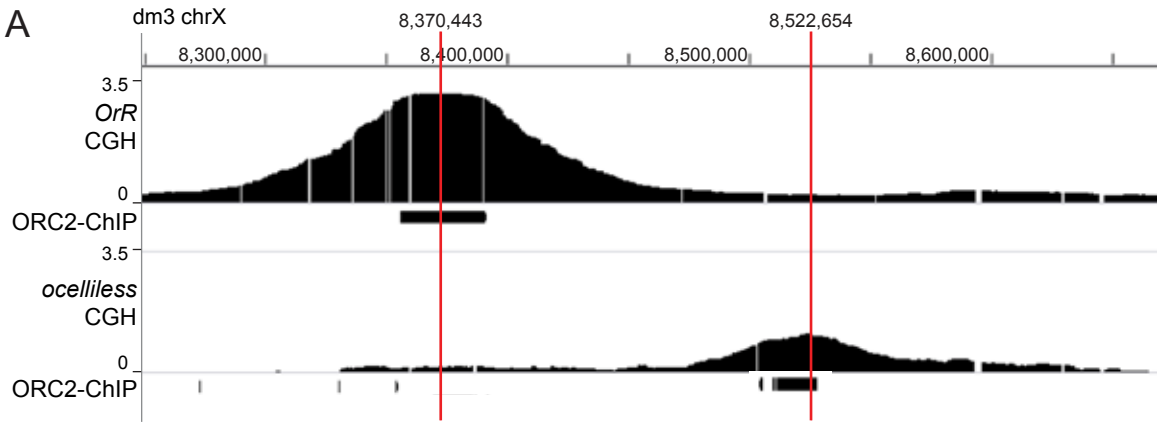
A
dm3 chrX
8,370,443
8,522,654
8,300,000
8,400,000
8,500,000
8,600,000
3.5
OrR
CGH
0
ORC2-ChIP
3.5
ocelliless
CGH
0
ORC2-ChIP

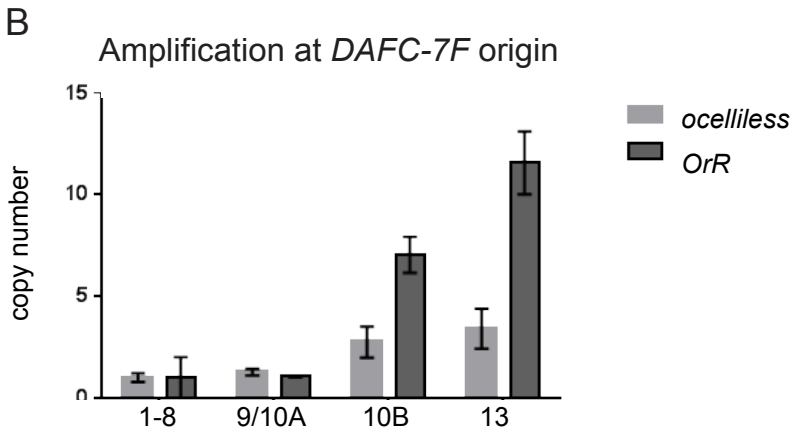
B
Amplification at DAFC-7F origin
copy number
15
10
5
0
1-8
9/10A
10B
13
ocelliless
OrR

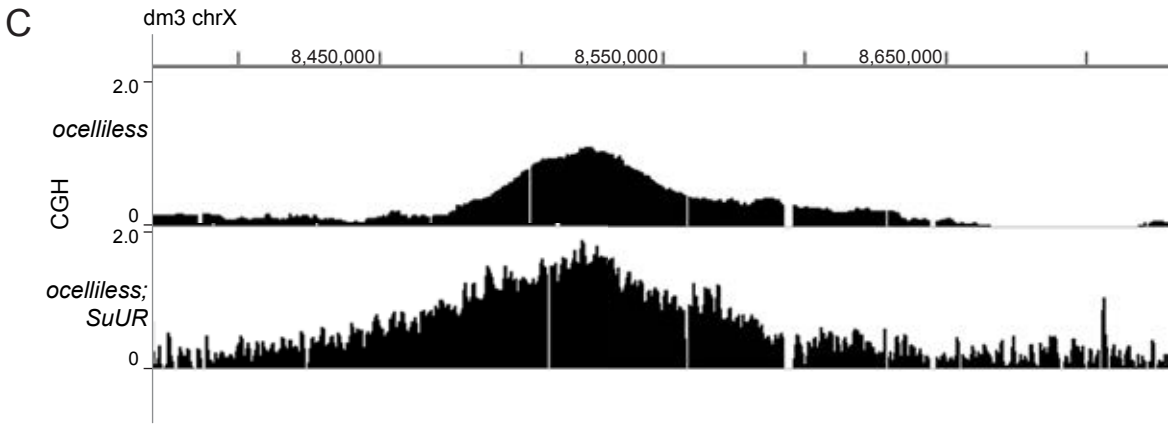
C
dm3 chrX
8,450,000
8,550,000
8,650,000
2.0
ocelliless
CGH
0
2.0
ocelliless;
SuUR
0

previous findings that amplification is abolished at the endogenous *7F* position (Spradling & Mahowald 1981). The ChIP-seq results reveal that the ORC binding domain is maintained over endogenous *DAFC-7F* sequences that are moved in the inversion. Consistent with previous observations, our results show that both ORC binding (Austin 1999) and developmental timing of origin firing (Spradling 1981, Kalfayan 1985, Orr-Weaver 1989, Carminati 1992) are regulated by cis-regulatory elements within the *ocelliless* inversion.

The *ocelliless* CGH data show that replication forks move further in the ectopic *8A* region than at the endogenous *DAFCs*. One possibility is that these forks escape negative regulation by the fork inhibitor Suppressor of Under-Replication (SuUR). It is interesting that fork progression is enhanced at *8A* in *ocelliless* to a similar extent as that observed the endogenous *DAFCs* in a *SuUR* null mutant (Sher *et al.* 2012, Nordman *et al.* 2014). To test the *8A* region escapes SuUR-mediated repression, we measured fork progression in an *oc; SuUR* double mutant by CGH analysis. Consistent with previous observations, fork progression is enhanced equally across the *ocelliless* ectopic amplicon (Fig. 2C). This result shows that the enhanced fork movement at *8A* is not caused by absence of SuUR, but rather the result of chromatin structure and/or sequence motifs that permit greater fork progression from the origin.

Slope of the Amplification Gradient Identifies Positions of Altered Fork Progression

Our CGH data from ectopic amplicons across the genome revealed variations in fork progression at ectopic sites. Additionally, inspection of CGH profiles from the endogenous *DAFCs* indicates there are differences in fork progression between these positions. To quantify fork progression along the amplification gradient, we developed an analysis to measure the rate of copy number decrease, or slope, along both sides of each amplification gradient. This analysis

utilizes a regression model with segmented relationships to divide each amplification gradient into the left and right sides and calculate their individual slopes. We find the slope is not uniform across all six *DAFCs*, nor is it equal on either side of the gradient within a single *DAFC* (Table 1). Moreover, the segmented model can find positions where the slope changes within one side of the gradient, called breakpoints, and tests the breakpoint significance using the Davies' test (Muggeo 2003). This analysis shows that five of the six *DAFCs* contain breakpoints along one side of the gradient (Fig. 3, Table 1). A notable example is *DAFC-66D*, in which the right side of the gradient can be divided into three distinct slopes (Fig. 3, bottom left). It is striking that a roughly 5kb region is particularly inhibitory to fork progression, as highlighted by the steep slope, between two regions of similar fork progression. Together, these results indicate not only that fork progression varies between the six endogenous *DAFCs*, but also the forks do not always move uniformly throughout a single amplified region.

Discussion

The collection of CGH profiles from ectopic amplicons presented here illustrates how chromosome position influences fork progression. Analysis of both sequence and chromatin elements at these ectopic sites will shed light on characteristics of hard-to-replicate regions and potential replication barriers. The *ocelliless* CGH profile reveals a striking asymmetry in fork progression on either side of the origin not seen for any of the ectopic amplicons generated by *P*-element insertion. The observation that the endogenous *DAFC-7F* sequences exhibit reduced fork progression in the context of the inversion suggests slow fork movement in this region is caused by some aspect of the chromatin or the chromosome architecture. Additionally, forks moving into the ectopic *8A* region do not appear to experience the same restrictions as those on

Table 1. Slopes and breakpoints along the six *DAFCs* from *OrR* 16C follicle cell CGH data

DAFC	**Left slope (copy number/position)**	**Right slope (copy number/position)**	**Location of breakpoints with $p<0.05$ (bp)**	**Slopes between breakpoints, left to right**
22B	4.396E-05	-3.258E-05	1881239	1.155E-05 5.488E-05
30B	1.848E-05	-3.741E-05	9574472	-2.153E-05 -7.350E-05
34B	4.845E-05	-4.580E-05	(none)	
62D	2.577E-05	-2.850E-05	2243222	5.030E-05 1.531E-05
66D	6.751E-05	-7.892E-05	8745842 8752932	-4.713E-05 -11.86E-05 -5.978E-05
7F	4.872E-05	-5.613E-05	8355576	6.581E-05 -0.1911E-05

Figure 3. Slope analysis at the six *DAFCs* from *OrR* 16C follicle cell CGH data

Each array probe is represented by the center coordinate and plotted against the normalized copy number, shown by black dots. Red lines show the average regression line for the left and right sides of the amplification gradient. The segmented regression lines are displayed in blue or green over the regions of altered slope. Chromosomal position is plotted on the x-axis, the log2 ratio of DNA copy number (as measured by CGH) is plotted on the y-axis.

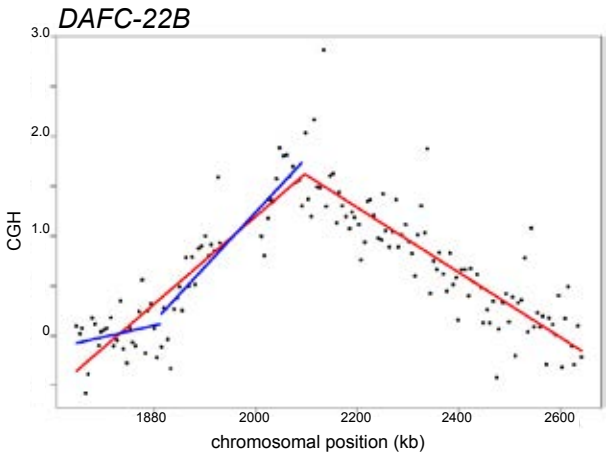
DAFC-22B
CGH
3.0
2.0
1.0
0
1880
2000
2200
2400
2600
chromosomal position (kb)

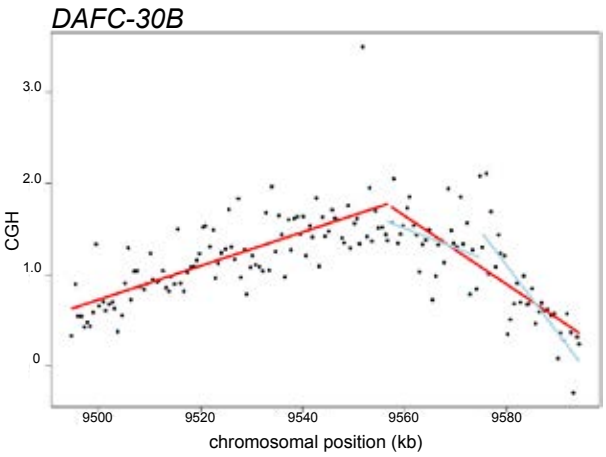
DAFC-30B
CGH
3.0
2.0
1.0
0
9500
9520
9540
9560
9580
chromosomal position (kb)

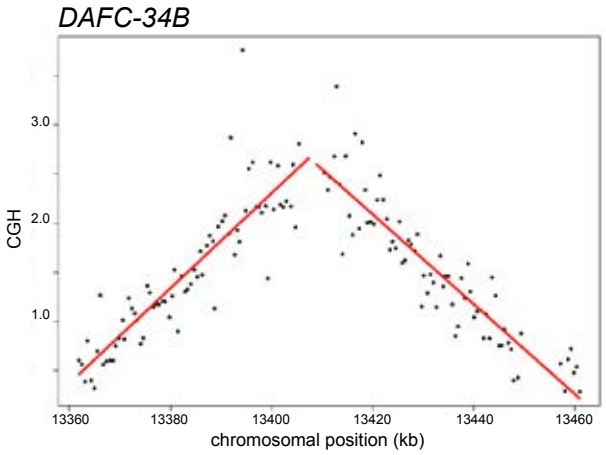
DAFC-34B
CGH
3.0
2.0
1.0
13360
13380
13400
13420
13440
13460
chromosomal position (kb)

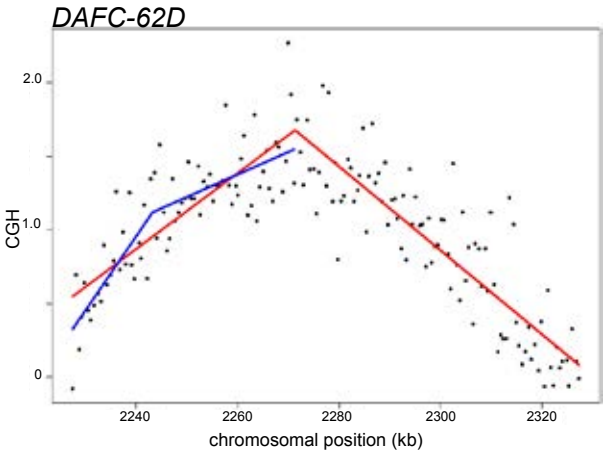
DAFC-62D
CGH
2.0
1.0
0
2240
2260
2280
2300
2320
chromosomal position (kb)

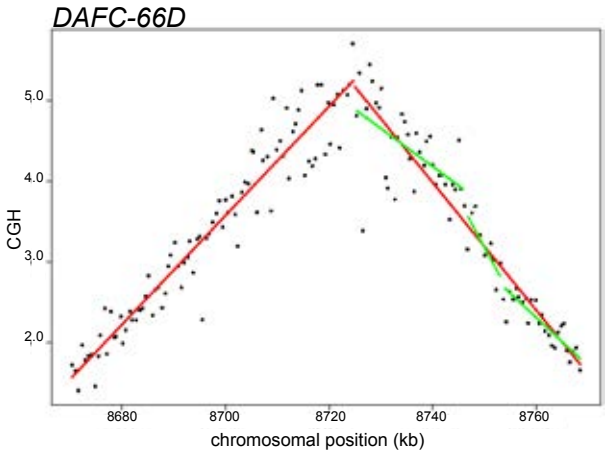
DAFC-66D
CGH
5.0
4.0
3.0
2.0
8680
8700
8720
8740
8760
chromosomal position (kb)

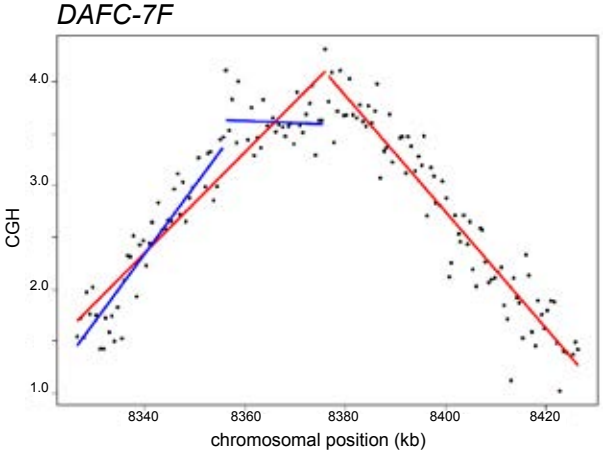
DAFC-7F
CGH
4.0
3.0
2.0
1.0
8340
8360
8380
8400
8420
chromosomal position (kb)

the other side of the gradient. This reveals that fork inhibition is restricted to the region between the inversion breakpoints. Furthermore, fork movement is enhanced in the *8A* region of *ocelliless* relative to endogenous *DAFCs*. Fork progression is increased even more in the absence of the fork destabilizer SuUR. Therefore increased fork progression in *8A* is not due to absence of SuUR activity, but may be the result of a chromatin and/or sequence landscape that is easier to replicate through.

CGH profiles of *P*-element derived ectopic amplicons indicate the position of insertion influences fork progression. It is possible that some of the observed changes in the CGH gradients are caused by differences in the transposon constructs. It is important to note that amplification of the transposons themselves is not included on the CGH gradients. Only endogenous sequences at the insertion positions contain probes that hybridize to ectopic amplicons and are visibly amplified after array normalization. Since different ectopic lines were competitively hybridized and normalized against each other, copy number of *DAFC-66D* probes is close to 1 in this array data. S6.9 and $A_{10}O_{31}$ contain the additional *E.coli lacZ* sequences, whereas both S6.9 and M9 constructs are missing large regions of *DAFC-66D*. It is possible that these extra and/or deleted sequences could affect forks even as they progress outside of the transgene sequence, either independently or via interactions with the surrounding insertion site. A more extensive survey from identical transgenes is required to determine whether fork progression is influenced solely by insertion position.

The slope analysis presents a powerful tool to quantify and compare fork progression at different genomic positions, as well as to pinpoint coordinates where fork movement changes. The breakpoints within the endogenous *DAFCs* reveal that fork progression can change over short distances. This is especially apparent for *DAFC-66D*, which exhibits three distinct slopes

along a single arm of the CGH gradient. The steepest slope between the first and second breakpoints spans only 5kb, and is sandwiched between two regions of similarly reduced slope. This indicates fork progression is strongly inhibited within the 5kb window, but forks that escape this region experience a more permissible environment. This suggests sequence motifs or sudden changes in the chromatin structure could alter fork movement here. It is possible that DNA secondary structures cause frequent fork pausing in this region of *DAFC-66D*, which would result in the observed steep slope. The six endogenous *DAFCs* sequences were searched for predicted G4 motifs (Menendez *et al.* 2012), but only a few isolated instances were discovered; no G4's were predicted in *DAFC-66D* (data not shown). However, G4's could be looked for directly using a specific antibody (Schaffitzel *et al.* 2001, Biffi *et al.* 2013) which would reveal whether these structures form during amplification.

Analysis of fork progression at positions of re-replication presents an interesting opportunity to study mechanism of chromosome fragility under condition of replication stress. Replication forks generated during re-replication move only a fraction of the distance covered by normal S-phase forks (Nguyen *et al.* 2001), and indeed previous measurements at the *DAFCs* showed these forks progress much slower than those generated during endocycles or mitotic S-phase (Claycomb *et al.* 2002). Additionally, re-replication during S-phase activates the DNA damage checkpoint and generates double-strand breaks (Mihaylov *et al.* 2002, Melixetian *et al.* 2004, Zhu *et al.* 2004, Green & Li 2005, Davidson *et al.* 2006, Finn & Li 2013, Neelsen *et al.* 2013), which were suggested to be the result of collisions between adjacent replication forks (Davidson *et al.* 2006). Therefore, genomic positions of slow fork movement are expected to increase the frequency of collisions, thus exacerbating damage and making such sites especially fragile during re-replication. The combination of our CGH survey with the slope analysis offers a

perfectly poised tool to discover sequence and chromatin features that are particularly toxic during re-replication, as well as under general conditions of replication stress.

Experimental Procedures

Fly Strains

All wild-type measurements were made with the *Oregon-R (OrR)* strain. *DAFC-66D* ectopic amplicon lines were previously described (Orr-Weaver & Spradling 1986, Orr-Weaver *et al.* 1989, Carminati *et al.* 1992). The *ocelliless* stock, $oc^{1}/FM7$, was obtained from the Bloomington Stock Center.

Isolation of 16C Follicle Cells by FACS

Follicle cells were isolated as described previously (Lilly & Spradling 1996) with the following modifications. Ovaries were dissected in Grace's media while transferring to ice. Ovaries were digested in 5mg/mL collagenase in Grace's media. The cell pellet was resuspened in 10μg/mL DAPI in PBS. 16C follicle cells were isolated by FACS using a MoFlo flow cytometer.

Comparative genome hybridization

Arrays were done from 16C follicle cells isolated by FACS from S6.9-5, R7.7-6, $A_{48}O_{28}$-8 and M9 ectopic amplicons. Stage 13 egg chambers were hand sorted for the $A_{48}O_{28}$-7, $A_{48}O_{28}$-8, $A_{10}O_{31}$-1, $A_{10}O_{31}$-13 and *ocelliless* arrays. Ovaries were dissected from fattened females in Grace's media. Approximately 100 stage 13 egg chambers were hand sorted per experiment and stored at -80°C. *OrR* embryos were collected for 2 hours and stored at -80°C. Egg chambers were

thawed in 300µL ChIP lysis buffer and embryos in 1% SDS in TE. Egg chambers and embryos were dounced for 10 strokes using a Type B pestle. DNA was fragmented from all follicle cell, egg chamber and embryo preparations by sonication in a Biorupter300 (Diagenode) at 4°C for 10 cycles of 30sec on 30sec off at maximum power. DNA was digested in *AluI* and *RsaI* and labeled using Invitrogen's BioPrime labeling kit. DNA was hybridized to custom Agilent tiling arrays with probes approximately every 250 basepairs. For *DAFC-66D* transgenes, DNA from two different transgene lines were competitively hybridized to a single array. DNA from *ocelliless* stage 13 egg chambers was competitively hybridized with *OrR* embryonic DNA. Array intensity was LOESS normalized and smoothed by genomic windows of 1 kb using the Ringo package in R (Toedling *et al.* 2007).

Sequencing *ocelliless* inversion breakpoints

DNA was isolated from whole flies homozygous for oc^{1}. Primers were designed based on approximate breakpoints determine by restriction site mapping (Spradling & Mahowald 1981). The upstream breakpoint at *7F* was amplified using the primers: 5'-GGACTACAAGTTCGTGGATGAT (forward) and 5'–CTCGACGAAGCCTCATAAATAC (reverse). The downstream breakpoint at *8A* was amplified using the primers: 5'–GAATAATGGCCTGTGTTGAGAC (forward) and 5'–AACACACACGACACAGACAGAC (reverse). PCR products were purified using the Qiagen PCR purification kit and sent to Genewiz, Inc. for Sanger sequencing. Sequences were aligned to chromosome X: 8284453 – 8585812 from the Drosophila dm3 genome annotation using DNASTAR Lasergene SeqMan Pro.

Quantitative real-time PCR

Ovaries were dissected from fattened females in Grace's media. Approximately 60 egg chambers were hand sorted from each stage per experiment and stored at -80°C. Egg chambers were thawed in 300µL ChIP lysis buffer and homogenized. DNA was fragmented by sonication in a Biorupter300 (Diagenode) at 4°C, 10 cycles of 30sec on 30sec off at maximum power. Copy number was measured by relative quantitative PCR using stage 1-8 egg chambers as the calibrator sample and the non-amplified *polalpha* locus as the endogenous control.

ChIP-sequencing

Ovaries were dissected from fattened *ocelliless* homozygous females in Grace's media and fixed in 4% formaldehyde for 15 minutes. A total of 3,000 stage 10 egg chambers were sorted by hand and stored at -80°C. To isolate follicle cell nuclei, egg chambers were resuspended in 500µL mHB buffer (0.34M sucrose, 15.0 mM NaCL, 60.0 mM KCL, 0.2mM EDTA, 0.2mm EGTA, 0.5% NP-40, 0.15mM spermidine, 0.15mM spermine). Egg chambers were dounced 10 strokes and filtered with 40µm nylon filter and spun for 5 minutes at 500 x g (Lui *et al.* 2012). The follicle cell nuclei pellet was suspended in 300µL ChIP lysis buffer (50mM HEPES/KOH pH 7.5, 140mM NaCl, 1mm EDTA, 1% Triton X-100, 0.1% Na-Deoxycholate). Chromatin was fragmented by sonication in a Biorupter300 (Diagenode) at 4°C for 30 cycles of 30sec on 30sec off at maximum power. Supernatants were incubated overnight in 1:250 anti-dmORC2 serum (Steve Bell). Chromatin was pulled down with Dynabeads magnetic beads (1:1 ratio of A and G beads, ThermoFisher Scientific). Crosslinks were reversed by overnight incubation in 1% SDS at 65°C overnight, and DNA isolated by phenol-chloroform extraction. Libraries were made using the NEBNext Ultra DNA Library Prep (#E7370) according to the manufacturer's instructions.

Libraries were sequenced on the Illumina Hi-Seq 2000. Peaks were called using MACS with $p \leq$ 1E-5 and FDR < 5%, normalizing to input.

Slope analysis

Segmented regression analysis was used to find breakpoints along the left and right sides of each *DAFC* from *OrR* 16C follicle cell CGH data (Kim *et al.* 2011). Each probe along the amplification gradients was assigned a single genomic coordinate at the center of the probe. The CGH value, or DNA copy number, for each probe was plotted against the center coordinate. Every *DAFC* was divided into left and right sides using a regression model with segmented relationships, as implemented by the R package 'segmented'. Each side of the *DAFC* was then examined for potential breakpoints, as indicated by a change of slope, again using a segmented model. Davies' test was used to assay the significance ($p<0.05$) of any potential breakpoint, after which the slope on each side of the breakpoint was calculated (Muggeo 2003).

Acknowledgements

We thank Steve Bell for anti-dmORC2 serum. The Bloomington Stock Center provided the *ocelliless* flies. FACS was done by the MIT Koch Institute Flow Cytometry Core and sequencing for ChIP-seq experiments was done by the MIT BioMicro Center. This work was supported by NIH grant GM57940 to Terry Orr-Weaver and the MIT School of Science Fellowship in Cancer Research.

References

Abbas, T., Keaton, M.A., Dutta, A. (2013). Genomic instability in cancer. Cold Spring Harb. Perspect. Biol. *5*, a012914.

Andreyeva, E.N., Kolesnikova, T.D., Belyaeva, E.S., Glaser, R.L., Zhimulev, I.F. (2008). Local DNA underreplication correlates with accumulation of phosphorylated H2Av in the *Drosophila melanogaster* polytene chromosomes. Chromosome Res. *16*, 851-862.

Austin, R. J., Orr-Weaver, T. L., Bell, S. P. (1999). *Drosophila* ORC specifically binds to *ACE3*, an origin of DNA replication control element. Genes Dev. *13*, 2639-2649.

Belyaeva, E.S., Zhimulev, I.F., Volkova, E.I., Alekseyenko, A.A., Moshkin, Y.M., Koryakov, D.E. (1998). Su(UR)ES: a gene suppressing DNA underreplication in intercalary and pericentric heterochromatin of *Drosophila melanogaster* polytene chromosomes. Proc. Natl. Acad. Sci. *95*, 7532-7537.

Besnard, E., Babled, A., Lapasset, L., Milhavet, O., Parrinello, H., Dantec, C., Marin, J.M., Lemaitre, J.M. (2012). Unraveling cell type-specific and reprogrammable human replication origin signatures associated with G-quadruplex consensus motifs. Nat. Struct. Mol. Biol. *19*, 837-844.

Biffi, G., Tannahill, D., McCafferty, J., Balasubramanian, S. (2013). Quantitative visualization of DNA G-quadruplex structures in human cells. Nat. Chem. *5*, 182-186.

Carminati, J.L., Johnston, C.G., Orr-Weaver, T.L. (1992). The *Drosophila ACE3* chorion element autonomously induces amplification. Mol. Cell. Biol. *12*, 2444-2453.

Casper, A.M., Nghiem, P., Arlt, M.F., Glover, T.W. (2002). ATR regulates fragile site stability. Cell *11*, 779-789.

Claycomb, J.M., MacAlpine, D.M., Evans, J.G., Bell, S.P., Orr-Weaver, T.L. (2002). Visualization of replication initiation and elongation in *Drosophila*. J. Cell Biol. *159*, 225-236.

Claycomb, J.M., Benasutti, M., Bosco, G., Fenger, D.D., Orr-Weaver, T.L. (2004). Gene amplification as a developmental strategy: isolation of two developmental amplicons in *Drosophila*. Dev. Cell *6*, 145-155.

Claycomb, J.M., and Orr-Weaver T.L. (2005). Developmental gene amplification: insights into DNA replication and gene expression. Trends Genet. *21*, 149-62.

Davidson, I.F., Anatoily, L., Blow, J.J. (2006). Deregulated replication licensing causes DNA fragmentation consistent with head-to-tail fork collision. Mol. Cell *24*, 433-443.

Debatisse, M., Le Tallec, B., Letessier, A., Dutrillaux, B., Brison, O. (2012). Common fragile sites: mechanisms of instability revisited. Trends Genet. *28*, 22-32.

de Cicco, D.V., Spradling, A.C. (1984). Localization of a cis-acting element responsible for the developmentally regulated amplification of Drosophila chorion genes. Cell *38*, 45-54.

Finn, K., Li, J.J. (2013). Single-stranded annealing induced by re-initiation of replication origins provides a novel and efficient mechanism for generating copy number expansion via non-allelic homologous recombination. PLoS Genetics *9*, e1003192.

Follonier, C., Oehler, J., Herrador, R., Lopes, M. (2013). Friedreich's ataxia-associated GAA repeats induce replication-fork reversal and unusual molecular junctions. Nat. Struct. Mol. Biol. *20*, 486-94.

Gerhardt, J., Tomishima, M.J., Zaninovic, N., Colak, D., Yan, Z., Zhan, Q., Rosenwaks, Z., Jaffrey, S.R., Schildkraut, C.L. (2014). The DNA replication program is altered at the FMR1 locus in fragile X embryonic stem cells. Mol. Cell *53*, 19-31.

Glover, T.W., Berger C., Coyle J., Echo B. (1984). DNA polymerase alpha inhibition by aphidicolin induces gaps and breaks at common fragile sites in human chromosomes. Hum. Genet. *67*, 136–142.

Green, B. M., and Li. J.J. (2005). Loss of rereplication control in *Saccharomyces cerevisiae* results in extensive DNA damage. Mol. Biol. Cell *16*, 421-432.

Hoshina, S., Yura, K., Teranishi, H., Kiyasu, N., Tominaga, A., Kadoma, H., Nakatsuka, A., Kunichika, T., Obuse, C., Waga, S. (2013). Human origin recognition complex binds preferentially to G-quadruplex-preferable RNA and single-stranded DNA. J. Biol. Chem. 288, 30161-30171.

Kim, J.C., Nordman, J., Xie, F., Kashevsky, H., Eng, T., Li, S., MacAlpine, D.M., Orr-Weaver, T.L. (2011). Integrative analysis of gene amplification in *Drosophila* follicle cells: parameters of origin activation and repression. Genes Dev. *25*, 1384-1398.

Letessier, A. Millot, G.A., Koundrioukoff, S., Lachagès, A.M., Vogt, N., Hansen, R.S., Malfoy, B., Brison, O., Debatisse, M. (2011). Cell-type-specific replication initiation programs set fragility of the FRA3B fragile site. Nature *470*, 120–123.

Lilly, M.A., Spradling, A.C. (1996). The *Drosophila* endocycle is controlled by Cyclin E and lacks a checkpoint ensuring S-phase completion. Genes Dev. *10*, 2514-2526.

Liu J., McConnell, K., Dixon, M., Calvi, B.R. (2012). Analysis of model replication origins in *Drosophila* reveals new aspects of the chromatin landscape and its relationship to origin activity and the prereplicative complex. Mol. Biol. Cell *23*, 200-212.

Liu, G., Chen, X., Leffak, M. (2013). Oligodeoxynucleotide binding to (CTG) · (CAG) microsatellite repeats inhibits replication fork stalling, hairpin formation, and genome instability. Mol. Cell. Biol. *33*, 571-581.

London, T.B., Barber, L.J., Mosedale, G., Kelly, G.P., Balasubramanian, S., Hickson, I.D., Boulton, S.J., Hiom, K. (2008). FANCJ is a structure-specific DNA helicase associated with the maintenance of genomic G/C tracts. J. Biol. Chem. *283*, 36132–36139.

Maizels, N., Gray, L.T. (2013). The G4 genome. PLoS Genet. *9*, e1003468.

Makunin, I.V., Volkova, E.I., Belyaeva, E.S., Nabirochkina, E.N., Pirrotta, V., Zhimulev, I.F. (2002). The Drosophila suppressor of underreplication protein binds to late-replicating regions of polytene chromosomes. Genetics *160*, 1023-1034.

Menendez, C., Frees, S., Bagga, P.S. (2012). QGRS-H Predictor: a web server for predicting homologous quadruplex forming G-rich sequence motifs in nucleotide sequences. Nucleic Acids Res. *40*, W96-W103.

Melixetian, M., Ballabeni, A., Masiero, L., Gasparini, P., Zamponi, R., Bartek, J., Lukas, J., Helin, K., (2004). Loss of Geminin induces rereplication in the presence of functional p53. J. Cell Biol. *165*, 473-482.

Mihaylov, I.S., Kondo, T., Jones, L., Ryzhikov, S., Tanaka, J., Zheng, J., Higa, L. A., Minamino, N., Cooley, L., Zhang, H. (2002). Control of DNA replication and chromosome ploidy by Geminin and Cyclin A. Mol. Cell. Biol. *22*, 1868-1880.

Mirkin, E.V., Mirkin, S.M. (2007). Replication fork stalling at natural impediments. Microbiol. Mol. Biol. Rev. *71*, 13-35.

Muggeo, V.M. (2003). Estimating regression models with unknown break-points. Stat. Med. *22*, 3055-3071.

Neelsen, K.J., Zanini, I.M.Y., Mijic, S., Herrador, R., Zellweger, R., Chaudhuri, A.R., Creavin, K.D., Blow, J.J., Lopes, M. (2013). Deregulated origin licensing leads to chromosomal breaks by rereplication of a gapped DNA template. Genes Dev. *27*, 2537-2542.

Nguyen, V.Q., Co, C., Li, J.J. (2001). Cyclin-dependent kinases prevent DNA re-replication through multiple mechanisms. Nature *411*, 1068-1073.

Nordman, J., Li, S., Eng, T., MacAlpine, D., Orr-Weaver, T.L. (2011). Developmental control of the DNA replication and transcription programs. Genome Res. *21*, 175–181.

Nordman, J.T., Kozhevnikova, E.N., Verrijzer, C.P., Pindyurin, A.V., Andreyeva, E.N., Shloma, V.V., Zhimulev, I.F., Orr-Weaver, T.L. (2014). DNA copy-number control through inhibition of replication fork progression. Cell Rep. *9*, 841-849.

Nordman, J.T., Orr-Weaver, T.L. (2015). Understanding replication fork progression, stability, and chromosome fragility by exploiting the Suppressor of Underreplication protein. Bioessays *37*, 856-861.

Orr-Weaver, T.L., Spradling, A.C. (1986). *Drosophila* chorion gene amplification requires an upstream region regulating *s18* transcription. Mol. Cell Biol. *6*, 4624-4633.

Orr-Weaver, T.L., Johnston, C.G., Spradling, A.C. (1989). The role of ACE3 in *Drosophila* chorion gene amplification. EMBO J. *8*, 4153-4162.

Ozeri-Galai, E., Lebofsky, R., Rahat, A., Bester, A.C., Bensimon, A., Kerem, B. (2011). Failure of origin activation in response to fork stalling leads to chromosomal instability at fragile sites. Mol. Cell *43*, 122–131.

Ozeri-Galai, E., Bester, A.C., Kerem, B. (2012). The complex basis underlying common fragile site instability in cancer. Trends Genet. *26*, 295-302.

Paeschke, K., Capra, J.A., Zakian, V.A. (2011). DNA replication through G-quadruplex motifs is promoted by the *Saccharomyces cerevisiae* Pif1 DNA helicase. Cell *145*, 678-691.

Palumbo, E., Matricardi, L., Tosoni, E., Bensimon, A., Russo, A. (2010). Replication dynamics at common fragile site FRA6E. Chromosoma *119*, 575–587.

Park, E.A., MacAlpine, D. M., Orr-Weaver, T.L. (2007). *Drosophila* follicle cell amplicons as models for metazoan DNA replication: a *cyclinE* mutant exhibits increased replication fork elongation. Proc. Natl. Acad. Sci. USA *104*, 16739-16746.

Sabouri, N., Capra, J.A., Zakian, V.A. (2014). The essential *Schizosaccharomyces pombe* Pfh1 DNA helicase promotes fork movement past G-quadruplex motifs to prevent DNA damage. BMC Biol. *12*, 101.

Sanders, C.M. (2010). Human Pif1 helicase is a G-quadruplex DNA-binding protein with G-quadruplex DNA-unwinding activity. Biochem. J. *430*, 119–128.

Schaffitzel, C., Berger, I., Postberg, J., Hanes, J., Lipps, H.J., Pluckthun, A. (2001). *In vitro* generated antibodies specific for telomeric guanine-quadruplex DNA react with *Stylonychia lemnae* macronuclei. Proc. Natl. Acad. Sci. USA *98*, 8572-8577.

Schwab, R.A., Nieminuszczy, J., Shin-Ya, K., Niedzwiedz, W. (2013). FANCJ couples replication past natural fork barriers with maintenance of chromatin structure. J. Cell. Biol. *201*, 33-48.

Shah, S.N., Opresko, P.L., Meng, X., Lee, M.Y., Eckert, K.A. (2010). DNA structure and the Werner protein modulate human DNA polymerase delta-dependent replication dynamics within the common fragile site FRA16D. Nucleic Acids Res. *38*, 1149–1162.

Sher, N., Bell, G.W., Li, S., Nordman, J., Eng, T., Eaton, M.L., Macalpine, D.M., Orr-Weaver, T.L. (2012). Developmental control of gene copy number by repression of replication initiation and fork progression. Genes Res. *22*, 64-75.

Spradling, A.C., Mahowald, A.P. (1979). Drosophila bearing the *ocelliless* mutation underproduce two major chorion proteins both of which map near this gene. Cell *16*, 609-616.

Spradling, A.C., Mahowald, A.P. (1980). Amplification of genes for chorion proteins during oogenesis in *Drosophila melanogaster*. Proc. Natl. Acad. Sci. USA *77*, 1096-1100.

Spradling, A.C., Mahowald, A.P. (1981). A Chromosome Inversion Alters the Pattern of Specific DNA Replication in Drosophila Follicle Cells. Cell *27*, 203-209.

Spradling, A.C., Orr-Weaver, T.L. (1987). Regulation of DNA Replication During *Drosophila* Development. Ann. Rev. Genet. *21*, 373-403.

Toedling, J., Skylar, O., Krueger, T., Fischer, J.J., Sperling, S., Huber, W. (2007). Ringo—an R/Bioconductor package for analyzing ChIP–chip readouts. BMC Bioinformatics *8*,. doi: 10.1186/1471-2105-8-221.

Valton, A.L., Hassan-Zadeh, V., Lema, I., Boggetto, N., Alberti, P., Saintomé, C., Riou, J.F., Prioleau, M.N. (2014). G4 motifs affect origin positioning and efficiency in two vertebrate replicators. EMBO J. *33*, 732-746.

Wu, Y., Shin-Ya, K., Brosh, R.M. (2008). FANCJ helicase defective in Fanconi anemia and breast cancer unwinds G-quadruplex DNA to defend genomic stability. Mol. Cell. Biol. *28*, 4116–4128.

Zhang, H., Freudenreich, C.H. (2007). An AT-rich sequence in human common fragile site FRA16D causes fork stalling and chromosome breakage in *S. cerevisiae*. Mol. Cell *27*, 367–379.

Zhu, W., Chen, Y., Dutta, A. (2004). Rereplication by depletion of Geminin is seen regardless of p53 status and activates a G2/M checkpoint. Mol. Cell. Biol. *16*, 7140-7150.

Chapter Three: Replication Fork Progression during Re-replication requires the DNA Damage Checkpoint and Double-Strand Break Repair

Jessica L. Alexander[1, 2], M. Inmaculada Barrasa[1], Terry L. Orr-Weaver[1, 2]

[1]Whitehead Institute for Biomedical Research, 9 Cambridge Center, Cambridge, MA 02142, USA
[2]Department of Biology, Massachusetts Institute of Technology, 77 Massachusetts Ave., 68-132, Cambridge, MA 02139, USA

This chapter was published in Current Biology 25(12): 1654-1660 (2015).
M. Inmaculada Barrasa developed and performed γH2Av ChIP-seq analysis
Jessica L. Alexander performed all other experiments and analysis

Summary

Replication origins are under tight regulation to ensure activation occurs only once per cell cycle (Bell & Dutta 2002, Abbas & Dutta 2013). Origin re-firing in a single S-phase leads to the generation of DNA double-strand breaks (DSBs) and activation of the DNA damage checkpoint (Mihaylov *et al.* 2002, Melixetian *et al.* 2004, Zhu *et al.* 2004, Green & Li 2005, Davidson *et al.* 2006, Abbas & Dutta 2013). If the checkpoint is blocked, cells enter mitosis with partially re-replicated DNA that generates chromosome breaks and fusions (Melixetian *et al.* 2004). These types of chromosomal aberrations are common in numerous human cancers, suggesting re-replication events contribute to cancer progression. It was proposed that fork instability and DSBs formed during re-replication are the result of head-to-tail collisions and collapse of adjacent replication forks (Davidson *et al.* 2006). However, previously studied systems lack the resolution to determine whether the observed DSBs are generated at sites of fork collisions. Here we utilize the Drosophila ovarian follicle cells, which exhibit re-replication under precise developmental control (Spradling & Mahowald 1980, Calvi *et al.* 1998, Claycomb & Orr-Weaver 2005) to model the consequences of re-replication at actively elongating forks. Re-replication occurs from specific replication origins at six genomic loci, termed *Drosophila Amplicons in Follicle Cells* (*DAFCs*) (Claycomb *et al.* 2004, Claycomb & Orr-Weaver 2005, Kim *et al.* 2011). Precise developmental timing of *DAFC* origin firing permits identification of forks at defined points after origin initiation (Claycomb *et al.* 2002, Park *et al.* 2007). Here we show that *DAFC* re-replication causes fork instability and generates DSBs at sites of potential fork collisions. Immunofluorescence and ChIP-seq demonstrate the DSB marker γH2Av is enriched at elongating forks. Fork progression is reduced in the absence of DNA damage checkpoint components and nonhomologous end-joining (NHEJ), but not homologous

recombination. NHEJ appears to continually repair forks during re-replication to maintain elongation.

Results & Discussion

Fork instability and double-strand breaks occur during amplification

Drosophila marks DSBs by phosphorylation the H2Av histone tail, forming γH2Av (Madigan *et al.* 2002), which can therefore be used to monitor DSB generation. The nuclear localization of γH2Av was visualized by immunofluorescence in amplifying follicle cells using a phospho-specific antibody. Follicle cells were co-labeled with the thymidine analog ethynyl deoxyuridine (EdU), which specifically marks the *DAFCs* due to the absence of genome-wide replication (Calvi *et al.* 1998, Claycomb *et al.* 2002). Drosophila egg chambers are divided into developmental stages based on their distinct morphologies, each of which lasts for a defined period of time. This enables isolation of the follicle cells at specific times in development by ovary dissection. Origin firing at the *DAFCs* begins at stage 10B across all follicle cells of a given egg chamber (Calvi *et al.* 1998). At this stage EdU is visible in single foci corresponding to each *DAFC* origin and the surrounding forks (Fig. 1A, C) (Calvi *et al.* 1998, Claycomb *et al.* 2002). By stages 12 and 13, the origin of the most highly amplified site, *DAFC-66D*, no longer fires, but existing replication forks continue to travel; this results in the resolution of two adjacent EdU foci around the *DAFC-66D* origin, called the double-bar structure (Claycomb *et al.* 2002). (Fig. 1A, F).

We found that intense γH2Av staining directly overlaps with sites of EdU incorporation in all amplifying follicle cells observed (Fig. 1B-G). In stage 10B when replication forks have just begun to progress away from the origin, γH2Av was already visible at each EdU focus (Fig. 1B,

Figure 1. Markers of DNA damage and replication fork stress co-localize with sites of re-replication.

(A) The onion skin model of amplification. EdU is drawn in red overlaying sites of actively replicating DNA. EdU labeling during origin initiation and fork progression in stage 10B results in incorporation throughout the amplicons (left). In stage 13 when forks continue to progress without further origin firing events, EdU incorporation gives rise to the double-bar structure (right).

(B-G) Immunofluorescence images of stage 10B (B-D) and 13 (E-G) follicle cell nuclei reveal the double-strand break marker γH2Av (D, G) co-localizes with EdU (C, F). As forks progress in stage 13 and EdU incorporation forms the double-bar structure (F), the γH2Av signal also resolves into to double-bars (G). This co-localization pattern was present in every follicle cell nucleus of every egg chamber observed (53 stage 10Bs and 49 stage 13s). (B, E) Merged image with EdU is shown in red, γH2Av in green, DAPI in blue. Each image is a single plane of a follicle cell nucleus. The prominent EdU focus corresponds to *DAFC-66D* (arrows). Scale bars, 1μm.

(H-M) RPA immunofluorescence reveals direct overlap with EdU in stage 10B (H-J) and 13 (K-M) follicle cells. RPA follows the pattern of fork progression highlighted by EdU, resolving into a double-bar structure in stage 13 (M). This co-localization pattern was present in every follicle cell nucleus of every egg chamber observed (51 stage 10Bs and 60 stage 13s). (H, K) Merged image with EdU is shown in red, RPA in green, DAPI in blue. Each image is a single plane of a follicle cell nucleus. The prominent EdU focus corresponds to *DAFC-66D* (arrows). Scale bars, 1 μm.

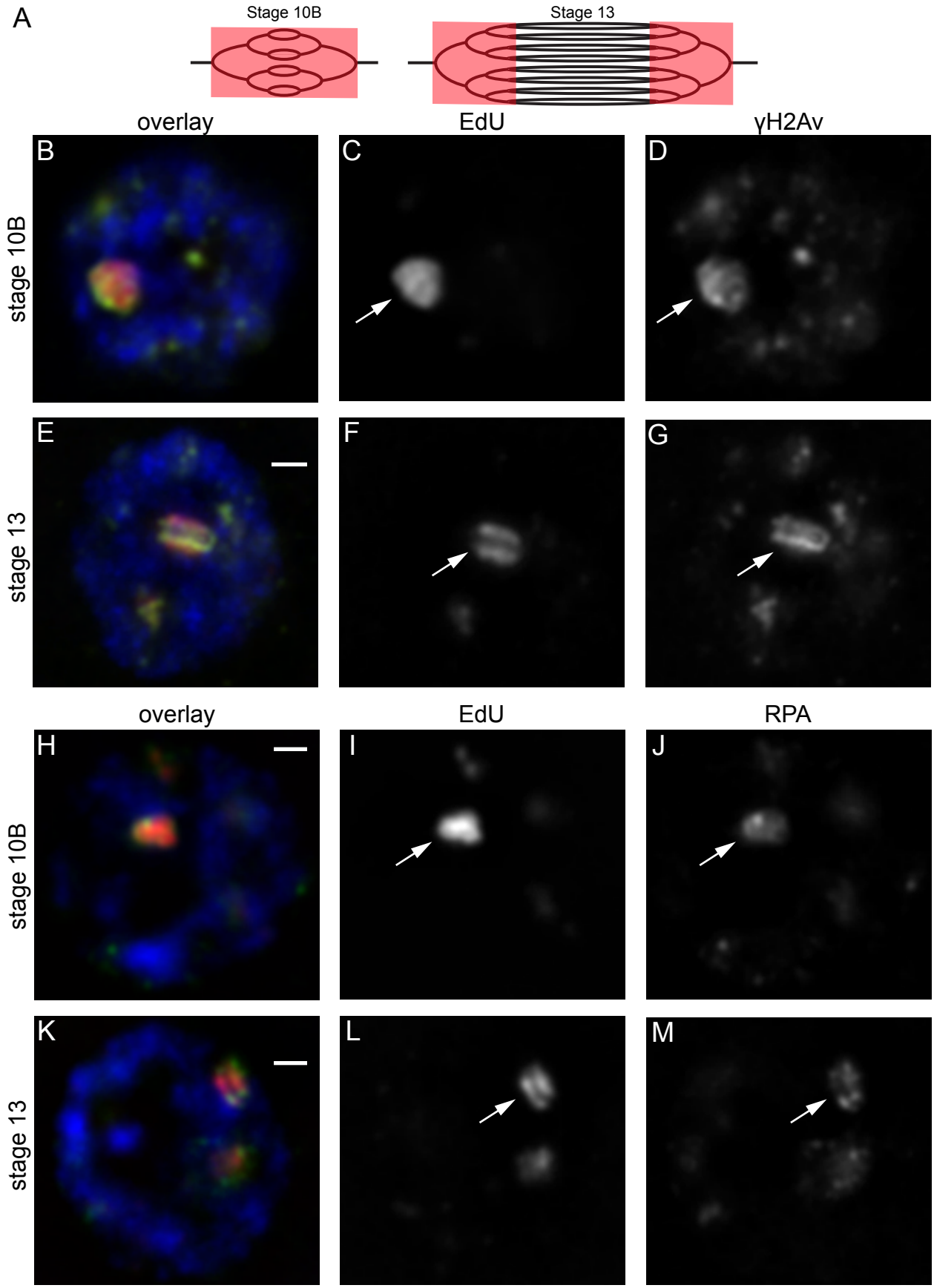
A
Stage 10B
Stage 13
overlay
EdU
γH2Av
B
C
D
stage 10B
E
F
G
stage 13
overlay
EdU
RPA
H
I
J
stage 10B
K
L
M
stage 13

D). Strikingly, in stage 13 γH2Av resolved into a double-bar pattern overlapping EdU (Fig. 1E, G). These results demonstrate that DSBs are generated during amplification. Additionally, the resolution of γH2Av into double-bars in stage 13 strongly suggests that DSBs are occurring at the active replication forks and that these breaks are repaired as the forks progress.

The γH2Av localization pattern was confirmed using a second antibody (Fig. 2A) (Lake *et al.* 2013). The antibody specificity was verified in $H2Av^{\Delta CT}$ mutant follicle cells, in which the only form of H2Av expressed lacks the phosphorylation site (Clarkson *et al.* 1999). No γH2Av signal was detected during any stage of amplification in $H2Av^{\Delta CT}$ follicle cells (Fig. 2B). To confirm the observed DNA damage was not generated by EdU incorporation, follicle cells were co-labelled for γH2Av and the *DAFC* fork marker DUP (Fig. 2C) (Claycomb *et al.* 2002). Here γH2Av signal overlapped with DUP as single foci in stage 10B and double-bars in stage 13, as was seen with EdU.

To determine if the γH2Av signal at the *DAFCs* is generated by DSBs or single-stranded DNA (ssDNA), staining was done in follicle cells lacking ATR and ATM activity (Fig. 2D-F). Both activated kinases phosphorylate H2Av; ATR is activated in response to extended RPA tracks on ssDNA, whereas ATM is specifically activated by DSBs (Harper & Elledge 2007). In the absence of either single kinase, γH2Av localization was the same as in wild-type follicle cells (Fig. 2E, F). However, when neither kinase was active, γH2Av was completely absent (Fig. 2D). This demonstrates that both ssDNA and DSBs generate γH2Av during re-replication.

To confirm our results with γH2Av staining, we sought to localize RPA as a second marker of fork stalling and damage. RPA forms long tracks on single-stranded DNA caused by fork stalling, as well as after resection of DSBs (Byun *et al.* 2005, Jazayeri *et al.* 2006). RPA staining therefore marks both fork stress and sites of DSB repair. Similar to γH2Av, we found that strong

Figure 2. γH2Av and RPA localization are specific to sites of re-replication

(A) Immunofluorescence for γH2Av using a mouse-monoclonal antibody shows the pattern of co-localization with EdU is nearly identical to that seen with the commercial antibody. γH2Av stains as a single focus in stage 10B (top right), and again is seen to resolve into double-bars in stage 13 (bottom right). Merged image with EdU is shown in red, γH2Av in green, DAPI in blue (left). Each image is a single plane of one nucleus. Scale bars, 2 μm.

(B) γH2Av immunofluorescence in $H2Av^{\Delta CT}$ follicle cells using the commercial antibody displays no signal during amplification. The EdU signal is identical to what is observed in wild-type follicle cells in both stages 10B (top middle) and 13 (bottom middle), but no γH2Av signal was detected in this phosphorylation mutant (right). Merged image with EdU is shown in red, γH2Av in green, DAPI in blue (left). Each image is a single plane of one nucleus. Images were taken at exposures equal to that of wild-type images (Fig. 1). No signal was detected at higher exposures (not shown). Scale bars, 2 μm.

(C) Co-immunofluorescence of DUP and γH2Av confirm DSBs track with active replication forks in the absence of EdU incorporation. Both DUP (middle) and γH2Av (right) form a single focus in stage 10B (top) and resolve into double-bars in stage 13 (bottom). Merged images with DUP shown in red, γH2Av in green, DAPI in blue (left). Each image is a single plane of one nucleus. Scale bars, 2 μm.

(D-F) There is no detectable γH2Av signal in the absence of ATR and ATM activity. The Drosophila homologs of ATR and ATM are *mei-41* and *tefu*, respectively. γH2Av staining was done in a *mei-41* null and *tefu* temperature sensitive line, $mei\text{-}41^{D3}$; $tefu^{atm\text{-}8}$. (D) After 24 hours at the restrictive temperature there is no detectable γH2Av in $mei\text{-}41^{D3}$; $tefu^{atm\text{-}8}$ follicle cells at stage 10B or 13. (E) $mei\text{-}41^{D3}$; $tefu^{atm\text{-}8}$/*TM3* follicle cells lack ATR activity, but have one

functional ATM allele. (F) *mei-41*^{D3}*/FM7; tefu*$^{atm-8}$ follicle cells lack ATM activity, but have one functional ATR allele. In both single mutants (E and F) γH2Av staining is visible in the same pattern observed in wild-type follicle cells, overlapping sites of EdU incorporation. These results show that both ATM and ATR activity generate γH2Av at the *DAFCs*, demonstrating γH2Av marks DSBs and single-stranded DNA at these sites of re-replication. Merged images with EdU shown in red, γH2Av in green, DAPI in blue (left). Each image is a single plane of two to four nuclei. Scale bars, 5 μm.

(G) Immunofluorescence in endocycling follicle cells reveals γH2Av is not specific to EdU-positive cells. Background signal is detected in all endocycling cells regardless of cell cycle stage (top right). Compare to γH2Av immunofluorescence during re-replication in stage 10B from the same experiment taken at equal exposures (bottom right). Merged images with EdU shown in red, γH2Av in green, DAPI in blue (left). Each image is a single plane of three nuclei. Scale bars, 5 μm.

(H) RPA immunofluorescence in endocycling follicle cells reveals this marker does not overlap with sites of EdU incorporation. Some background signal is observed in all nuclei regardless of cell cycle stage (top right). Compare to RPA immunofluorescence during re-replication in stage 10B from the same experiment taken at equal exposures (bottom right). Merged images with EdU shown in red, γH2Av in green, DAPI in blue (left). Each image is a single plane of three to four nuclei. Scale bars, 5 μm.

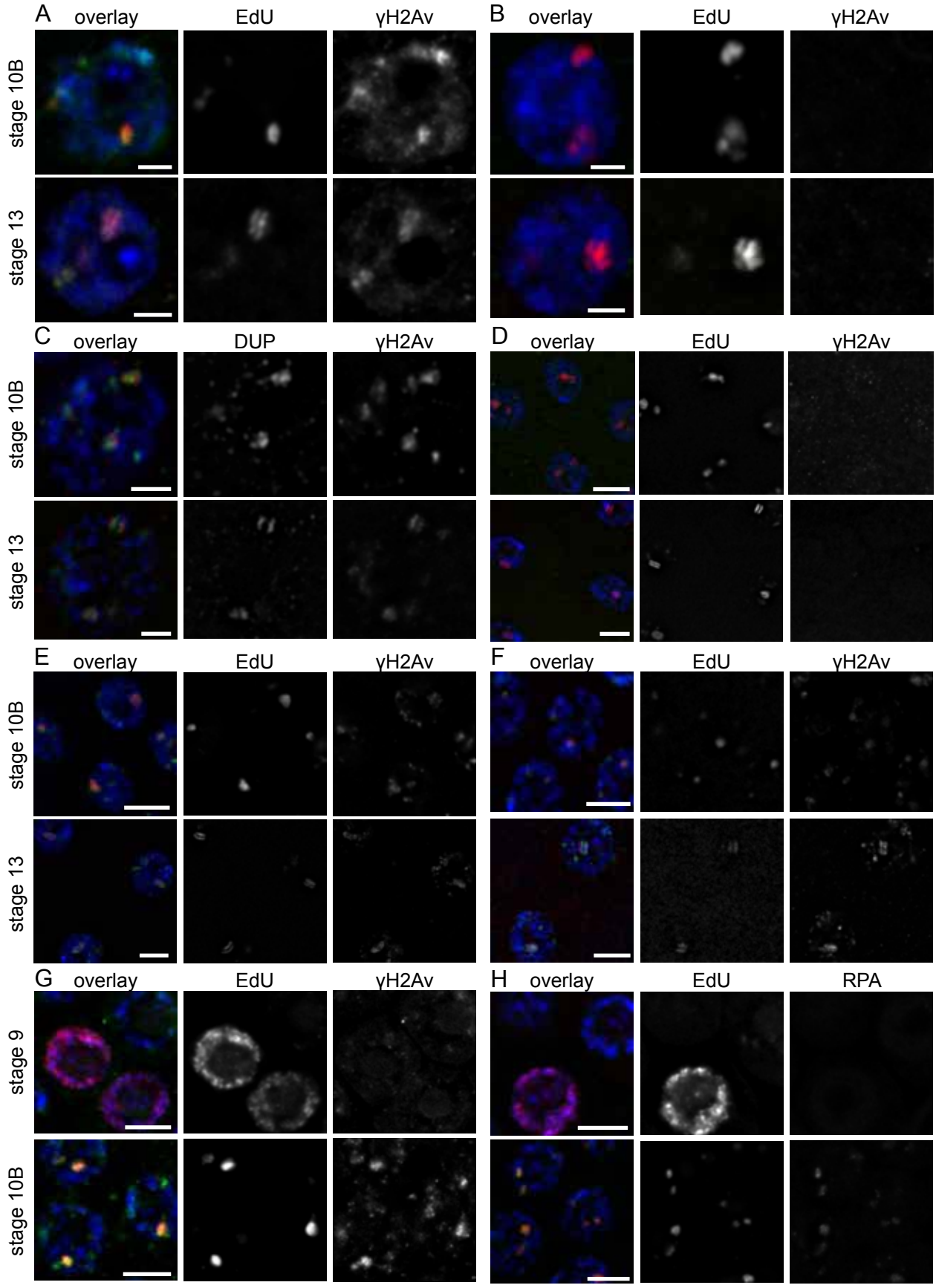
A
overlay
EdU
γH2Av
B
overlay
EdU
γH2Av
stage 10B
stage 13
C
overlay
DUP
γH2Av
D
overlay
EdU
γH2Av
stage 10B
stage 13
E
overlay
EdU
γH2Av
F
overlay
EdU
γH2Av
stage 10B
stage 13
G
overlay
EdU
γH2Av
H
overlay
EdU
RPA
stage 9
stage 10B

RPA staining directly overlapped with sites of EdU incorporation during all amplification stages observed (Fig. 1H-M). Additionally, RPA resolved into a double-bar structure in stage 13, following the pattern of EdU (Fig. 1M). Together the RPA and γH2Av results indicate replication forks stall and collapse during re-replication at the *DAFCs*.

To confirm that the RPA and γH2Av signals observed were not general markers of DNA replication, we examined staining in earlier follicle cells undergoing S-phase. Prior to the onset of amplification, the follicle cells undergo three endocycles (Calvi *et al.* 1998). The endocycle is an alternative cell cycle that undergoes consecutive G- and S-phases without an intervening mitosis. S-phase of the endocycle resembles that of a canonical S-phase in that origins fire only once per cell cycle, and therefore do not exhibit re-replication (Nordman *et al.* 2011). Although diffuse nuclear staining was detected for both RPA and γH2Av, neither signal was specific to EdU positive cells (Fig. 2G-H). This shows that neither RPA nor γH2Av can be detected at replication forks during S-phase in the absence of fork stress. There was γH2Av at genomic regions outside the *DAFCs* during amplification stages, which was absent in staining controls (Fig. 2B, D) indicating it is specific and generated in response to DNA damage. The appearance of γH2Av throughout the nucleus during the endocycles is consistent with previous observations that DSBs occur in the heterochromatin in follicle cells (Hong *et al.* 2007, Mehrotra *et al.* 2008). The γH2Av staining that is not coincident with the amplicons also is at heterochromatin as evidenced by intense DAPI staining.

To evaluate γH2Av localization at the *DAFCs* and across the genome at the molecular level, we analyzed γH2Av enrichment by ChIP-seq. Enrichment was assessed in both stage 10B and 13 follicle cell nuclei to observe changes in γH2Av accumulation at the initial and final points in amplification. The same ChIP-seq experiment was done from $H2Av^{\Delta CT}$ follicle cells to control

for non-specific antibody binding (Fig. 4). To determine where γH2Av is enriched along each *DAFC*, the position of γH2Av peaks was compared to Comparative Genomic Hybridization (CGH) analysis from wild-type egg chambers. CGH analysis measures the DNA copy number over chromosomal position, and demonstrates that fork progression expands the amplification gradient of each *DAFC* between stages 10B to 13 (Fig. 3, first and third lines). Comparison of ChIP-seq with the CGH gradients enabled us to analyze the γH2Av enrichment profile relative to the active replication forks.

We found that γH2Av was significantly enriched at all six *DAFC*s in both stages compared to enrichment across the genome and in the $H2Av^{\Delta CT}$ control (Table 1). The ChIP-seq enrichment profiles shifted from a single broad region of enrichment in stage 10B to two adjacent peaks on either side of the origin in stage 13, reflecting the double-bar structure seen by γH2Av immunofluorescence at *DAFC-66D* (Fig. 3, second and fourth lines). Previous analysis of *DAFC-66D* measured a 70kb gap between the double-bars by stage 13 (Claycomb *et al.* 2002), much larger than the gaps between γH2Av ChIP-seq peaks. However, previous measurements were made at individual follicle cells, whereas the ChIP-seq data is averaged across $3x10^6$ cells. Co-localization of γH2Av staining and EdU indicate γH2Av is at active replication forks (Fig. 1E-G). Therefore the reduced double-bar distance measured by ChIP-seq is likely the result of the large population average.

Interestingly, the resolution provided by ChIP-seq revealed enrichment at *DAFC-66D* is resolved into double-bars by stage 10B. In stage 13, the positions are maintained with increased levels of enrichment. We propose that fork stress and accumulation of DSBs in the double-bar structure early at *DAFC-66D* increases the frequency of fork collisions in those same positions. Therefore γH2Av enrichment is enhanced over the same sequences, rather than spreading away

Figure 3. γH2Av enrichment at the *DAFCs* during re-replication stages.

CGH and γH2Av ChIP-seq from *OrR* stage 10B and 13 follicle cells at each of the six *DAFCs*. Chromosomal position is indicated above each panel. CGH profiles are the log2 ratio (0-5) of egg chamber to embryonic DNA (first and third lines). ChIP-seq enrichment is the RPM of ChIP/input (0-26) for 1kb windows sliding every 100bp, and is the geometric mean of two biological replicates (second and fourth lines). Genomic coordinates are displayed above.

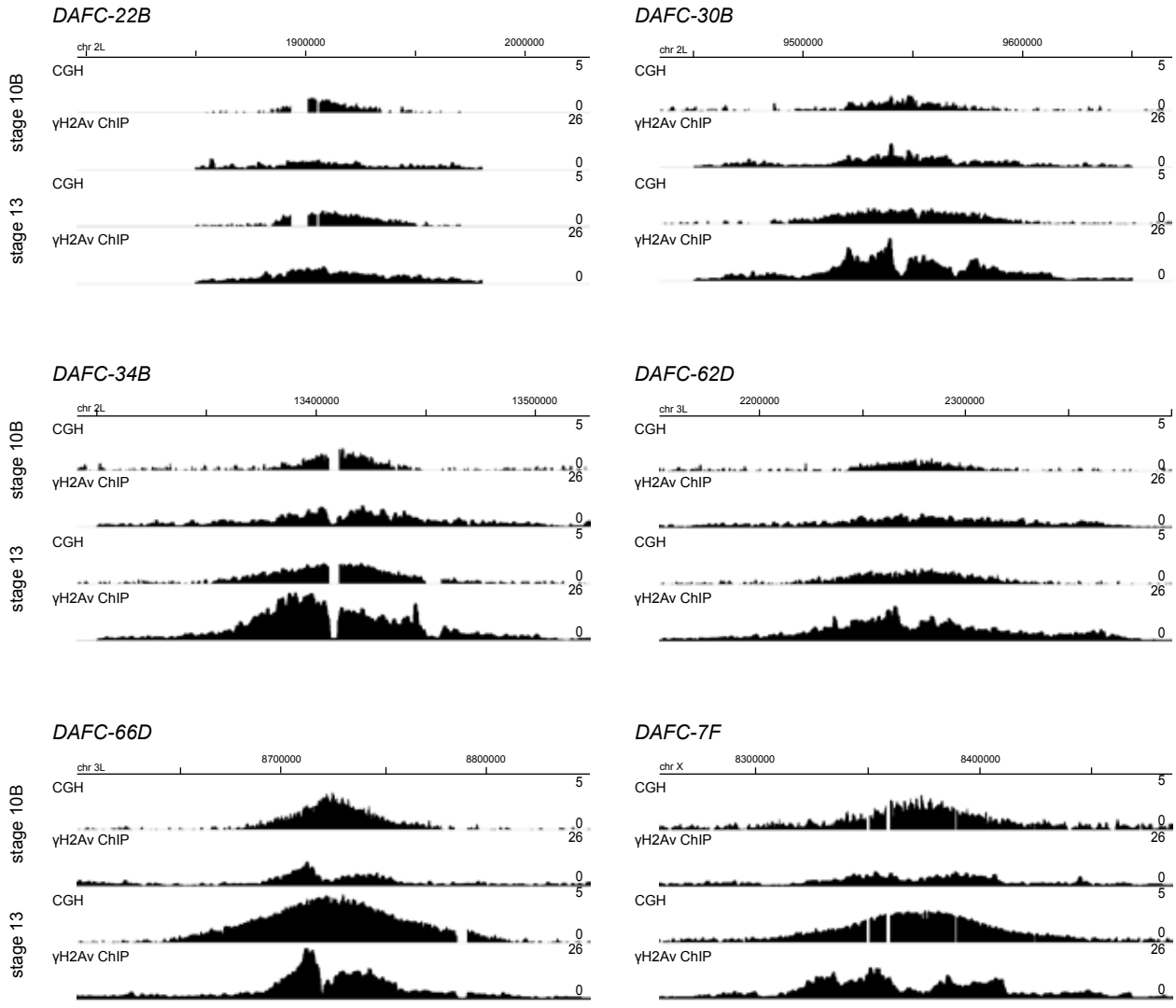
DAFC-22B
chr 2L
1900000
2000000
stage 10B
CGH
5
0
γH2Av ChIP
26
0
stage 13
CGH
5
0
γH2Av ChIP
26
0
DAFC-30B
chr 2L
9500000
9600000
CGH
5
0
γH2Av ChIP
26
0
CGH
5
0
γH2Av ChIP
26
0
DAFC-34B
chr 2L
13400000
13500000
stage 10B
CGH
5
0
γH2Av ChIP
26
0
stage 13
CGH
5
0
γH2Av ChIP
26
0
DAFC-62D
chr 3L
2200000
2300000
CGH
5
0
γH2Av ChIP
26
0
CGH
5
0
γH2Av ChIP
26
0
DAFC-66D
chr 3L
8700000
8800000
stage 10B
CGH
5
0
γH2Av ChIP
26
0
stage 13
CGH
5
0
γH2Av ChIP
26
0
DAFC-7F
chr X
8300000
8400000
CGH
5
0
γH2Av ChIP
26
0
CGH
5
0
γH2Av ChIP
26
0

Figure 4. γH2Av peaks are specific to the phosphorylated histone

γH2Av ChIP-seq from *H2Av*$^{\Delta CT}$ stage 10B and 13 follicle cells at each of the six *DAFCs*. CGH data is from *OrR* stage 10B and 13 egg chambers. Chromosomal position is indicated above each panel. CGH profiles are the log2 ratio (0-5) of egg chamber to embryonic DNA (first and third lines). ChIP-seq enrichment is the RPM of ChIP/input (0-26) for 1kb windows sliding every 100bp, and is the geometric mean of two biological replicates (second and forth lines). Genomic coordinates are displayed above.

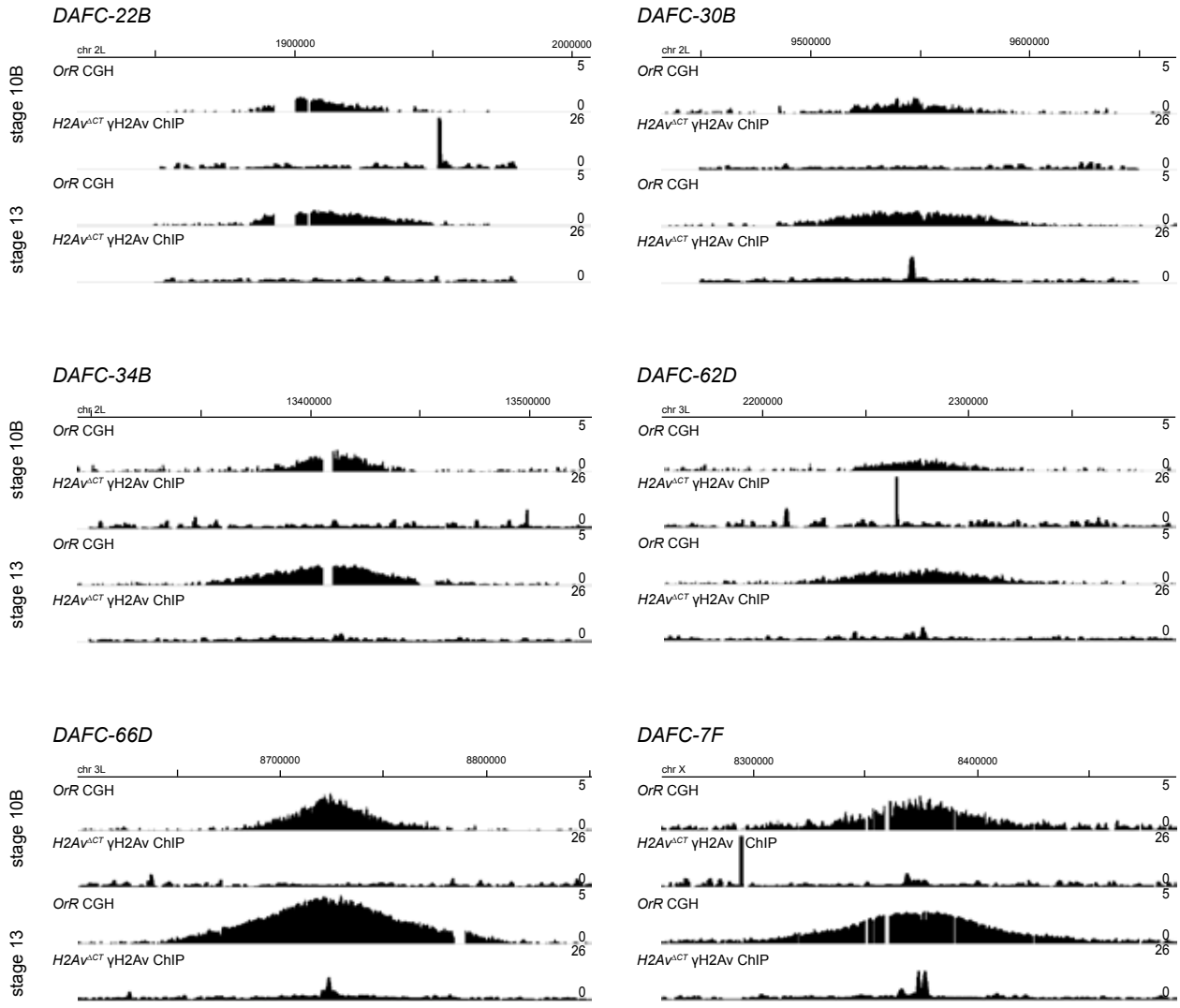
DAFC-22B
chr 2L
1900000
2000000
stage 10B
OrR CGH
H2Av^ΔCT γH2Av ChIP
stage 13
OrR CGH
H2Av^ΔCT γH2Av ChIP
DAFC-30B
chr 2L
9500000
9600000
OrR CGH
H2Av^ΔCT γH2Av ChIP
OrR CGH
H2Av^ΔCT γH2Av ChIP
DAFC-34B
chr 2L
13400000
13500000
stage 10B
OrR CGH
H2Av^ΔCT γH2Av ChIP
stage 13
OrR CGH
H2Av^ΔCT γH2Av ChIP
DAFC-62D
chr 3L
2200000
2300000
OrR CGH
H2Av^ΔCT γH2Av ChIP
OrR CGH
H2Av^ΔCT γH2Av ChIP
DAFC-66D
chr 3L
8700000
8800000
stage 10B
OrR CGH
H2Av^ΔCT γH2Av ChIP
stage 13
OrR CGH
H2Av^ΔCT γH2Av ChIP
DAFC-7F
chr X
8300000
8400000
OrR CGH
H2Av^ΔCT γH2Av ChIP
OrR CGH
H2Av^ΔCT γH2Av ChIP

Table 1. γH2Av ChIP-seq enrichment at the *OrR DAFCs* is significantly different from the genome and *H2Av$^{\Delta CT}$ DAFCs* (Relating to Figure 2)

Enrichment of γH2Av at each *DAFC* was compared to genome-wide enrichment by taking the median of the $\log_2$(RPM ChIP/RPM input) windows across each individual *DAFC* and the entire genome. This analysis was done for *OrR* and *H2Av$^{\Delta CT}$* ChIP, stages 10B and 13.

median of $\log_2$(RPM ChIP/RPM input) density distributions				
	OrR stage 10B	*H2Av$^{\Delta CT}$* stage 10B	*OrR* stage 13	*H2Av$^{\Delta CT}$* stage 13
genome	0	-0.04	-0.05	0
DAFC-22B	1.16	-0.50	1.91	-0.24
DAFC-30B	1.94	-0.16	2.69	0.55
DAFC-34B	2.39	0.19	3.51	0.27
DAFC-62D	2.00	0.05	2.79	0.08
DAFC-66D	1.98	0.04	2.98	0.76
DAFC-7F	2.10	0.15	2.92	0.72

[a] all *DAFC* medians are significantly different from the genome median

from the origin between stages 10B and 13. Together our ChIP-seq and cytological results demonstrate extensive fork stalling and DSBs occur at the active replication forks during re-replication.

The DNA damage response is essential for fork progression after re-replication

DSBs are generated from the earliest point of amplification in stage 10B, yet replication fork progression is still continues until the end of follicle cell development in stage 13. This suggests that the DNA damage response (DDR) and DSB repair may be essential for continued fork movement during re-replication. To test the requirement for repair at active replication forks, we measured fork progression at the *DAFCs* in several DDR mutants by Comparative Genomic Hybridization (CGH) analysis (Chapter2, Fig. 5). The shape of the amplification gradients generated by CGH is reflective of replication fork progression. A gradual decrease in copy number indicates uninhibited fork movement, whereas a rapid decrease indicates fork movement is impeded (Fig. 5A). CGH analysis is therefore a powerful tool to compare fork progression between different mutant lines. CGH analysis was performed at each site of re-replication except *DAFC-22B*; this site is a strain-specific amplicon (Kim *et al.* 2011), and therefore could not be compared across different genetic backgrounds. The number and timing of replication initiation events was first measured for each mutant by quantitative PCR. None of the mutants analyzed significantly affected replication initiation (Fig. 5D), confirming that any changes in the amplification gradients are not due to altered initiation kinetics. Additionally, fork progression was measured in appropriate controls to rule out changes in fork progression due to differences in genetic backgrounds (Fig. 6A and 8A).

Figure 5. Fork progression is reduced in the absence of DDR components.

(A) Blocked fork progression causes adjacent forks to pile up, resulting in close spacing as demonstrated by the replication forks highlighted in red (top). This is reflected in the CGH gradient by a sharp decrease in copy number. An example of one such region is highlighted in red on the wild-type *DAFC-66D* gradient (bottom).

(B) CGH of *DAFC-66D* from DDR mutants reveals impaired replication fork progression. DNA from stage 13 egg chambers was competitively hybridized with diploid embryonic DNA to microarrays with approximately one probe every 125bp. Chromosomal position is plotted on the x-axis, the log2 ratio of stage 13 DNA to embryonic DNA is plotted on the y-axis. In all mutants shown, the amplification gradient exhibits a rapid decrease in copy number compared to the wild type (top).

(C) The half-maximum distance was calculated in the wild-type and mutant backgrounds for each *DAFC*. Each half-maximum value is the average of three biological replicates. Significance measured by the Dunnett test for multiple comparisons, asterisks indicate $p<0.05$ and n.s. indicates not significant.

(D) The level of amplification was measured at the *DAFC-66D* origin of replication in each DSB signaling and repair mutant by quantitative real-time PCR. The copy number in stages 10B and 13 egg chambers is relative to the nonamplified *rosy* locus. Error bars are standard error of three replicates. None of the mutants were significantly different from the wild type as measured by the Dunnett test for multiple comparisons.

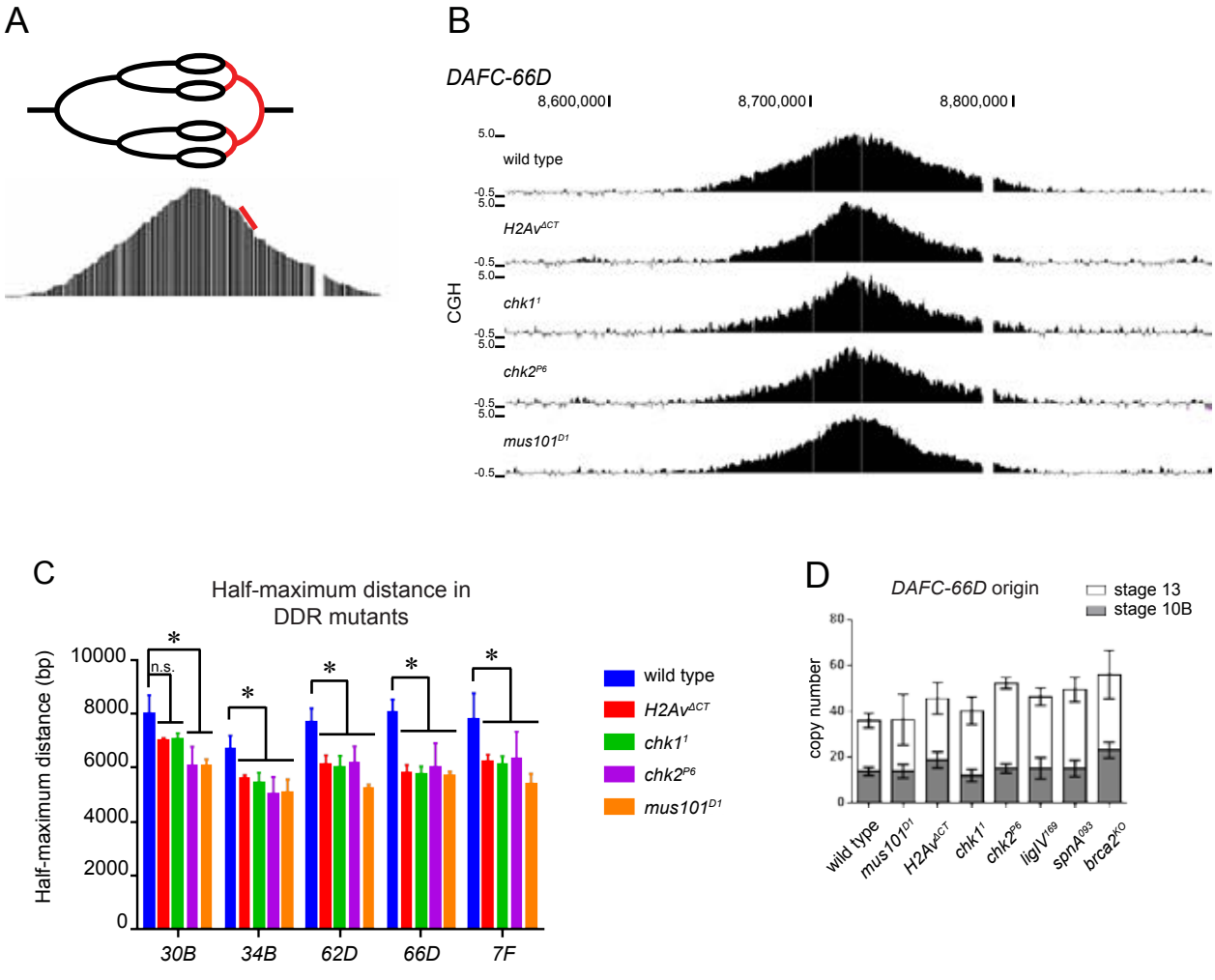
A
B
DAFC-66D
8,600,000
8,700,000
8,800,000
wild type
H2Av^ΔCT
chk1^1
chk2^P6
mus101^D1
CGH
C
Half-maximum distance in DDR mutants
Half-maximum distance (bp)
n.s.
30B
34B
62D
66D
7F
wild type
H2Av^ΔCT
chk1^1
chk2^P6
mus101^D1
D
DAFC-66D origin
stage 13
stage 10B
copy number
wild type
mus101^D1
H2Av^ΔCT
chk11
chk2^P6
ligIV^169
spnA^093
brca2^KO

Figure 6. CGH reveals impaired replication fork progression at every *DAFC* in DDR mutants

(A) The half-maximum distance was calculated in $chk2^{P6}/CyO$ heterozygous siblings of $chk2^{P6}$ and compared to *OrR* wild type for each *DAFC*. All $chk2^{P6}/CyO$ half-maximum distances were statistically the same as *OrR*. The $chk2^{P6}/CyO$ heterozygotes are significantly different from $chk2^{P6}$ at three of the five *DAFCs*. Significance measured by the Dunnett test for multiple comparisons, asterisks indicate $p<0.05$.

(B) DNA from stage 13 egg chambers was competitively hybridized with diploid embryonic DNA to microarrays with approximately one probe every 125bp. Chromosomal position is plotted on the x-axis, the log2 ratio of stage 13 DNA to embryonic DNA is plotted on the y-axis. Copy number decreases more rapidly at all *DAFCs* in each mutant background compared to wild type.

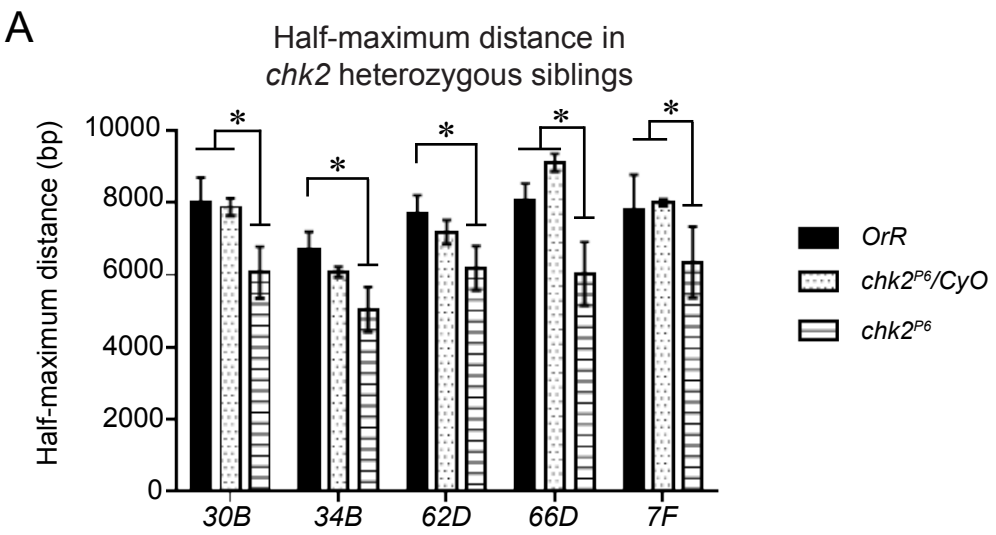
A
Half-maximum distance in
chk2 heterozygous siblings
Half-maximum distance (bp)
10000
8000
6000
4000
2000
0
30B
34B
62D
66D
7F
OrR
chk2P6/CyO
chk2P6

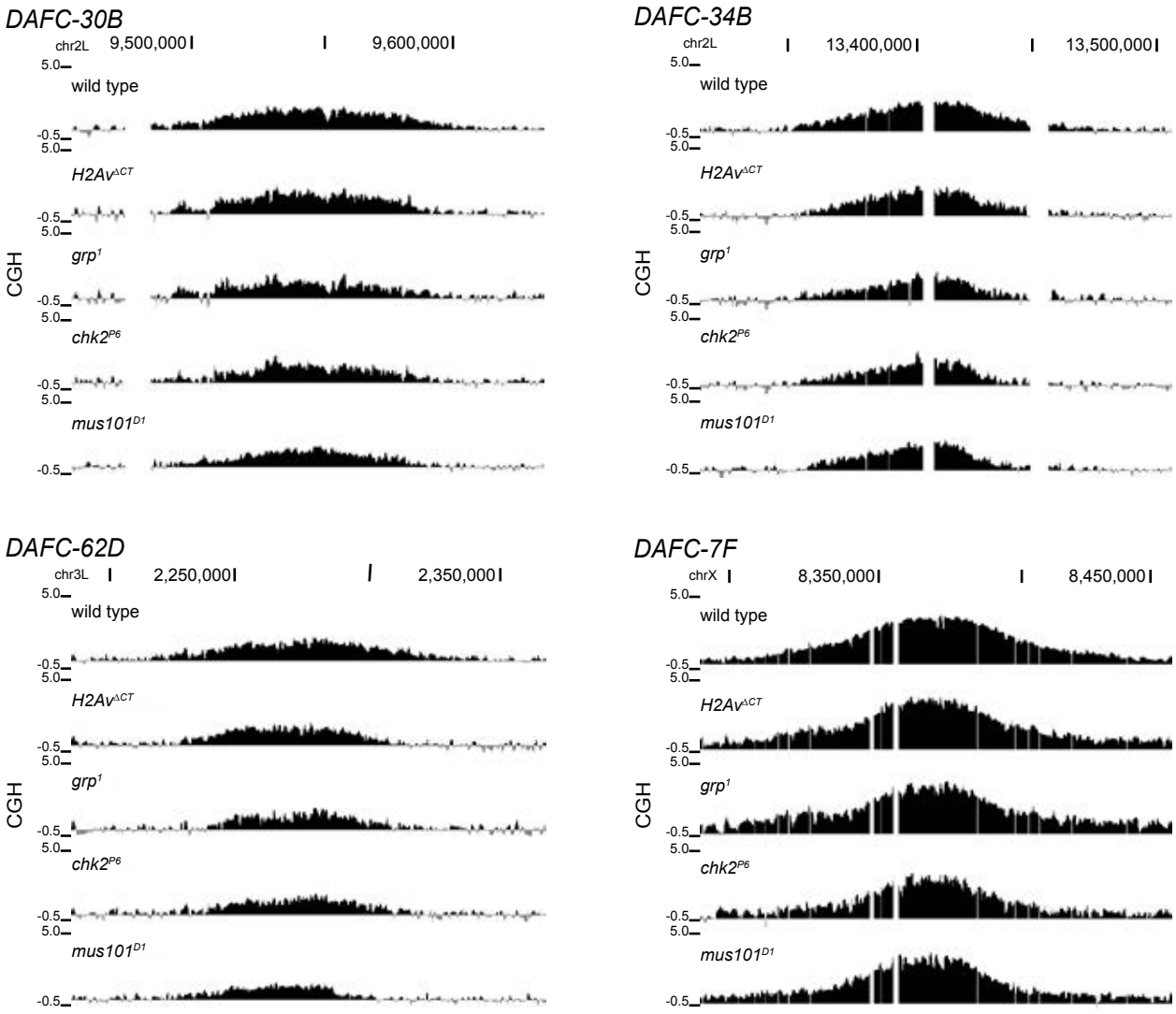
B
DAFC-30B
chr2L 9,500,000 9,600,000
DAFC-34B
chr2L 13,400,000 13,500,000
DAFC-62D
chr3L 2,250,000 2,350,000
DAFC-7F
chrX 8,350,000 8,450,000
wild type
H2Av^ΔCT
grp1
chk2P6
mus101D1
CGH
5.0
-0.5

CGH analysis was done for a collection of mutants previously shown to be involved in various stages of the DDR: *H2Av*$^{\Delta CT}$, *mus101*^{D1}, *chk1*^{1} and *chk2*^{P6} (Madigan *et al.* 2002, Harper & Elledge 2007, Kondo & Perrimon 2011). To measure fork progression quantitatively, we calculated the half-maximum distance for each *DAFC* from the wild-type and DDR mutant CGH data. The half-maximum distance is the number of basepairs between the left and right position of half-maximal copy number. Since inhibited fork movement causes a more rapid decrease in copy number, a reduced half-maximum distance indicates fork progression is impeded. The half-maximum distance was significantly reduced at nearly all *DAFCs* in the *H2Av*$^{\Delta CT}$, *mus101*^{D1}, *grp*^{1} (*chk1)*^{1} and *chk2*^{P6} mutant follicle cells (Fig. 5B-C, 6B). Together these results show that impairing the DNA checkpoint prevents complete fork progression, suggesting that checkpoint-mediated fork stabilization and repair are utilized during re-replication.

One site, *DAFC-30B*, does not exhibit a significant decrease in the half-maximum distance in *H2Av*$^{\Delta CT}$ or *chk1*^{1} (Fig. 5C). This site only undergoes two origin firings before the completion of stage 10B (Claycomb *et al.* 2004). It is likely that because this site completes re-replication at the earliest stages, these forks have enough time to repair and progress close to the wild-type distance by stage 13 even when DDR signaling is dampened.

It is well established that activation of Chk1 during S-phase prevents late origin firing (Abbas & Dutta 2013). However, the number of origin firings at each *DAFC* was unaffected by loss of Chk1 (Fig. 5D). It has been shown that Chk1 does not globally block origin firing, but rather limits new initiations to origins nearby stressed replication forks (Ge & Blow 2010). Therefore, it is not surprising that activation of the DNA damage checkpoint does not influence origin activation at the *DAFCs*. It is more likely that amplification results from the ability of

these origins to escape re-initiation controls, rather than inactivity of the DNA damage checkpoint.

Double-strand break repair is required for continued fork progression during re-replication

To elucidate the mechanism of repair, fork progression was measured in mutants known to be defective in specific repair pathways. The half-maximum distance was measured in the null mutants $spnA^{093}$ (*Rad51* homolog) (Staeva-Vieira *et al.* 2003) and $brca2^{KO}$ (Klovstad *et al.* 2008) to test the role of homologous recombination (HR), and $ligIV^{169}$ (McVey *et al.* 2008) to examine nonhomologous end joining (NHEJ) in repair after re-replication. We found that the half-maximum distance at each *DAFC* was significantly decreased in $ligIV^{169}$, but not $spnA^{093}$ or $brca2^{KO}$ follicle cells (Fig. 7, 8B). We demonstrated the effect was specific to loss of *ligIV* by testing the parental strain in which the excision was generated (Fig. 8). These results indicate HR is dispensable, whereas NHEJ is utilized for DSB repair during re-replication. The dependence of fork progression on DSB repair machinery further demonstrates that re-replication generates DSBs at the active replication forks, and these breaks must be repaired for subsequent forks to continue elongating.

The half-maximum measurements from DDR and *ligIV* mutants show only a 25-30% decrease in fork progression at each re-replicated site, rather than a complete replication block. There are two possible explanations for this effect: 1) each signaling and repair component is required to repair 30% of breaks that form on every copy of re-replicated DNA; or 2) DSBs are generated on 30% of the amplified strands. The former explanation seems unlikely for this collection of mutants, which represent diverse functions at different stages of DNA damage

Figure 7. LigIV is utilized for DSB repair during re-replication.

(A) CGH of *DAFC-66D* reveals impaired replication fork progression in the $ligIV^{169}$, but not the $spnA^{093}$ or $brca2^{KO}$ mutants. DNA from stage 13 egg chambers was competitively hybridized with diploid embryonic DNA to microarrays with approximately one probe every 125bp. Chromosomal position is plotted on the x-axis, the log2 ratio of stage 13 DNA to embryonic DNA is plotted on the y-axis.

(B) The half-maximum distance was calculated in the wild-type and mutant backgrounds for each *DAFC*. Each half-maximum value is the average of three biological replicates. Significance measured by the Dunnett test for multiple comparisons, asterisks indicate $p<0.05$. The $spnA^{093}$ and $brca2^{KO}$ mutants are not significantly different from wild type.

A

DAFC-66D

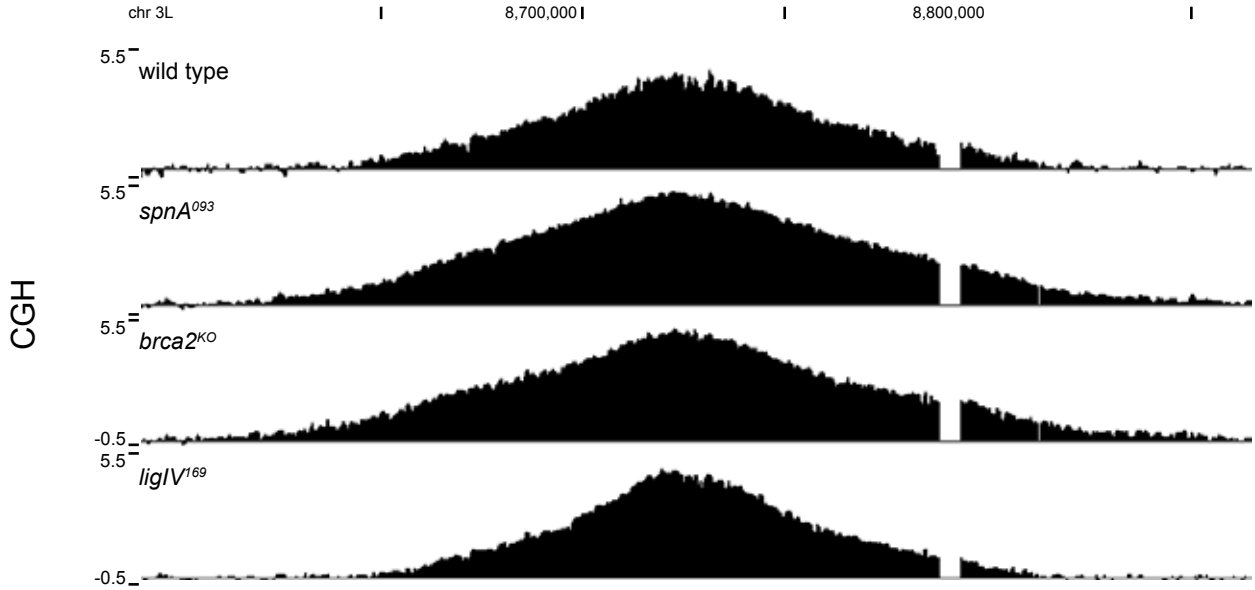
chr 3L
8,700,000
8,800,000
CGH
5.5
wild type
5.5
spnA093
5.5
brca2KO
-0.5
5.5
ligIV169
-0.5

B

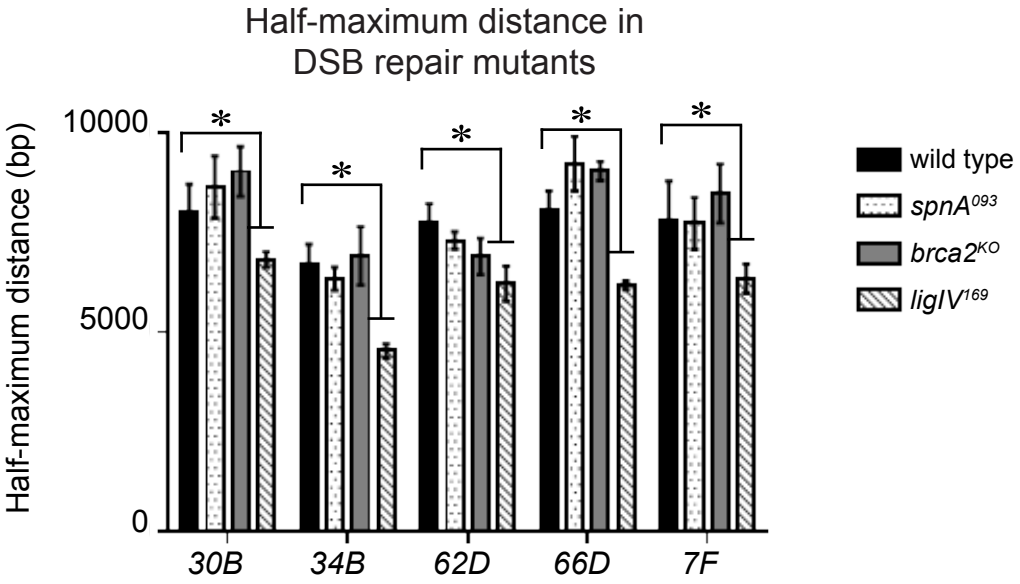
Half-maximum distance in
DSB repair mutants
Half-maximum distance (bp)
10000
5000
0
*
30B
34B
62D
66D
7F
wild type
spnA093
brca2KO
ligIV169

Figure 8. CGH reveals impaired replication fork progression at every *DAFC* in a *ligIV* mutant

(A) The half-maximum distances were calculated in the *P*-element insertion strain $DNL4^{EP10385}$ used to generate $ligIV^{169}$. The half-maximum distance is significantly different at each *DAFC* between the two lines, confirming reduced fork progression in $ligIV^{169}$ is not a feature of the strain background. Significance measured by the Sidak test for multiple comparisons, asterisks indicate $p<0.05$.

(B) DNA from stage 13 egg chambers was competitively hybridized with diploid embryonic DNA to microarrays with approximately one probe every 125bp. Chromosomal position is plotted on the x-axis, the log2 ratio of stage 13 DNA to embryonic DNA is plotted on the y-axis. Copy number decreases more rapidly at all *DAFCs* in the $ligIV^{169}$ mutant, whereas $spnA^{093}$ and $brca2^{KO}$ resemble the wild-type gradient.

A

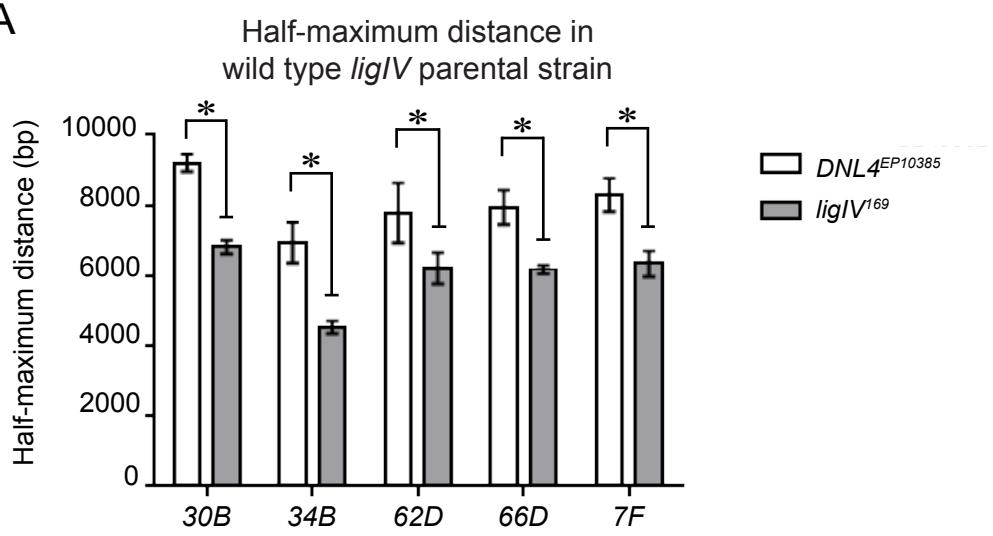
Half-maximum distance in
wild type *ligIV* parental strain
Half-maximum distance (bp)
10000
8000
6000
4000
2000
0
*
30B
34B
62D
66D
7F
DNL4EP10385
ligIV169

B

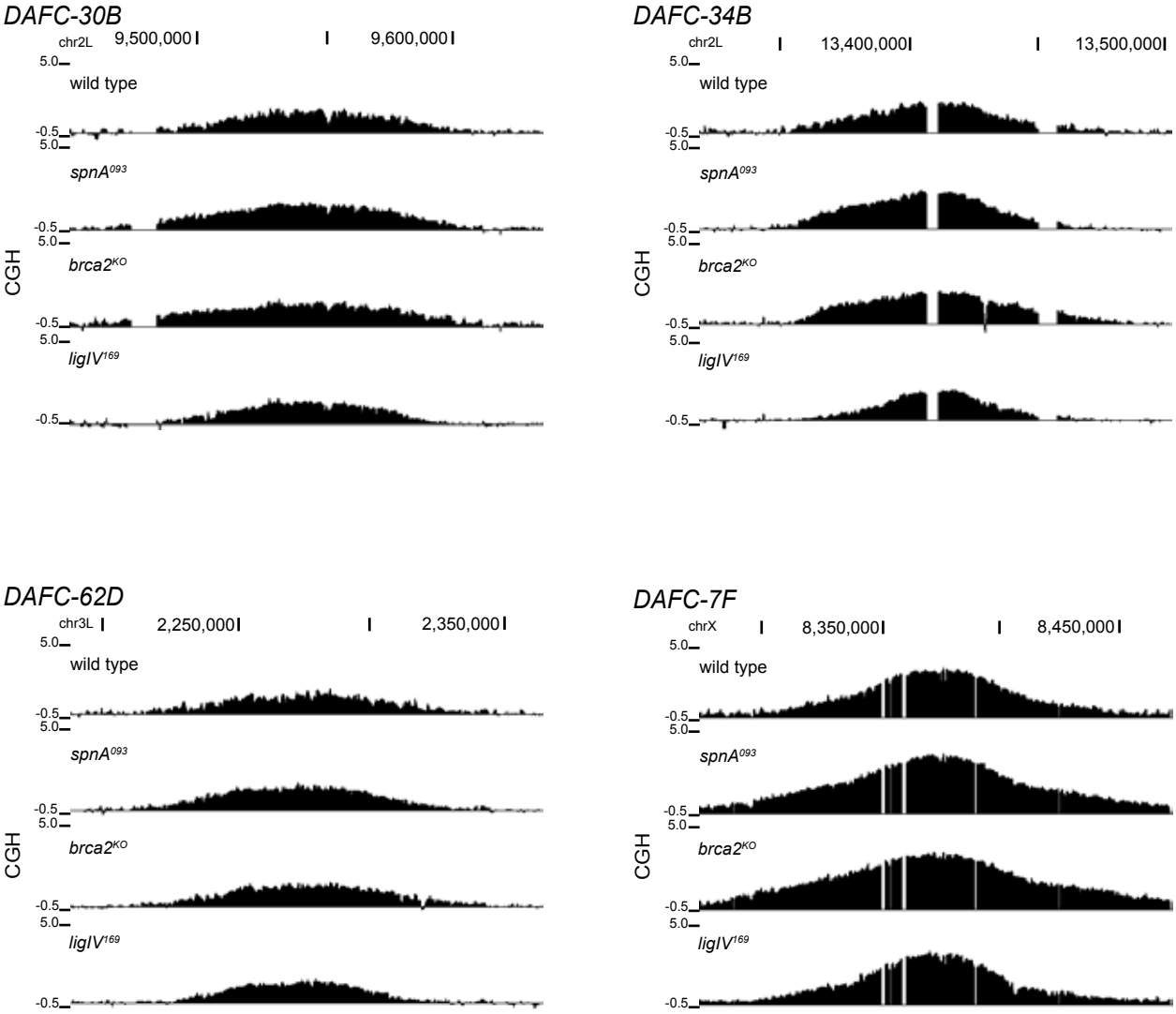
DAFC-30B
chr2L
9,500,000
9,600,000
DAFC-34B
chr2L
13,400,000
13,500,000
DAFC-62D
chr3L
2,250,000
2,350,000
DAFC-7F
chrX
8,350,000
8,450,000
wild type
spnA093
brca2KO
ligIV169
CGH
5.0
-0.5

detection and repair. We therefore prefer the latter argument, which can be explained by replication fork collisions. Such collision events are expected to be stochastic, and will not occur at the same position on each copy of DNA in every cell. Additionally, this variation in break position is averaged across all the copies of amplified DNA in each 16C cell and the approximately 100,000 cells per CGH experiment, explaining why copy number decreases as a gradient rather than a sharp drop at sites of damage. In addition to replication fork collision, it is possible the *DAFC* replication forks are inherently unstable.

Our results indicate that the NHEJ repair pathway is utilized to maintain fork progression at the *DAFCs*, whereas inhibition of HR has no significant effect. These results are supported by a recent study that found deletions within *DAFC-66D* from amplification stage follicles, consistent with end-joining repair (Yarosh & Spradling 2014). HR is often the preferred repair mechanism when homologous sequences are available to copy (Ciccia & Elledge 2010). The follicle cells undergo endocycles prior to amplification, increasing the genome ploidy to 16C (Calvi *et al.* 1998). This increase in genome content, coupled with amplification, provides many identical copies of the *DAFCs* available for HR repair. It was thus initially surprising that the follicle cells instead utilize the mutagenic NHEJ pathway. It is possible that the presence of too many templates is problematic for HR repair, and generates DNA structures that could actually slow repair and fork progression**.** Repair by NHEJ is also much faster than HR (Ciccia & Elledge 2010), allowing the cells to repair the damage as soon as possible so that replication forks can continue. The presence of multiple broken DNA ends within the *DAFCs* would also provide many substrates for NHEJ repair. Additionally, because the follicle cells are sloughed off the oocyte soon after amplification ends, potential mutations produced by NHEJ will not have deleterious effects for the organism. We propose that fast kinetics, coupled to the terminal

differentiation of the follicle cells, make NHEJ the ideal mechanism to repair damage generated during re-replication.

Conclusions

The gene amplification system is a well-established model of DNA replication. We establish for the first time that the gene amplification also is ideal to study how DNA damage is generated and repaired during re-replication. The resolution of the *DAFC* system enabled us to visualize DSBs directly at active forks, providing more direct evidence for the cause-and-effect relationship between re-replication and DSB generation. We show that loss of various checkpoint and repair components impairs fork progression, illustrating that checkpoint signaling is essential for repair of forks that are damaged during re-replication. Additionally, we propose that the *DAFCs* are a model of general fork instability that can be used to elucidate the pathways responsible for maintenance of fork progression under replication stress.

Experimental Procedures

Fly Strains

All experiments were done in the wild-type strain *Oregon-R (OrR)* unless otherwise noted. Analysis of *spnA* was done in a trans-heterozygous combination over a deletion that removes the *spnA* gene: $spnA^{093}/Df(3R)X3F$. The $mus101^{D1}$ allele is a separation of function mutant in which Mus101(TopBP1) can initiate replication but is defective in checkpoint signaling (Kondo & Perrimon 2011). The $mus101^{D1}$, *Df(3R)X3F* and $tefu^{atm-8}$ (Silva *et al.* 2004) stocks were obtained from the Bloomington stock center. The *w,* $P\{w^{+}, H2Av^{\Delta CT}\}$; $H2Av^{810}$ strain (Clarkson 1999) was provided by Kim McKim (Rutgers University). The alleles $spnA^{093}$, grp^{1} and chk^{P6} (Staeva-Vieira *et al.* 2003, Fogarty *et al.* 1994, Abdu *et al.* 2002) were provided by Trudi Schupbach (Princeton

University). The *brca2*^{KO}, *ligIV*^{169} and *DNL4*^{EP10385} (Klovstad *et al.* 2008, McVey *et al.* 2004) alleles were obtained from Mitch McVey (Tufts University). The *mei-41*^{D3} null allele (Laurencon *et al.* 2003) was provided by Norbert Perrimon (Harvard Medical School).

Immunofluorescence and EdU labelling

OrR and *w, P{w*$^{+}$*, H2Av*$^{\Delta CT}$*}; H2Av*^{810} females were fattened for two days on wet yeast at room temperature. Females from the *mei-41*^{D3}*/FM7; tefu*$^{atm-8}$*/TM3* stock were fattened for 3 days at 18°C, then moved to 29°C for 24 hours on fresh wet yeast. All ovaries were dissected in room temperature Grace's media. Ovaries were incubated in 50μM EdU in Grace's media for 30 minutes, fixed in 4% formaldehyde for 15 minutes, then permeabilized in PBX (0.1% TritonX in PBS) for 30 minutes. EdU detection was done using Invitrogen's Click-iT EdU Alexa Fluor 555 Imaging Kit following the manufacturer's instructions. Ovaries were blocked for one hour at room temperature (1% bovine serum albumin, 2% natural goat serum in PBX), then incubated in antibody overnight at 4°C. γH2Av antibody (Rockland, 600-401-914S) and RPA serum (Marton *et al.* 1994) were diluted 1:1000; the mouse monoclonal γH2Av antibody (Lake *et al.* 2013) was diluted 1:2000. FITC-conjugated secondary antibody was used at a concentration of 1:200, followed by DAPI staining.

For DUP immunofluorescence, *OrR* females were fattened for two days on wet yeast at room temperature. Ovaries were dissected in room temperature Grace's media, fixed in 8% paraformaldehyde for 5 minutes, and then permeabilized in PBX (0.1% TritonX in PBS) for 2 hours. Ovaries were blocked for one hour at room temperature (1% bovine serum albumin, 2% natural goat serum in PBX), then incubated at 4°C overnight in 1:1000 γH2Av antibody (Rockland, 600-401-914S) and 1:200 affinity purified guinea pig anti-DUP (Whittaker *et al.*

2000). Ovaries were incubated in 1:200 donkey anti-rabbit-FITC and 1:1000 donkey anti-guinea pig-Cy3, followed by DAPI staining.

Images were captured on a Nikon Eclipse Ti microscope with a Hamamatsu camera and a Nikon Apo TIRF 100× oil objective. Displayed images were deconvolved using the NIS elements software.

ChIP-sequencing

Ovaries were dissected from fattened *OrR* and *w, P{w^{+}, H2Av$^{\Delta CT}$}; H2Av^{810}* females in Grace's media and fixed in 4% formaldehyde for 15 minutes. Stage 10B and 13 egg chambers were sorted by hand and stored at -80°C. A total of 3,000 egg chambers were collected from each stage per ChIP-seq experiment. Two biological replicates were performed for each sample. To isolate follicle cell nuclei, egg chambers were resuspended in 500µL mHB buffer (0.34M sucrose, 15.0 mM NaCL, 60.0 mM KCL, 0.2mM EDTA, 0.2mm EGTA, 0.5% NP-40, 0.15mM spermidine, 0.15mM spermine). Stage 10B egg chambers were dounced 10 strokes, stage 13 egg chambers 20 strokes. Dounced egg chambers were filtered with 40µm nylon filter and spun for 5 minutes at 500 x g (Liu 2012). The follicle cell nuclei pellet was suspended in 300µL ChIP lysis buffer (50mM HEPES/KOH pH 7.5, 140mM NaCl, 1mm EDTA, 1% Triton X-100, 0.1% Na-Deoxycholate). Chromatin was fragmented by sonication in a Biorupter300 (Diagenode) at 4°C for 30 cycles of 30sec on 30sec off at maximum power. Supernatants were incubated overnight in 1:150 γH2Av antibody (Rockland, 600-401-914S). Chromatin was pulled down with Dynabeads magnetic beads (1:1 ratio of A and G beads, ThermoFisher Scientific). Crosslinks were reversed by overnight incubation in 1% SDS at 65°C overnight, and DNA isolated by phenol-chloroform extraction. Libraries were made using the NEBNext Ultra DNA Library Prep

(#E7370) according to the manufacturer's instructions. Libraries were sequenced on the Illumina Hi-Seq 2000.

Reads were mapped with bowtie setting the seed length to 40, using the option "--best", and leaving other settings as default. One kilobase windows were made sliding every 100 nucleotides, and the number of reads overlapping with the windows were counted using "bedtools coverage" (Quinlan & Hall 2010). The number of reads in each window was divided by the millions of reads mapped to obtain reads per million (RPM). The RPM from the ChIP was divided by the RPM of the corresponding input in each window. To avoid divisions by zero, 10^{-6} was added to each RPM value before taking the ratio. The two replicates were summarized by calculating the mean of the $\log_2$ ratios (ChIP/input).

To assess the statistical significance of enrichment at each *DAFC*, the distribution of the $\log_2$ RPM ChIP/input values of the windows across the genome was calculated for stages 10B and 13. The *DAFC* distributions were obtained from the windows overlapping with the area of 70kb (st10B) or 100kb (st13), centered at the origin. Enrichment was quantified by comparing the medians between distributions and statistical significance was determined by the Wilcoxon rank-sum (WRS) test with continuity correction. The same analysis was done for *OrR* and $H2Av^{\Delta CT}$ ChIP samples.

Comparative genome hybridization

Ovaries were dissected from fattened females in Grace's media. Approximately 100 stage 13 egg chambers were hand sorted per experiment and stored at -80°C. *OrR* embryos were collected for 2 hours and stored at -80°C. Egg chambers were thawed in 300µL ChIP lysis buffer and embryos in 1% SDS in TE. All tissues were dounced for 10 strokes using a Type A pestle. DNA

was fragmented by sonication in a Biorupter300 (Diagenode) at 4°C, 10 cycles of 30sec on 30sec off at maximum power. DNA labeling done as previously described (Blitzblau *et al.* 2007). DNA was hybridized to custom Agilent tiling arrays with probes approximately every 125 basepairs. Array intensity was LOESS normalized and smoothed by genomic windows of 500bp using the Ringo package in R (Toedling *et al.* 2007).

The half-maximum distance was calculated from smoothed CGH data. The half-maximum point is the genomic coordinate at which the copy number drops to half of the maximum copy number at the origin. This coordinate was calculated independently for the left and right sides of the amplification gradient, and the distance between these two points is the half-maximal distance. This distance was calculated individually for each replicate at each *DAFC*, and the average values across three biological replicates are displayed. Half-maximum distances from $chk2^{P6}/CyO$ and $DNL4^{EP10385}$ are the average of two biological replicates.

Quantitative real-time PCR

Ovaries were dissected from fattened females in Grace's media. Approximately 60 egg chambers were hand sorted from each stage per experiment and stored at -80°C. Egg chambers were thawed in 300µL ChIP lysis buffer and homogenized. DNA was fragmented by sonication in a Biorupter300 (Diagenode) at 4°C, 10 cycles of 30sec on 30sec off at maximum power. Copy number was measured by relative quantitative PCR using stage 1-8 egg chambers as the calibrator sample and the non-amplified *rosy* locus as the endogenous control.

Accession Numbers

The CGH and ChIP-seq data sets have been deposited in the Gene Expression Omnibus (http://www.ncbi.nlm.nih.gov/geo/). CGH data sets for wild-type controls are under accession numbers GSM432742 and GSM1354444. All mutant CGH and all ChIP-seq data sets are under accession number GSE66691.

Acknowledgements

We thank Brian Hua for sharing unpublished data and for affinity purified DUP antibody. Bioinformatics support was provided by George Bell for CGH half-maximum analysis. Paul Fisher provided the RPA antibody, Scott Hawley and Jeff Sekelsky the γH2Av monoclonal antibody, and Kim McKim, Trudi Schupbach, Mitch McVey, and the Bloomington Stock Center were the sources for Drosophila stocks. Sequencing for ChIP-seq experiments was done by the MIT BioMicro Center. We thank Tom DiCesare for graphics help. We are grateful for helpful comments on the manuscript from Mitch McVey, Steve Bell and Adam Martin. This work was supported by NIH grant GM57940 to Terry Orr-Weaver and the MIT School of Science Fellowship in Cancer Research. Terry Orr-Weaver is an American Cancer Society Research Professor.

References

Abbas, T., Keaton, M.A., Dutta, A. (2013). Genomic instability in cancer. Cold Spring Harb. Perspect. Biol. *5*, a012914.

Abdu U., Brodsky M., Schupbach T. (2002). Activation of a meiotic checkpoint during *Drosophila* oogenesis regulates the translation of Gurken through Chk2/Mnk. Curr. Biol. *12*, 1645-1651.

Bell, S.P., Dutta, A. (2002). DNA replication in eukaryotic cells. Annu. Rev. Biochem. *71*, 333–374.

Blitzblau, H.G., Bell, G.W., Rodriguez, J., Bell, S.P., Hochwagen, A. (2007). Mapping of meiotic single-stranded DNA reveals double-stranded-break hotspots near centromeres and telomeres. Curr. Biol. *17*, 2003-2012.

Byun, T.S., Pacek, M., Yee, M., Walter, J.C., Cimprich, K.A. (2005). Functional uncoupling of MCM helicase and DNA polymerase activities activates the ATR-dependent checkpoint. Genes Dev. *19*, 1040-1052.

Calvi, B. R., Lilly, M.A., Spradling, A.C. (1998). Cell cycle control of chorion gene amplification. Genes Dev. *12*, 734-744.

Ciccia, A. and Elledge, S.J. (2010). The DNA damage response: making it safe to play with knives. Mol. Cell *40*, 179-204.

Clarkson, M.J., Wells, J.R.E., Gibson, F., Saint, R., Tremethick, D.J. (1999). Regions of variant histone His2AvD required for *Drosophila* development. Nature *399*, 694-697.

Claycomb, J.M., MacAlpine, D.M., Evans, J.G., Bell, S.P., Orr-Weaver, T.L. (2002). Visualization of replication initiation and elongation in *Drosophila*. J. Cell Biol. *159*, 225-236.

Claycomb, J.M., Benasutti, M., Bosco, G., Fenger, D.D., Orr-Weaver, T.L. (2004). Gene amplification as a developmental strategy: isolation of two developmental amplicons in *Drosophila*. Dev. Cell *6*, 145-155.

Claycomb, J.M., and Orr-Weaver T.L. (2005). Developmental gene amplification: insights into DNA replication and gene expression. Trends Genet. *21*, 149-62.

Davidson, I.F., Anatoily, L., Blow, J.J. (2006). Deregulated replication licensing causes DNA fragmentation consistent with head-to-tail fork collision. Mol. Cell *24*, 433-443.

Fogarty, P., Kaplin, R., Sullivan, W. (1994). The *Drosophila* maternal-effect mutation *grapes* causes a metaphase arrest at nuclear cycle 13. Development *120*, 2131-2142.

Ge, X.Q. and Blow, J.J. (2010). Chk1 inhibits replication factory activation but allows dormant origin firing in existing factories. J. Cell Biol. *191*, 1285-1297.

Green, B. M., Li. J.J. (2005). Loss of rereplication control in *Saccharomyces cerevisiae* results in extensive DNA damage. Mol. Biol. Cell *16*, 421-432.

Harper, J.W., Elledge, S.J. (2007). The DNA damage response: ten years after. Mol. Cell *28*, 739-745.

Hong, A., Narbonne-Reveau, K., Riesgo-Escovar, J., Fu, H., Aladjem, M. I., Lilly, M. A. (2007). The cyclin-dependent kinase inhibitor Dacapo promotes replication licensing during *Drosophila* endocycles. EMBO J. *26*, 2071-2082.

Jazayeri, A., Falck, J., Lukas, C., Bartek, J., Smith, G.C.M, Lukas, J., Jackson, S.P. (2006) ATM- and cell cycle-dependent regulation of ATR in response to DNA double-strand breaks. Nat. Cell Biol. *8*, 37-45.

Kim, J.C., Nordman, J., Xie, F., Kashevsky, H., Eng, T., Li, S., MacAlpine, D.M., Orr-Weaver, T.L. (2011). Integrative analysis of gene amplification in *Drosophila* follicle cells: parameters of origin activation and repression. Genes Dev. *25*, 1384-1398.

Klovstad, M., Abdu, U., Schüpbach, T. (2008). *Drosophila brca2* is required for mitotic and meiotic DNA repair and efficient activation of the meiotic recombination checkpoint. PLoS Genet. *4*, e31.

Kondo, S., Perrimon, N. (2011). A genome-wide RNAi screen identifies core components of the G_2-M DNA damage checkpoint. Sci. Signal *4*, rs1.

Lake, C.M., Holsclaw, J.K., Bellendir, S.P., Sekelsky, J., Hawley, R.S. (2013). The Development of a monoclonal antibody recognizing the *Drosophila melanogaster* phosphorylated histone H2A variant (γ-H2AV). G3 *3*, 1539-1543.

Laurencon, A., Purdy, A., Sekelsky, J., Hawley, R.S., Su, T.T. (2003). Phenotypic analysis of separation-of-function alleles of *mei-41*, Drosophila ATM/ATR. Genetics *601*, 589-601.

Liu J., McConnell, K., Dixon, M., Calvi, B.R. (2012). Analysis of model replication origins in *Drosophila* reveals new aspects of the chromatin landscape and its relationship to origin activity and the prereplicative complex. Mol. Biol. Cell *23*, 200-212.

Madigan, A.P., Chotkowski, H.L., Glaser, R.L. (2002). DNA double-strand break-induced phosphorylation of *Drosophila* histone variant H2Av helps prevent radiation-induced apoptosis. Nucleic Acids Res. *30*, 3698-3705.

Marton R.F., Thommes P., Cotterill S. **(**1994). Purification and characterization of dRP-A: a single-stranded DNA binding protein from *Drosophila melanogaster*. FEBS Letters *342*, 139-144.

McVey, M., Radut, D., Sekelsky, J.J. (2004). End-joining repair of double-strand breaks in *Drosophila melanogaster* is largely DNA ligase IV independent. Genetics *168*, 2067–2076.

Mehrotra, S., Maqbool, S. B., Kolpakas, A., Murnen, K., Calvi, B. R. (2008). Endocycling cells do not apoptose in response to DNA rereplication genotoxic stress. Genes Dev. *22*, 3158-3171.

Melixetian, M., Ballabeni, A., Masiero, L., Gasparini, P., Zamponi, R., Bartek, J., Lukas, J., Helin, K., (2004). Loss of Geminin induces rereplication in the presence of functional p53. J. Cell Biol. *165*, 473-482.

Mihaylov, I.S., Kondo, T., Jones, L., Ryzhikov, S., Tanaka, J., Zheng, J., Higa, L. A., Minamino, N., Cooley, L., Zhang, H. (2002). Control of DNA replication and chromosome ploidy by Geminin and Cyclin A. Mol. Cell. Biol. *22*, 1868-1880.

Nordman, J., Li, S., Eng, T., MacAlpine, D., Orr-Weaver, T.L. (2011). Developmental control of the DNA replication and transcription programs. Genome Res. *21*, 175-181.

Park, E.A., MacAlpine, D. M., Orr-Weaver, T.L. (2007) *Drosophila* follicle cell amplicons as models for metazoan DNA replication: a *cyclinE* mutant exhibits increased replication fork elongation. Proc. Natl. Acad. Sci. USA *104*, 16739-16746.

Quinlan, A.R., Hall, I.M. (2010). BEDTools: a flexible suite of utilities for comparing genomic features. Bioinformatics *26*, 841-842.

Silva, E., Tiong, S., Pedersen, M., Homola, E., Royou, A., Fasulo, B., Siriaco, G., Campbell, S.D. (2004). ATM is required for telomere maintenance and chromosome stability during *Drosophila* development. Curr. Biol. *14*, 1341-1347.

Spradling A.C., Mahowald A.P. (1980). Amplification of genes for chorion proteins during oogenesis in *Drosophila melanogaster*. Proc. Natl. Acad. Sci. USA *77*, 1096-1100.

Staeva-Vieira, E., Yoo, S., Lehmann, R. (2003). An essential role of DmRad51/SpnA in DNA repair and meiotic checkpoint control. EMBO J. *22*, 5863-5874.

Toedling, J., Skylar, O., Krueger, T., Fischer, J.J., Sperling, S., Huber, W. (2007). Ringo—an R/Bioconductor package for analyzing ChIP–chip readouts. BMC Bioinformatics *8*,. doi: 10.1186/1471-2105-8-221.

Whittaker, A.J., Royzman, I., Orr-Weaver, T.L. (2000). *Drosophila* Double parked: a conserved, essential replication protein that colocalizes with the origin recognition complex and links DNA replication with mitosis and the down-regulation of S phase transcripts. Genes Dev *14*, 1765-1776.

Yarosh, W., Spradling, A.C. (2014). Incomplete replication generates somatic DNA alterations within *Drosophila* polytene salivary gland cells. Genes Dev. *28*, 1840-1855.
Zhu, W., Chen, Y., Dutta, A. (2004). Rereplication by depletion of Geminin is seen regardless of p53 status and activates a G2/M checkpoint. Mol. Cell. Biol. *16*, 7140-7150.

Chapter Four:
Several Mechanisms contribute to Double-Strand Break Repair during Re-replication

Jessica L. Alexander[1], Kelly Beagan[2], Mitch McVey[2], Terry L. Orr-Weaver[1]

[1]Whitehead Institute for Biomedical Research, and Dept. of Biology, MIT, 9 Cambridge Center, Cambridge, MA 02142, USA
[2]Department of Biology, Tufts University, 200 Boston Ave., Medford, MA 02155

Jessica L. Alexander and Kelly Beagan performed the *ligIV; mus308* qPCR and CGH for *ku80*, *ku70*, *mus308* and *ligIV; mus308*
Jessica L. Alexander performed all other experiments and analysis

Abstract

Re-replication generates double-strand breaks (DSBs) at sites of fork collisions and causes a variety of genomic damage including chromosome breakage, fusions, repeat expansion and aneuploidy. However, the primary mechanism used to repair re-replication DSBs varies across different experimental systems. Additionally, repair pathway choice appears to contribute to the nature and severity of chromosome aberrations caused by re-replication events. Using developmentally regulated re-replication in the Drosophila follicle cells, we have tested the role of several repair pathways using re-replication fork progression as a readout for DSB repair efficiency. We previously reported that fork progression is reduced in $ligIV^{169}$ null mutants, indicating nonhomologous end joining (NHEJ) is required for efficient DSB repair. Here we show that the Ku70-80 heterodimer, the essential upstream NHEJ complex, is dispensable for fork progression at most re-replication sites. This suggests resection-mediated pathway(s) efficiently repair DSBs when Ku70-80 resection inhibition is alleviated. We find that microhomology-mediated end joining, which requires limited DSB resection, restores fork progression in the absence of NHEJ in a site-specific manner. Conversely, we find that fork progression is enhanced in the absence of both Drosophila Rad51 homologs, *spnA* and *spnB*, revealing homologous recombination repair is active during follicle cell re-replication, but inhibits fork elongation. In addition, mutants in two break-induced replication components also exhibit reduced fork progression. Therefore, we find that several DSB repair pathways are active during re-replication in the follicle cells and their contribution to productive fork progression is influenced by the genomic position, reaction kinetics and repair pathway competition.

Introduction

Re-replication generates double-strand breaks (DSBs) (Green & Li 2005, Davidson *et al.* 2006, Zhu & Dutta 2006, Finn & Li 2013, Neelsen *et al.* 2013, Alexander *et al.* 2015) and can lead to DNA fragmentation, chromosome breakage and fusions, repeat expansion and an increased rate of chromosome missegregation (Melixetian *et al.* 2004, Green & Li 2005, Davidson *et al.* 2006, Green *et al.* 2010, Finn & Li 2013, Neelsen *et al.* 2013, Hanlon & Li 2015). These types of genomic damage are commonly observed across multiple types of human cancers (Abbas & Dutta 2013). Re-replication can be induced experimentally by Cdt1 overexpression or depletion of its inhibitor Geminin (Mihaylov *et al.* 2002, Vaziri *et al.* 2003, Melixetian *et al.* 2004, Thomer *et al.* 2004, Zhu *et al.* 2004, Arias & Walter 2005, Li & Blow 2005, Maiorano *et al.* 2005, Davidson *et al.* 2006). Overexpression of Cdt1 also drives oncogenic transformation in cell culture and is observed in various human cancers cell lines (Arenston *et al.* 2002, Karakaidos *et al.* 2004, Xouri *et al.* 2004, Seo *et al.* 2005). Thus re-replication events may very well be a source of gene amplification and chromosome aberrations seen in cancer cells, and thus a major driving force in cancer progression.

Although the damage associated with re-replication has been widely observed, the reported mechanism of DSB repair varies across the literature. 53BP1, which promotes nonhomologous end joining (NHEJ) and inhibits homologous recombination (HR) (Ceccaldi *et al.* 2016), forms distinct foci when re-replication is induced (Neelson *et al.* 2013). Others report Rad51 foci in re-replicating cells (Melixetian *et al.* 2004, Zhu & Dutta 2006) or a genetic requirement for HR genes for repair and cell survival after re-replication (Archambault *et al.* 2005, Truong *et al.* 2014). Interestingly, microhomology-mediated end joining (MMEJ) also was shown to be utilized for repair, although to a lesser degree than HR (Truong *et al.* 2014).

The preferred pathway for DSB repair is largely governed by cell cycle stage (Ceccaldi *et al.* 2016). HR is promoted by S-CDK activity and thus is utilized during S and G2-phases of the cell cycle (Ceccaldi *et al.* 2016), consistent with the timing of re-replication events. NHEJ is active throughout the cell cycle, but is preferred during G0/G1 when there is no competition from HR (Ceccaldi *et al.* 2016). Pathway choice is ultimately the result of competition between repair proteins for DSB substrates, and the winner is influenced by availability and activity of pathway components. Studies in budding yeast demonstrate that HR and NHEJ compete for DSB repair after re-replication (Hanlon & Li 2015). The authors found that the frequency of aneuploidy is increased when re-replication is induced near a centromere and relies on the HR pathway for missegregation (Hanlon & Li 2015). This frequency is tripled in a NHEJ mutant, indicating that both HR and NHEJ repair re-replication DSBs (Hanlon & Li 2015). It is likely that HR and NHEJ, as well as other repair pathways, compete for DSB substrates generated by re-replication in other model systems as well.

Repair pathway choice may also be influenced by the structure of the DSB. Re-replication is predicted to generate single-sided DSBs (ssDSBs) when head-to-tail forks collide (Abbas & Dutta 2013). Break-induced replication (BIR) can be utilized for DSB repair when there is homology to only one side of the break and establishes a single replication fork (Malkova *et al.* 1996, 2005, Signon *et al.* 2001), making this pathway an interesting possibility for repair of ssDSBs (Kraus *et al.* 2001, Abbas & Dutta 2013). Additionally, most BIR events require Rad51 (Signon et al. 2001, Davis & Symington 2004); therefore reported genetic requirements for Rad51 (Truong *et al.* 2014) and Rad51 foci formation (Melixetian *et al.* 2004, Zhu & Dutta 2006) during re-replication may reflect BIR rather than or in addition to HR activity.

Here we utilize the Drosophila ovarian follicle cells, which exhibit re-replication under

precise developmental control, to define the mechanisms of DSB repair required to maintain fork elongation during re-replication. Re-replication occurs at six loci, termed *Drosophila Amplicons in Follicle Cells* (*DAFCs*). The *DAFCs* have specific replication origins that utilize the same machinery as the canonical S-phase (Claycomb & Orr-Weaver 2005). Bidirectional fork movement away from the origin produces a gradient of amplified DNA spanning approximately 100kb at each *DAFC* (Claycomb *et al.* 2004, Kim *et al.* 2011). The follicle cells are somatic cells of the ovary, and are one of three cell types that constitute the egg chamber. Drosophila egg chambers are divided into developmental stages based on their distinct morphologies, each of which lasts for a defined period of time. This enables isolation of the follicle cells at specific times in development by ovary dissection. Origin firing at the *DAFCs* begins at a specific developmental stage, 10B, across all follicle cells of a given egg chamber in the absence of genome-wide replication (Calvi *et al.* 1998). The precise timing of origin firing permits identification of replication forks at defined points after replication initiation, allowing real-time tracking of fork progression (Claycomb *et al.* 2002, Park *et al.* 2007). Defined timing of replication initiation also enables fork progression to be compared between different mutant lines, making it possible to dissect the pathways involved in maintaining fork elongation after re-replication events.

Unrepaired DSBs within the *DAFCs* will block all subsequent replication forks on the same strand from moving beyond the break site. Therefore, removal of DSB repair pathways utilized during re-replication will reduce overall fork progression. We previously found that fork progression at the *DAFCs* is reduced in the $ligIV^{169}$ null mutant (Alexander *et al.* 2015). This suggests that NHEJ is required to efficiently repair DSBs at damaged re-replication forks in order to maintain continued fork progression. To further characterize the role of NHEJ in re-

replication DSB repair, we measured fork progression in the absence of the Ku70-80 heterodimer. We find that fork progression is unaffected by loss of Ku70-80 at most *DAFCs*, indicating resection-mediated pathways compensate for loss of NHEJ. End-joining repair via MMEJ requires limited DSB resection (Chiruvella *et al.* 2013, Truong *et al.* 2013); although loss of the MMEJ component *mus308* does not globally impact fork progression, we find that simultaneously removing both NHEJ and MMEJ drastically impairs fork progression at two of the five *DAFCs*. In addition, we show that the HR pathway is activated at the *DAFCs* but is inhibitory to fork progression. Together, these results demonstrate that multiple mechanisms contribute to DSB repair during re-replication in the follicle cells. We propose that the extent of fork progression reflects both the kinetics of repair and competition between DSB repair pathways.

Results

End-joining repair is required for continued fork progression during re-replication

To determine which DSB repair mechanisms are required during re-replication, we measured fork progression in several end-joining repair mutants using Comparative Genomic Hybridization (CGH) paired with half-maximum distance analysis. This analysis uses CGH to measure copy number across each of the *DAFCs*, followed by calculating the distance between the left and right sides of half-maximum copy number. Reduced fork progression results in a more rapid decrease in copy number and therefore lower half-maximum values (Alexander *et al.* 2015).

To further test the requirement for NHEJ repair during re-replication, we measured fork progression in *ku70* and *ku80* null mutants. Ku70 and Ku80 initiate the NHEJ pathway by

binding the two broken ends of a DSB and blocking resection-mediated repair (Ceccaldi *et al.* 2016). To our surprise, the half-maximum distance is significantly reduced in both *ku70* and *ku80* at only one of the five sites, *DAFC-62D* (Fig. 1A, left). This result indicates that loss of *ku* gene function affects fork progression in a site-specific manner, unlike the *ligIV* mutant in which fork progression was equally reduced at all sites of re-replication (Alexander *et al.* 2015). We hypothesize that this discrepancy is due to where these components act in the NHEJ pathway. Ligase IV is essential for the final step of NHEJ to ligate the broken DNA ends together; therefore the *ligIV* mutant fails to repair DSBs at the final step of the pathway, slowing DSB repair and consequently fork progression. Conversely, in the absence of the Ku70-80 heterodimer, NHEJ cannot be initiated and a resection-mediated pathway is utilized instead (Ceccaldi *et al.* 2016). However, the reduced half-maximum distance at *DAFC-62D* in *ku70* and *ku80* indicates the alternative to NHEJ does not efficiently repair DSBs at all sites, suggesting the back-up pathway may exhibit site specificity.

MMEJ is an alternative mechanism of end-joining repair that does not rely on classical NHEJ factors. MMEJ requires limited resection using the same initial machinery as HR to expose single-stranded DNA ends (Truong *et al.* 2013). MMEJ requires DNA Polymerase θ (Pol θ), encoded by *mus308* in Drosophila (Chan *et al.* 2010, Kent *et al.* 2015, Mateos-Gomez *et al.* 2015). Pol θ binds to ssDNA on both ends of a DSB and aligns short 4-10bp microhomology sequences (Chan *et al.* 2010, Kent *et al.* 2015). Suitable microhomologies can also be generated by Pol θ, resulting in insertions templated from sequences outside the break site (Chan *et al.* 2010, Yu & McVey 2010, Hogg *et al.* 2012, Kent *et al.* 2015). To test the role of Mus308-mediated repair during re-replication, we measured fork progression at the *DAFCs* in a *mus308* null mutant, $mus308^{null}$. The half-maximum distance is not significantly reduced compared to

Figure 1. **MMEJ can compensate for loss of NHEJ to repair re-replication DSBs in a site-specific manner**

(A) The half-maximum distance was calculated in the wild-type and mutant backgrounds for each *DAFC*. (left) Half-maximum distances of NHEJ mutants are compared to wild-type. (right) *mus308* and *ligIV* distances are compared to wild-type, *ligIV; mus308* distances are compared to *ligIV*. All *ligIV; mus308* distances are significantly reduced compared to wild-type. Significance was measured by the Dunnett test for multiple comparisons, asterisks indicate $p<0.05$.

(B) CGH at *DAFC-7F* in wild-type and repair mutants. DNA from stage 13 egg chambers was competitively hybridized with diploid embryonic DNA to microarrays with approximately one probe every 125bp. Chromosomal position is plotted on the x-axis, the log2 ratio of stage 13 DNA to embryonic DNA is plotted on the y-axis.

A

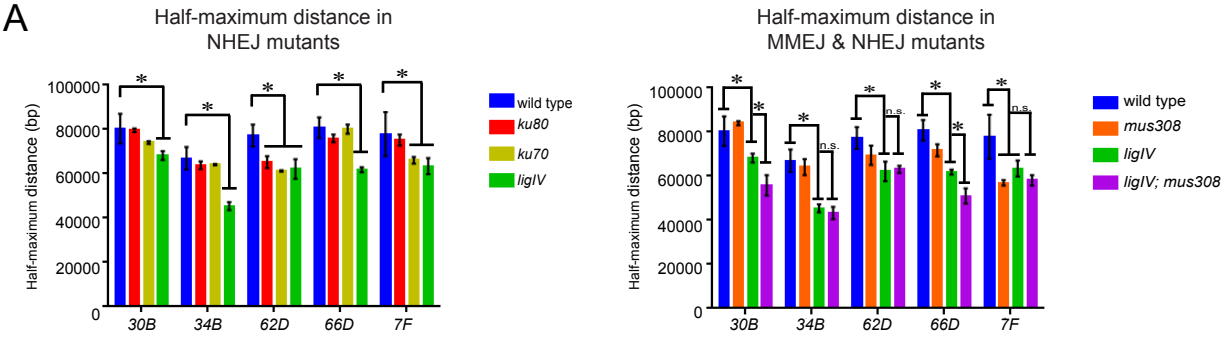
Half-maximum distance in NHEJ mutants
Half-maximum distance (bp)
100000
80000
60000
40000
20000
0
30B
34B
62D
66D
7F
wild type
ku80
ku70
ligIV
Half-maximum distance in MMEJ & NHEJ mutants
n.s.
wild type
mus308
ligIV
ligIV; mus308

B

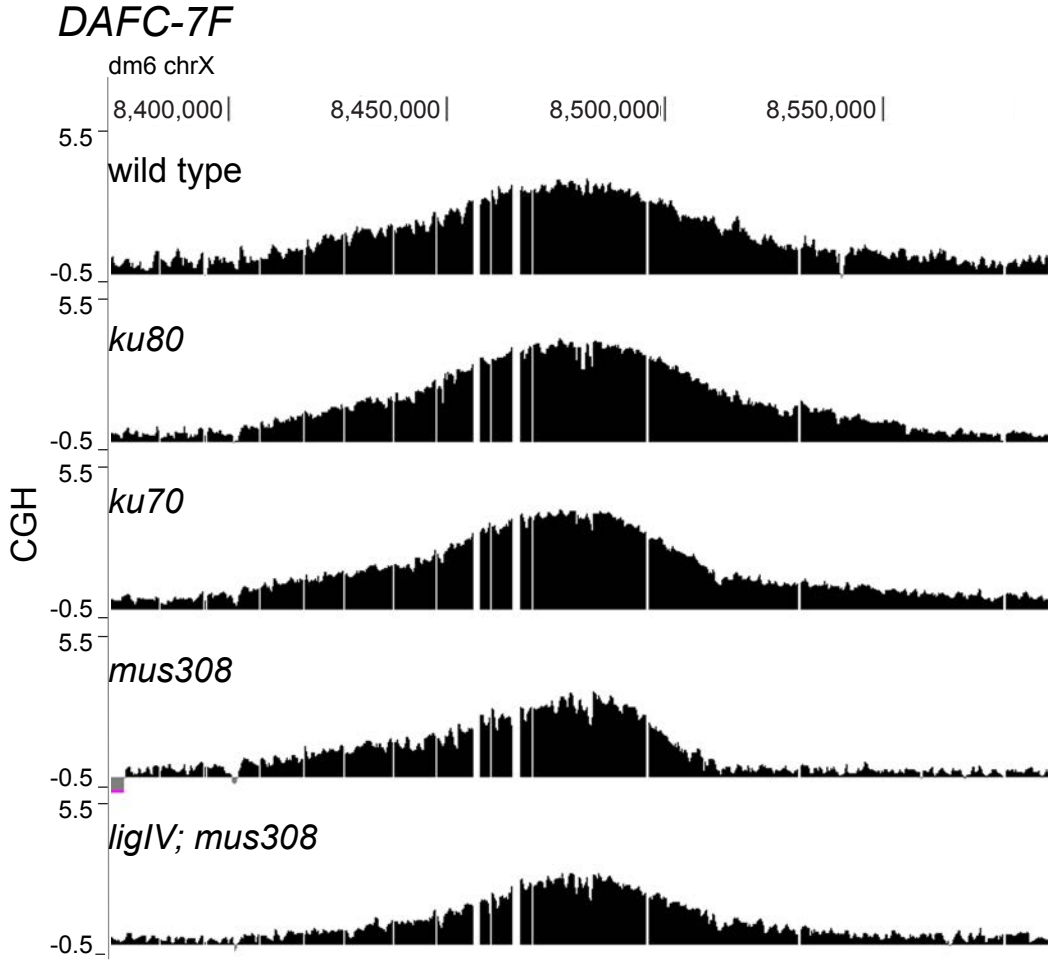
DAFC-7F
dm6 chrX
8,400,000
8,450,000
8,500,000
8,550,000
CGH
5.5
-0.5
wild type
ku80
ku70
mus308
ligIV; mus308

wild-type *OrR* at any of the sites except *DAFC-7F* (Fig. 1A, right). This suggests that the Mus308 pathway is not the primary mechanism of DSB repair at most of the *DAFCs*.

The reduced-half maximum at *DAFC-7F* in *mus308* is caused by an asymmetric decrease in the gradient, in which the copy number decreases more rapidly on the right side of *DAFC-7F* (Fig. 1B). Interestingly, the half-maximum distance is significantly reduced at *DAFC-7F* in the *ku70*, but not the *ku80* mutant; this is due an asymmetric decrease in copy number at the same position observed in *mus308* (Fig. 1B). It therefore seems that this locus is particularly sensitive to loss of repair components that do not affect fork progression at all or most other positions.

The *mus308* half-maximum distances reveal that the MMEJ pathway is not the primary DSB repair mechanism during re-replication. This is supported by previous results showing that absence of *ligIV* alone is sufficient to reduce fork progression at all *DAFCs* (Alexander *et al.* 2015). However, the fact that fork progression is reduced but not completely halted in *ligIV* mutants suggests there is another repair mechanism that is activated when NHEJ fails. This is also supported by the results in *ku70* and *ku80* discussed above. To test if MMEJ can repair re-replication induced DSBs in the absence of NHEJ, we measured fork progression at the *DAFCs* in a *ligIV; mus308* double-mutant. We found that the half-maximum distance is significantly reduced compared to the *ligIV* single mutant at two of *DAFCs*, whereas the other three sites are not significantly different from *ligIV* (Fig. 1A, right) (note that all five sites have a reduced half-maximum distance compared to wild-type). These results indicate that the MMEJ pathway efficiently repairs DSBs in the absence of NHEJ at some, but not all of the *DAFCs*. It is noteworthy that that *DAFC-62D* and *DAFC-7F*, the only two sites that require *ku80* and/or *ku70* for complete fork progression, are unaffected by the additional loss of *mus308* in a *ligIV* null

background. These results suggest that DSB repair at *DAFC-62D* and *DAFC-7F* is especially dependent on the NHEJ pathway.

The CGH measurements show that copy number at the *DAFC* origins is reduced in *ligIV; mus308*, indicating there are fewer origin firing events in the double-mutant (Fig. 1B, 2). To confirm that the reduced half-maximum distances are not due to a delay in origin firing, we measured copy number at the *DAFCs* over development by qPCR. We found that although the total copy number is reduced, the proper timing of origin firing is maintained (Fig. 3). Therefore, the half-maximum distances in *ligIV; mus308* reflect fork progression.

Repair by homologous recombination inhibits follicle cell re-replication fork progression

We previously found that fork progression is not decreased in *spnA/Rad51* or *brca2* null follicle cells, from which we concluded that HR is not utilized for repair at the *DAFCs*. However, the Drosophila genome contains two Rad51 homologs: the ubiquitously-expressed gene *spnA* (Staeva-Vieira *et al.* 2003) and the ovary-specific gene *spnB* (Ghabrial *et al.* 1998). The only previously known role for SpnB was in meiotic DSB repair in the oocyte (Ghabrial *et al.* 1998). To be confident that we were measuring fork progression in the complete absence of Rad51 activity, we performed CGH and measured the half-maximum distance across each *DAFC* in *spnA, spnB* double-mutant follicle cells. We found fork progression is ***increased*** at all *DAFCs* in the double-mutant, although this increase is statistically significant at only three of the five *DAFCs*: *DAFC-30B*, *-66D* and *-7F* (Fig. 4). Additionally, re-analysis of all HR mutant data revealed that the half-maximum distance is also significantly increased in *brca2* follicle cells at these same three sites, and at *DAFC-66D* in *spnA* single mutants (Fig. 4). These results

Figure 2. CGH across all *DAFCs* in NHEJ and MMEJ mutants

CGH at *DAFC-30B, -34B, -62D* and *-66D* in wild-type and repair mutants. DNA from stage 13 egg chambers was competitively hybridized with diploid embryonic DNA to microarrays with approximately one probe every 125bp. Chromosomal position is plotted on the x-axis, the log2 ratio of stage 13 DNA to embryonic DNA is plotted on the y-axis.

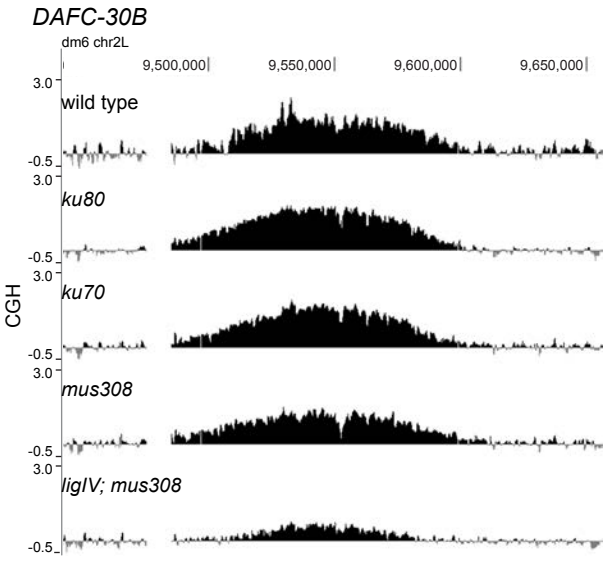
DAFC-30B
dm6 chr2L
9,500,000
9,550,000
9,600,000
9,650,000
wild type
ku80
ku70
mus308
ligIV; mus308
CGH
3.0
-0.5

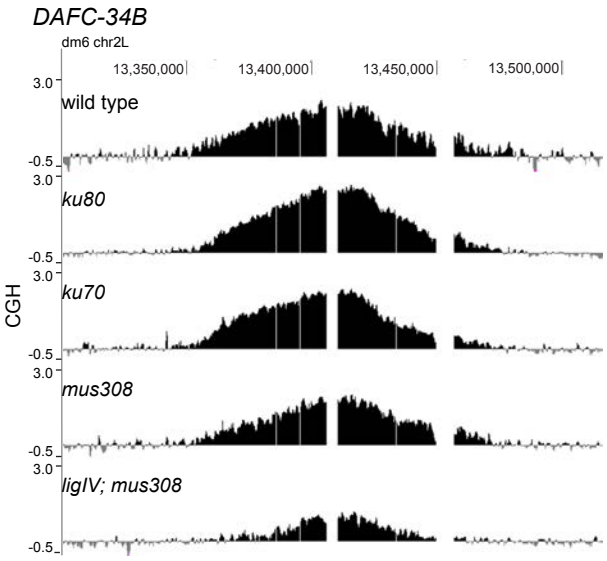
DAFC-34B
dm6 chr2L
13,350,000
13,400,000
13,450,000
13,500,000
wild type
ku80
ku70
mus308
ligIV; mus308
CGH
3.0
-0.5

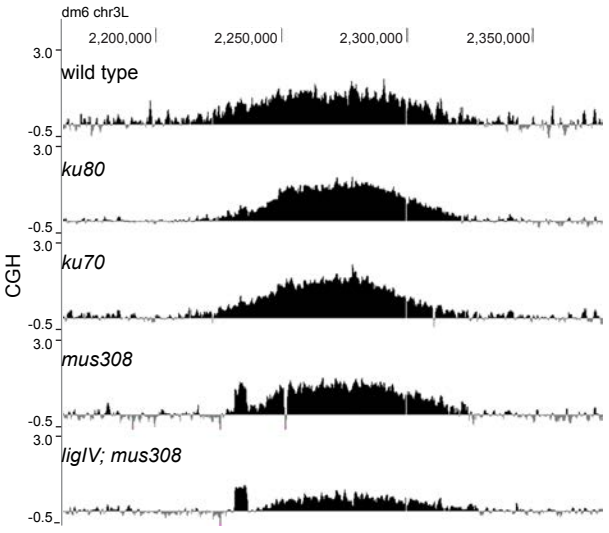
DAFC-62D
dm6 chr3L
2,200,000
2,250,000
2,300,000
2,350,000
wild type
ku80
ku70
mus308
ligIV; mus308
CGH
3.0
-0.5

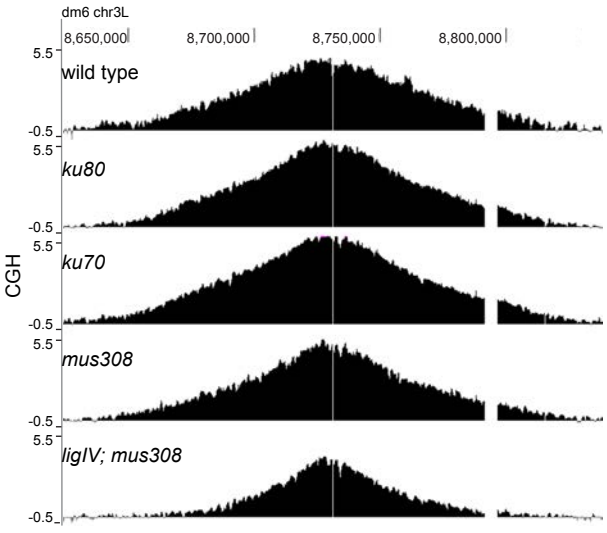
DAFC-66D
dm6 chr3L
8,650,000
8,700,000
8,750,000
8,800,000
wild type
ku80
ku70
mus308
ligIV; mus308
CGH
5.5
-0.5

Figure 3. Developmental timing of origin firing is the same in *ligIV; mus308* and sibling controls

The level of amplification was measured at the (A) *DAFC-66D* (B) *DAFC-7F* and (C) *DAFC-30B* origins of replication in *ligIV; mus308* and *ligIV; mus308/TM3* follicle cells by quantitative real-time PCR. The copy number is relative to the nonamplified *rosy* locus with stage 1-8 egg chambers as the calibrator sample. Error bars are standard error of three technical replicates.

A

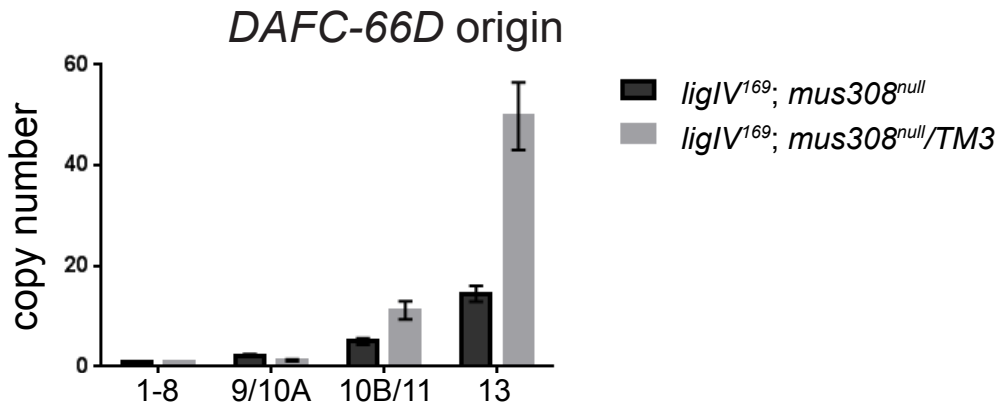
DAFC-66D origin
copy number
60
40
20
0
1-8
9/10A
10B/11
13
ligIV169; mus308null
ligIV169; mus308null/TM3

B

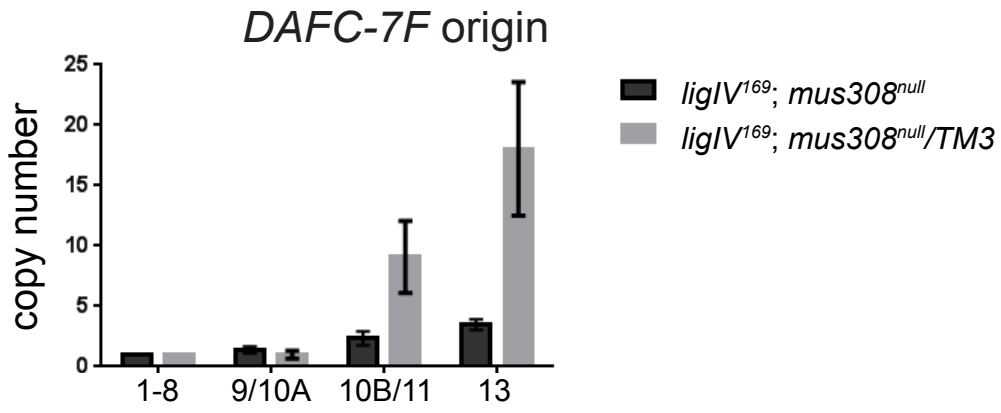
DAFC-7F origin
copy number
25
20
15
10
5
0
1-8
9/10A
10B/11
13
ligIV169; mus308null
ligIV169; mus308null/TM3

C

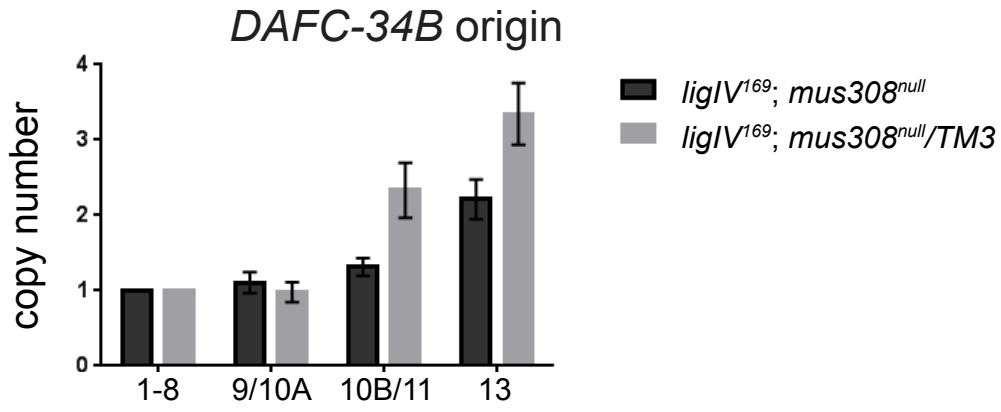
DAFC-34B origin
copy number
4
3
2
1
0
1-8
9/10A
10B/11
13
ligIV169; mus308null
ligIV169; mus308null/TM3

Figure 4. Loss of HR repair enhances re-replication fork progression

(A) The half-maximum distance was calculated in the wild-type and mutant backgrounds for each *DAFC*. Significance was measured by the Dunnett test for multiple comparisons, asterisks indicate $p<0.05$.

(B) CGH at *DAFC-30B, -34B, -62D, -66D* and *-7F* in wild-type and HR mutants. DNA from stage 13 egg chambers was competitively hybridized with diploid embryonic DNA to microarrays with approximately one probe every 125bp. Chromosomal position is plotted on the x-axis, the log2 ratio of stage 13 DNA to embryonic DNA is plotted on the y-axis.

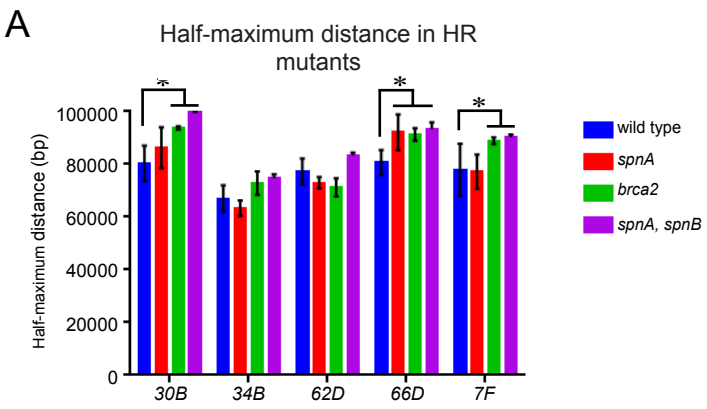
A
Half-maximum distance in HR mutants
Half-maximum distance (bp)
100000
80000
60000
40000
20000
0
30B
34B
62D
66D
7F
wild type
spnA
brca2
spnA, spnB

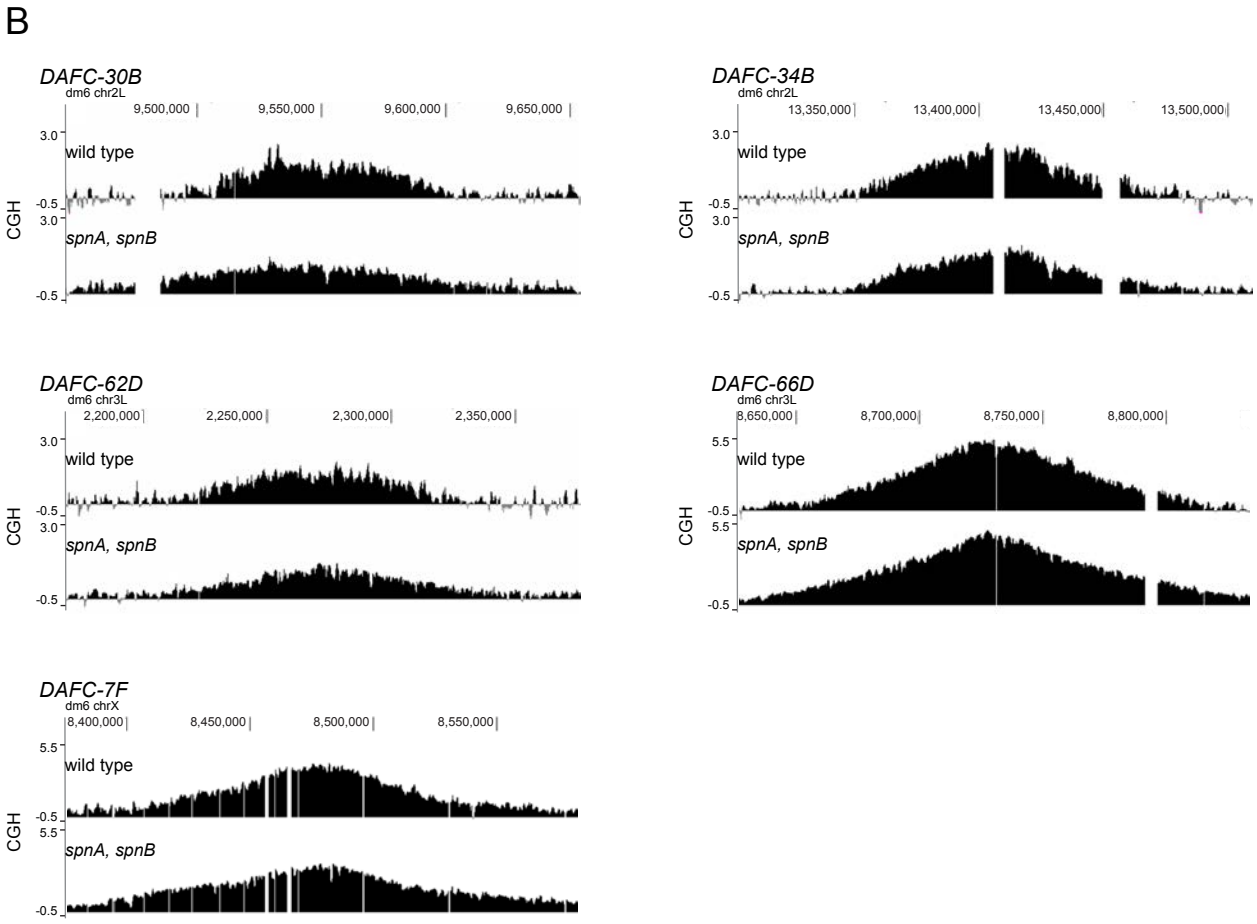
B
DAFC-30B
dm6 chr2L
9,500,000
9,550,000
9,600,000
9,650,000
wild type
spnA, spnB
CGH
DAFC-34B
dm6 chr2L
13,350,000
13,400,000
13,450,000
13,500,000
DAFC-62D
dm6 chr3L
2,200,000
2,250,000
2,300,000
2,350,000
DAFC-66D
dm6 chr3L
8,650,000
8,700,000
8,750,000
8,800,000
DAFC-7F
dm6 chrX
8,400,000
8,450,000
8,500,000
8,550,000

demonstrate that HR is active during re-replication in the follicle cells, and its activity is inhibitory to replication fork progression.

Fork progression is reduced in two Break-Induced Replication mutants

To test the role of BIR in repair of re-replication DSBs, we measured fork progression in the BIR mutants *pol32* and *pif1*. Pol32 is required for BIR (Lydeard *et al.* 2007) and the Pif1 helicase facilitates processive BIR repair (Wilson 2013 *et al.*, Saini *et al.* 2013, Vasianovich *et al.* 2014). The half-maximum distances are significantly reduced at all *DAFCs* in *pol32* and *pif1* follicle cells (Fig. 5). However, both Pol32 and Pif1 are involved in other aspects of fork progression. Pol32 is a non-essential subunit of Polδ, but *in vitro* studies show that polymerase processivity is reduced in the absence of Pol32 (Burgers & Gerik 1998). In addition, the Pif1 helicase is required for replication across G-quadruplex secondary structures and hard-to-replicate regions (Sanders 2010, Paeschke *et al.* 2011, Sabouri *et al.* 2012, Sabouri *et al.* 2014). However, it is important to note that if fork progression was unaffected by loss of these factors, BIR could be excluded as a possible repair mechanism. Therefore, although the measured decrease in fork progression in *pol32* and *pif1* cannot be definitively attributed to BIR repair, these results warrant further examination of the role of BIR during re-replication.

Discussion

We find that the NHEJ, MMEJ and HR pathways are all activated to repair DSBs generated by re-replication in the Drosophila follicle cells. We previously found that replication fork progression at the *DAFCs* relies on *ligIV*, suggesting NHEJ is the primary repair pathway during re-replication. However, we show here that null mutations in *ku80* and *ku70* do not decrease fork

Figure 5. Fork progression is reduced in BIR mutants

(A) The half-maximum distance was calculated in the wild-type and mutant backgrounds for each *DAFC*. Significance was measured by the Dunnett test for multiple comparisons, asterisks indicate $p<0.05$.

(B) CGH at *DAFC-30B, -34B, -62D, -66D* and *-7F* in wild-type and BIR mutants. DNA from stage 13 egg chambers was competitively hybridized with diploid embryonic DNA to microarrays with approximately one probe every 125bp. Chromosomal position is plotted on the x-axis, the log2 ratio of stage 13 DNA to embryonic DNA is plotted on the y-axis.

A

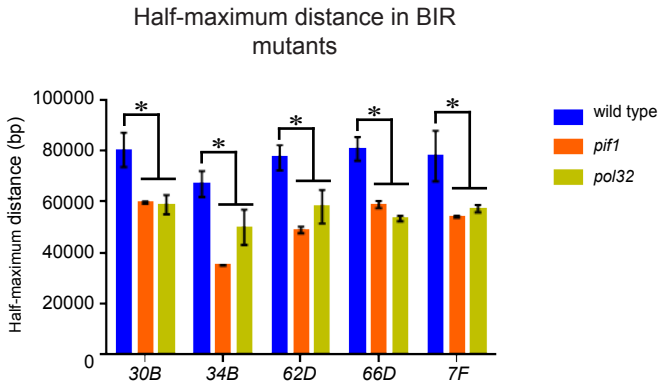
Half-maximum distance in BIR mutants
Half-maximum distance (bp)
100000
80000
60000
40000
20000
0
30B
34B
62D
66D
7F
wild type
pif1
pol32

B

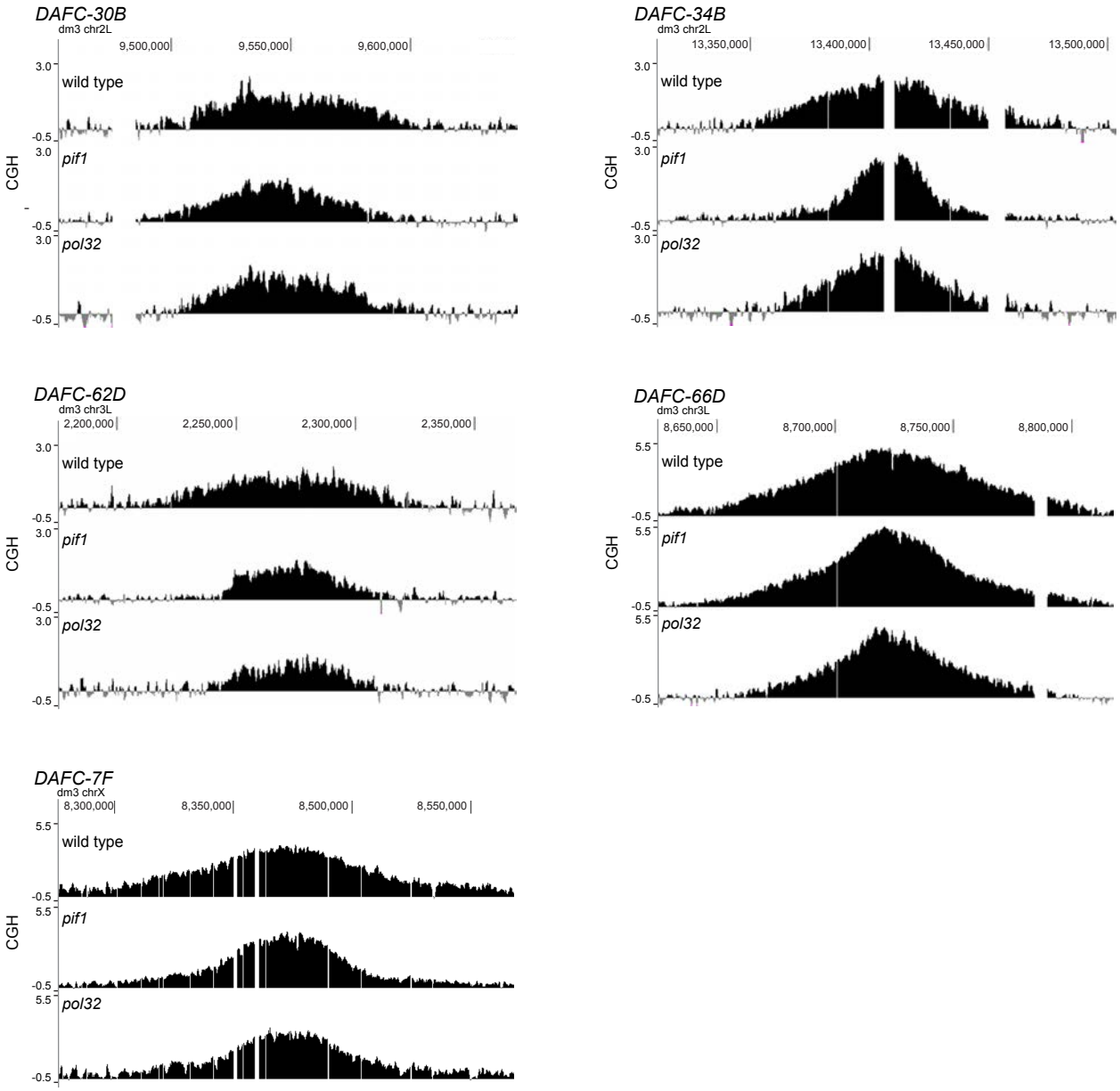
DAFC-30B
dm3 chr2L
9,500,000
9,550,000
9,600,000
DAFC-34B
dm3 chr2L
13,350,000
13,400,000
13,450,000
13,500,000
DAFC-62D
dm3 chr3L
2,200,000
2,250,000
2,300,000
2,350,000
DAFC-66D
dm3 chr3L
8,650,000
8,700,000
8,750,000
8,800,000
DAFC-7F
dm3 chrX
8,300,000
8,350,000
8,500,000
8,550,000
CGH
wild type
pif1
pol32

movement at most positions undergoing re-replication. It is likely that loss of the Ku70-80 heterodimer allows for resection of DSBs, creating substrates for other repair pathways. It is well documented that Ku70-80 binding to DSBs blocks resection by exonucleases, and likewise resection prevents binding of Ku70-80 (Ceccaldi *et al.* 2016). Loss of Ligase IV in the presence of Ku70-80 would simultaneously prevent resection of the DSBs and cause NHEJ to fail at the final step of the pathway. This abortive NHEJ therefore blocks repair by all possible pathways as long as Ku70-80 is bound to DSB ends, leading to overall reduced fork progression. Mutations in mouse *ligIV* and the *ku* genes also display different phenotypes on the organismal level. Null mutations in *ligIV* are lethal in mice (Barnes *et al.* 1998, Frank *et al.* 2000), while mutations in *ku70* or *ku80* are viable but exhibit growth defects, sensitivity to ionizing radiation, and impaired V(D)J recombination (Nussenzweig *et al.* 1996, Gu *et al.* 1997, Li *et al.* 2007).

It is surprising that loss of *ku70* reduces fork progression independently of *ku80*, and only within an approximately 20kb window within one of the re-replication gradients, *DAFC-7F*. Studies in mice revealed some differences in the phenotypes of *ku80* and *ku70* mutants (Nussenzweig *et al.* 1996, Gu *et al.* 1997). However, a more recent study showed the phenotypes are the same when genetic background and growth environment were rigorously controlled (Li *et al.* 2007). The *ku80* and *ku70* mutants analyzed here were generated from different strain backgrounds, and therefore it is a possibility that the variation in fork progression at *DAFC-7F* is a result of strain differences. We think this is unlikely because our analysis was done with a trans-heterozygous mutant for *ku70* and a null mutant over a deficiency for *ku80* (see Experimental Procedures for details). The S155 residue of human Ku70 was shown to be important for signaling to the DNA damage response (DDR) independent of its role in NHEJ repair (Fell & Schild-Poulter 2012). Although null mutants of one *ku* gene typically leads to

substantially decreased expression of the other (Fell & Schild-Poulter 2015), it is possible that low levels of Ku70 in *ku80* follicle cells could have a role in DDR and account for the difference in fork movement at *DAFC-7F*.

Decreased fork progression in *ku70* and *mus308* mutants is only observed within a defined region of *DAFC-7F*. This suggests that this region is especially dependent on end-joining pathways for repair, and absence of either NHEJ or MMEJ reduces repair efficiency and fork progression. Additionally, these results show that *DAFC-7F* is the only site that requires MMEJ repair when the NHEJ pathway is intact. The *C.elegans* Pol θ homolog repairs DSBs generated by collapse of replication forks at G-quadruplex (G4) secondary structures, and Pol θ mutants generate large deletions around G4 positions (Koole *et al.* 2014). Although modeling based on the primary sequence did not find G4 motifs at the *DAFCs* (data not shown), these structures have not been looked for directly during follicle cell amplification; it is possible that G4 and/or other secondary structures form when extensive single-stranded DNA is generated during re-replication. Thus, this region of *DAFC-7F* may contain sequence motifs that are especially sensitive to loss of Mus308.

It is curious that there is no additional decrease in the half-maximum distance in *ligIV; mus308* double-mutant over either single mutant at *DAFC-7F*. This suggests a third pathway repairs DSBs at *DAFC-7F* which is equally efficient in the absence of one or both end-joining mechanisms. The half-maximum distances in the *ligIV; mus308* double-mutant reveal that *DAFC-34B* and *-62D* also are not affected by the additional loss of MMEJ in the absence of NHEJ repair. Conversely, it appears that MMEJ does repair DSBs at *DAFC-30B* and *-66D* and partially compensates for loss of NHEJ at these sites. MMEJ is also utilized for repair after re-replication in human cells, but with reduced efficiency compared to HR (Truong *et al.* 2014).

This is consistent with our observation that MMEJ cannot repair all re-replication DSBs. It is interesting that *DAFC-62D* is the only site that exhibits a significantly decreased half-maximum distance in both *ku80* and *ku70*. These results suggest that NHEJ is the only pathway that can efficiently repair DSBs and support fork progression at *DAFC-62D* within the developmental window of follicle cell amplification. It is also possible that HR dominates repair in the absence of NHEJ at *DAFC-34B* and *-62D*, or in the absence of either end joining pathway at *-7F*. Indeed, the half-maximum distance is significantly increased at *DAFC-7F* in *brca2* and *spnA, spnB*. Although it is not statistically significant, the half-maximum distances at *DAFC-34B* and *-62D* also are increased in *spnA, spnB*, indicating HR is active at these three sites. Alternatively, another untested pathway could be active at *DAFC-34B*, *-62D* and *-7F*. It is important to note that these possibilities are not mutually exclusive, and several factors likely influence the activity of different repair pathways at each *DAFC*.

Increased fork progression in *spnA, spnB* mutants reveals that HR is active during re-replication in the follicle cells and competes with NHEJ for DSB substrates. However, the kinetics of HR likely makes this pathway too slow for productive DSB repair before the end of follicle cell development. Experiments measuring repair of targeted DSBs estimate HR takes 5-7 hours to complete, whereas NHEJ takes 30-70 minutes (Rapp & Greulich 2004, Mao *et al.* 2008, Hicks *et al.* 2011). Amplification in the follicle cells occurs over a 7.5 hour developmental window. Our CGH experiments were performed on stage 13 follicle cell DNA, the final stage of development, which lasts for 1 hour; this places our CGH measurements 6.5-7.5 hours after the first origin firing. Therefore DSB repair by HR cannot promote fork progression within this developmental timescale. This is illustrated by the increased half-maximum distances in HR

mutants. Absence of HR likely directs more DSBs to the faster NHEJ pathway, thus enhancing overall fork progression.

Measuring fork progression at the *DAFCs* by CGH is a sensitive and robust tool for the discovery of factors and pathways required for fork progression. However, it is limited to pathways with unique genetic components. For example, because Pol32 and Pif1 have other roles in fork progression, we cannot conclusively determine whether BIR is required for repair based on the reduced half-maximum distances in these mutants. Therefore, other methods are required to establish the role of BIR in re-replication DSB repair.

Deep sequencing of repair junctions would circumvent these constraints. Analysis of repair products from amplifying follicle cells would simultaneously reveal all repair pathways utilized at every site of re-replication. Side-by-side analysis of repair mutants would also shed light on the back-up mechanisms used for repair, whose products may be too rare or absent in wild-type samples to detect. A recent study analyzed repair junctions by comparing stage 11-14 egg chamber DNA to embryonic DNA sequences, and found large deletions throughout *DAFC-66D* (Yarosh & Spradling 2014). However, egg chambers include the nurse cells, which are undergoing apoptosis during these late stages (Cavaliere *et al.* 1998). A similar experimental design using purified follicle cell DNA from amplifying stages (i.e. 10B or 13) compared to pre-amplification stages (i.e. stage 9) would reveal repair-junctions that result from re-replication induced DSBs. This analysis would reveal the frequency and site-specificity of repair pathways utilized during re-replication, as well as for general DSB repair at various chromosomal positions.

Experimental Procedures

Fly Strains

Analysis of *ku70* was done in the trans-heterozygous combination $ku70^{Ex8/7B2}$ (Johnson-Schlitz *et al.* 2007). Analysis of *ku80* was done in a trans-heterozygous combination over a deletion that removes the *ku80* gene: $ku80^{168}$*/ Df(2L)TE35D-1*. All *ligIV* experiments were done with the $ligIV^{169}$ null allele (McVey *et al.* 2004). Analysis of BIR was done with the $pol32^{L2}$ (Kane *et al.* 2012) and $pif1^{167}$ alleles. The *spnA, spnB* double mutant was generated from the $spnA^{093}$ (Staeva-Vieira *et al.* 2003) and $spnB^{BU}$ (Ghabrial *et al.* 1998) alleles, provided by Trudi Schupbach. The $ku80^{168}$ mutation was generated by Mitch McVey from an imprecise excision screen using P{GSV2}GS50089, located in the 5' UTR of *ku80*. The deletion removes 1360bp 3' of the *P* insertion site, which includes more than half of the coding sequence. The $mus308^{null}$ mutants were generated through the imprecise excision of the *P*-element P{GD4232}v47606. This allele contains a 14kb deletion that spans the *mus308* gene and its promoter region.

Comparative genome hybridization

Ovaries were dissected from fattened females in Grace's media. Approximately 100 stage 13 egg chambers were hand sorted per experiment and stored at -80°C. *OrR* embryos were collected for 2 hours and stored at -80°C. Egg chambers were thawed in 300µL ChIP lysis buffer and embryos in 1% SDS in TE. All tissues were dounced for 10 strokes using a Type A pestle. DNA was fragmented by sonication in a Biorupter300 (Diagenode) at 4°C, 10 cycles of 30sec on 30sec off at maximum power. DNA labeling done as previously described (Blitzblau *et al.* 2007). DNA was hybridized to custom Agilent tiling arrays with probes approximately every 125 basepairs.

Array intensity was LOESS normalized and smoothed by genomic windows of 500bp using the Ringo package in R (Toedling *et al.* 2007).

The half-maximum distance was calculated from smoothed CGH data. The half-maximum point is the genomic coordinate at which the copy number drops to half of the maximum copy number at the origin. This coordinate was calculated independently for the left and ride sides of the amplification gradient, and the distance between these two points is the half-maximal distance. This distance was calculated individually for each replicate at each *DAFC*, and the average values of two biological replicates are displayed. Half-maximum distances from *OrR*, $lig4^{169}$, *ku80*, $pol32^{L2}$ and $pif1^{167}$ are the average of three biological replicates.

Quantitative real-time PCR

Ovaries were dissected from fattened females in Grace's media. Approximately 60 egg chambers were hand sorted from each stage per experiment and stored at -80°C. Egg chambers were thawed in 300µL ChIP lysis buffer and homogenized. DNA was fragmented by sonication in a Biorupter300 (Diagenode) at 4°C, 10 cycles of 30sec on 30sec off at maximum power. Copy number was measured by relative quantitative PCR using stage 1-8 egg chambers as the calibrator sample and the non-amplified *rosy* locus as the endogenous control.

Acknowledgements

We thank George Bell for bioinformatics support with CGH and half-maximum analysis. The excision screen that generated the $mus308^{null}$ allele was performed by Nikolai Renedo. Trudi Schupbach provided Drosophila stocks. This work was supported by NIH grant GM57940 to Terry Orr-Weaver and the MIT School of Science Fellowship in Cancer Research.

References

Abbas, T., Keaton, M.A., Dutta, A. (2013). Genomic instability in cancer. Cold Spring Harb. Perspect Biol. *5*, a012914.

Alexander, J.L., Barrasa, I.M., Orr-Weaver, T.L. (2015). Replication fork progression during re-replication requires the DNA damage checkpoint and double-strand break repair. Curr. Biol. *25*, 1654-1660.

Archambault. V., Ikui, A.E., Drapkin, B.J., Cross, F.R. (2005). Disruption of mechanisms that prevent re-replication triggers a DNA damage response. Mol. Cell. Biol. *25*, 6707–6721.

Arentson, E., Faloon, P., Seo, J., Moon, E., Studts, J.M., Fremont, D.H. Choi., K. (2002). Oncogenic potential of the DNA replication licensing protein CDT1. Oncogene *21*, 1150–1158.

Arias, E.E., Walter, J.C. (2005). Replication-dependent destruction of Cdt1 limits DNA replication to a single round per cell cycle in *Xenopus* egg extracts. Genes. Dev. *19*, 114–126.

Barnes, D.E., Stamp, G., Rosewell, I., Denzel, A., Lindahl, T. (1999). Targeted disruption of the gene encoding DNA ligase IV leads to lethality in embryonic mice. Curr. Biol. *8*, 1395-1398.

Blitzblau, H.G., Bell, G.W., Rodriguez, J., Bell, S.P., Hochwagen, A. (2007). Mapping of meiotic single-stranded DNA reveals double-stranded-break hotspots near centromeres and telomeres. Curr. Biol. *17*, 2003-2012.

Burgers, P. M., and Gerik, K. J. (1998) Structure and processivity of two forms of Saccharomyces cerevisiae DNA polymerase delta. J. Biol. Chem. *273*, 19756–19762.

Calvi, B. R., Lilly, M.A., Spradling, A.C. (1998). Cell cycle control of chorion gene amplification. Genes Dev. *12*, 734-744.

Cavaliere, V., Taddei, C., Gargiulo, G. (1998). Apoptosis of nurse cells at the late stages of oogenesis of *Drosophila melanogaster*. Dev. Genes Evol. *208*, 106-112.

Ceccaldi, R., Rondinelli, B., D'Andrea, A.D. (2016). Repair Pathway Choices and Consequences at the Double-Strand Break. Trends Cell. Biol. *26*, 52-64.

Chan, S.H., Yu, A.M., McVey, M. (2010). Dual roles for DNA polymerase theta in alternative end-joining repair of double-strand breaks in Drosophila. PLoS Genet. *6*, e1001005.

Chiruvella, K.K., Liang, Z., Wilson, T.E. (2013). Repair of double-strand breaks by end joining. Cold Spring Harb. Perspect Biol. *5*, a012757.

Claycomb, J.M., MacAlpine, D.M., Evans, J.G., Bell, S.P., Orr-Weaver, T.L. (2002). Visualization of replication initiation and elongation in *Drosophila*. J. Cell Biol. *159*, 225-236.

Claycomb, J.M., Benasutti, M., Bosco, G., Fenger, D.D., Orr-Weaver, T.L. (2004). Gene amplification as a developmental strategy: isolation of two developmental amplicons in *Drosophila*. Dev. Cell *6*, 145-155.

Claycomb, J.M., and Orr-Weaver T.L. (2005). Developmental gene amplification: insights into DNA replication and gene expression. Trends Genet. *21*, 149-62.

Davidson, I.F., Anatoily, L., Blow, J.J. (2006). Deregulated replication licensing causes DNA fragmentation consistent with head-to-tail fork collision. Mol. Cell *24*, 433-443.

Davis, A.P., Symington, L.S. (2004). Replication in Yeast RAD51-Dependent Break-Induced Replication in Yeast. Mol. Cell. Biol. *6*, 2344-2351.

Fell, V.L., Schild-Poulter, C. (2012). Ku Regulates Signaling to DNA Damage Response Pathways through the Ku70 von Willebrand A Domain. Mol. Cell. Biol. *32*, 76-87.
Fell, V.L., Schild-Poulter, C. (2015). The Ku heterodimer: Function in DNA repair and beyond. Mutat. Res. Rev. Mutat. Res. *763*, 15-29.
Finn, K., Li, J.J. (2013). Single-stranded annealing induced by re-initiation of replication origins provides a novel and efficient mechanism for generating copy number expansion via non-allelic homologous recombination. PLoS Genet. *9*, e1003192.
Frank, K.M., Sharpless, N.E., Gao, Y., Sekiguchi, J.M., Ferguson, D.O., Zhu, C., Manis, J.P., Horner, J., DePinho, R.A., Alt, F.W. (2000). DNA ligase IV deficiency in mice leads to defective neurogenesis and embryonic lethality via the p53 pathway. Mol. Cell *5*, 993-1002.
Ghabrial, A.Ray, R.P., Schupbach, T. (1998). *okra* and *spindle-B* encode components of the *RAD52* DNA repair pathway and affect meiosis and patterning in *Drosophila* oogenesis. Genes Dev. *12*, 2711-2723.
Green, B. M., and Li. J.J. (2005). Loss of rereplication control in *Saccharomyces cerevisiae* results in extensive DNA damage. Mol. Biol. Cell *16*, 421-432.
Green, B.M., Finn, K.J., Li, J.J. (2010). Loss of DNA replication control is a potent inducer of gene amplification. Science *329*, 943–946.
Gu, Y., Seidl, K.J., Rathbun, G.A., Zhu, C., Manis, J.P., van der Stoep, N., Davidson, L., Cheng, H.L., Sekiguchi, J.M., Frank, K., Stanhope-Baker, P., Schlissel, M.S., Roth, D.B., Alt, F.W. (1997). Growth retardation and leaky SCID phenotype of Ku70-deficient mice. Immunity *7*, 653-665.
Hanlon, S.L., Li, J.J. (2015). Re-replication of a centromere induces chromosomal instability and aneuploidy. PLoS Genet. *4*, e1005039.
Hicks, W.M., Yamaguchi, M., Haber, J.E. (2011). Real-time analysis of double-strand DNA break repair by homologous recombination. Proc. Natl. Acad. Sci. USA *108*, 3108-3115.
Hogg, M., Sauer-Eriksson, A.E., Johansson, E. (2012). Promiscuous DNA synthesis by human DNA polymerase theta. Nucleic Acids Res. *40*, 2611–2622.
Johnson-Schlitz, D.M., Flores, C., Engels, W.R. (2007). Multiple-pathway analysis of double-strand break repair mutations in Drosophila. PLoS Genet. *3*, e50.
Kane, D., P., Shusterman, M., Rong, Y., McVey, M. (2012). Competition between Replicative and Translesion Polymerases during Homologous Recombination Repair in Drosophila. PLoS Genet. *8*, e 1002659.
Karakaidos, P., Taraviras, S., Vassiliou, L.V., Zacharatos, P., Kastrinakis, N.G., Kougiou, D., Kouloukoussa, M., Nishitani, H., Papavassiliou, A.G., Lygerou, Z., Gorgoulis, V.G. (2004). Over- expression of the replication licensing regulators hCdt1 and hCdc6 characterizes a subset of non-small-cell lung carcinomas: Synergistic effect with mutant p53 on tumor growth and chromosomal instability - Evidence of E2F-1 transcriptional control over hCdt1. Am. J. Pathol. *165*, 1351–1365.
Kent, T., Chandramouly, G., McDevitt, S.M., Ozdemir, A.Y., Pomerantz, R.T. (2015). Mechanism of microhomology-mediated end-joining promoted by human DNA polymerase θ. Nat. Struct. Mol. Biol. *22*, 230-237.
Kim, J.C., Nordman, J., Xie, F., Kashevsky, H., Eng, T., Li, S., MacAlpine, D.M., Orr-Weaver, T.L. (2011). Integrative analysis of gene amplification in *Drosophila* follicle cells: parameters of origin activation and repression. Genes Dev. *25*, 1384-1398.

Koole, W., van Schende, R., Karambelas, A.E., van Heteren, J.T., Okihara, K.L., Tijsterman, M. (2014). A Polymerase Theta-dependent repair pathway suppresses extensive genomic instability at endogenous G4 DNA sites. Nat. Commun. *5*, 3216.

Kraus, E., Leung, W., Haber, J.E. (2001). Break-induced replication: A review and an example in budding yeast. Proc. Natl. Acad. Sci. USA *98*, 8255-8262.

Li, A., Blow, J.J. (2005). Cdt1 downregulation by proteolysis and geminin inhibition prevents DNA re-replication in *Xenopus*. EMBO J. *24*, 395–404.

Li, H., Vogel, H., Holcomb, V.B., Gu, Y., Hasty, P. (2007). Deletion of Ku70, Ku80, or both causes early aging without substantially increased cancer. Mol. Cell. Biol. *27*, 8205-8214.

Lydeard, J.R., Jain, S., Yamaguchi, M., Haber, J.E. (2007). Break-induced replication and telomerase-independent telomere maintenance require Pol32. Nature *448*, 820-823.

Maiorano, D., Krasinska, L., Lutzmann, M., Mechali, M. (2005). Recombinant Cdt1 induces rereplication of G2 nuclei in *Xenopus* egg extracts. Curr. Biol. *15*, 146–153.

Malkova, A., Ivanov, E.L., Haber, J.E. (1996). Double-strand break repair in the absence of RAD51 in yeast: a possible role for break-induced DNA replication. Proc. Natl. Acad. Sci. USA *93*, 7131-7136.

Malkova, A., Naylor, M.L., Yamaguchi, M., Ira, G., Haber, J.E. (2005). RAD51-Dependent Break-Induced Replication Differs in Kinetics and Checkpoint Responses from RAD51-Mediated Gene Conversion. Mol. Cell. Biol. *25*, 933-944.

Mao, Z., Bozzella, M., Seluanov, A., Gorbunova, V. (2008). Comparison of nonhomologous end joining and homologous recombination in human cells. DNA Repair (Amst). *7*, 1765-1771.

Mateos-Gomez, P.A., Gong, F., Nair, N., Miller, K.M., Lazzerini-Denchi, E., Sfeir, A. (2015). Mammalian polymerase θ promotes alternative NHEJ and suppresses recombination. Nature *518*, 254-257.

McVey, M., Radut, D., Sekelsky, J.J. (2004). End-joining repair of double-strand breaks in *Drosophila melanogaster* is largely DNA ligase IV independent. Genetics *168*, 2067–2076.

Melixetian, M., Ballabeni, A., Masiero, L., Gasparini, P., Zamponi, R., Bartek, J., Lukas, J., Helin, K., (2004). Loss of Geminin induces rereplication in the presence of functional p53. J. Cell Biol. *165*, 473-482.

Mihaylov, I.S., Kondo, T., Jones, L., Ryzhikov, S., Tanaka, J., Zheng, J., Higa, L. A., Minamino, N., Cooley, L., Zhang, H. (2002). Control of DNA replication and chromosome ploidy by Geminin and Cyclin A. Mol. Cell. Biol. *22*, 1868-1880.

Neelsen, K.J., Zanini, I.M.Y., Mijic, S., Herrador, R., Zellweger, R., Chaudhuri, A.R., Creavin, K.D., Blow, J.J., Lopes, M. (2013). Deregulated origin licensing leads to chromosomal breaks by rereplication of a gapped DNA template. Genes Dev. *27*, 2537-2542.

Nussenzweig, A., Chen, C., da Costa Soares, V., Sanchez, M., Sokol, K., Nussenzweig, M.C., Li, G.C. (1996). Requirement for Ku80 in growth and immunoglobulin V(D)J recombination. Nature *382*, 551-555.

Paeschke, K., Capra, J.A., Zakian, V.A. (2011). DNA replication through G-quadruplex motifs is promoted by the *Saccharomyces cerevisiae* Pif1 DNA helicase. Cell *145*, 678-691.

Park, E.A., MacAlpine, D. M., Orr-Weaver, T.L. (2007) *Drosophila* follicle cell amplicons as models for metazoan DNA replication: a *cyclinE* mutant exhibits increased replication fork elongation. Proc. Natl. Acad. Sci. USA *104*, 16739-16746.

Rapp, A., Greulich, K.O. (2004). After double-strand break induction by UV-A, homologous recombination and nonhomologous end joining cooperate at the same DSB if both systems are available. J. Cell Sci. *117*, 4935-4945.

Sabouri, N., McDonald, K.R., Webb, C.J., Cristea, I.M., Zakian, V.A. (2012). DNA replication through hard-to-replicate sites, including both highly transcribed RNA Pol II and Pol III genes, requires the S. pombe Pfh1 helicase. Genes Dev. *26*, 581–593.

Sabouri, N., Capra, J.A., Zakian, V.A. (2014). The essential *Schizosaccharomyces pombe* Pfh1 DNA helicase promotes fork movement past G-quadruplex motifs to prevent DNA damage. BMC Biol. *12*, 101.

Saini, N., Ramakrishnan, S., Elango, R., Ayyar, S., Zhang, Y., Deem, A., Ira, G., Haber, J.E., Lobachev, K.S., Malkova, A. (2013). Migrating bubble during break-induced replication drives conservative DNA synthesis. Nature *502*, 389-392.

Sanders, C.M. (2010). Human Pif1 helicase is a G-quadruplex DNA-binding protein with G-quadruplex DNA-unwinding activity. Biochem. J. *430*, 119–128.

Seo, J., Chung, Y.S., Sharma, G.G., Moon, E., Burack, W.R., Pandita, T.K., Choi, K. (2005). Cdt1 transgenic mice develop lymphoblastic lymphoma in the absence of p53. Oncogene *24*, 8176–8186.

Signon, L., Malkova, A., Naylor, M.L., Klein, H., Haber, J.E. (2001). Genetic Requirements for *RAD51* - and *RAD54* -Independent Break-Induced Replication Repair of a Chromosomal Double-Strand Break. Mol. Biol. Cell *21*, 2048-2056.

Staeva-Vieira, E., Yoo, S., Lehmann, R. (2003). An essential role of DmRad51/SpnA in DNA repair and meiotic checkpoint control. EMBO *22*, 5863-5874.

Thomer, M., May, N.R., Aggarwal, B.D., Kwok, G., Calvi, B.R. (2004). *Drosophila double-parked* is sufficient to induce re-replication during development and is regulated by cyclin E/CDK2. Development *131*, 4807-4818.

Toedling, J., Skylar, O., Krueger, T., Fischer, J.J., Sperling, S., Huber, W. (2007). Ringo—an R/Bioconductor package for analyzing ChIP–chip readouts. BMC Bioinformatics *8*,. doi: 10.1186/1471-2105-8-221.

Truong, L.N., Li, Y., Shi, L.Z., Hwang, P.Y., He, J., Wang, H., Razavian, N., Berns, M.W., Wu X. (2013). Microhomology-mediated End Joining and Homologous Recombination share the initial end resection step to repair DNA double-strand breaks in mammalian cells. Proc. Natl. Acad. Sci. USA. *110*, 7720-7725.

Truong, L.N., Li, Y., Sun, E., Ang, K., Hwang, P.Y.H., Wu, X. (2014). Homologous recombination is a primary pathway to repair DNA double-strand breaks generated during DNA rereplication. J. Biol. Chem. *289*, 28910-28923.

Vasianovich, Y., Harrington, L.A., Makovets, S. (2014). Break-Induced Replication Requires DNA Damage-Induced Phosphorylation of Pif1 and Leads to Telomere Lengthening. PLoS Genet. *10*, e1004679.

Vaziri, C., Saxena, S., Jeon, Y., Lee, C., Murata, K., Machida, Y., Wagle, N., Hwang, D.S., Dutta, A. (2003). A p53-dependent checkpoint pathway prevents rereplication. Mol. Cell *11*, 997–1008.

Wilson, M.A., Kwon, Y., Xu, Y., Chung, W.H., Chi, P., Niu, H., Mayle, R., Chen, X., Malkova, A., Sung, P., Ira, G. (2013). Pif1 helicase and Polδ promote recombination-coupled DNA synthesis via bubble migration. Nature *502*, 393-639.

Xouri, G., Lygerou, Z., Nishitani, H., Pachnis, V., Nurse, P., Taraviras, S. (2004). Cdt1 and geminin are down-regulated upon cell cycle exit and are over-expressed in cancer-derived cell lines. Eur. J. Biochem. *271*, 3368–3378.

Yarosh, W., Spradling, A.C. (2014). Incomplete replication generates somatic DNA alterations within *Drosophila* polytene salivary gland cells. Genes Dev. *28*, 1840-1855.

Yu, A.M., McVey, M. (2010). Synthesis-dependent microhomology-mediated end joining accounts for multiple types of repair junctions. Nucleic Acids Res. *38*, 5706-5717.

Zhu, W., Chen, Y., Dutta, A. (2004). Rereplication by depletion of Geminin is seen regardless of p53 status and activates a G2/M checkpoint. Mol. Cell. Biol. *16*, 7140-7150.

Zhu, W., Dutta, A. (2006). An ATR- and BRCA1-mediated Fanconi anemia pathway is required for activating the G2/M checkpoint and DNA damage repair upon rereplication. Mol. Cell. Biol. *26*, 4601-4611.

Chapter Five:
Conclusions and Perspectives

In this thesis I have established the *Drosophila Amplicons in Follicle Cells* (*DAFCs*) as a model system for re-replication induced damage. We find that double-strand breaks (DSBs) are coincident with elongating forks, supporting the model that collisions between adjacent replication forks leads to collapse and DSBs (Davidson *et al.* 2006). Furthermore, the half-maximum distance analysis described here measures global fork progression across each *DAFC*; this analysis has enabled us to quantitatively compare how loss of various DNA damage response and repair components influence fork movement. Using fork progression as a read-out for DSB repair efficiency, we have begun to define the mechanisms of DSB repair during re-re-plication. Our current results indicate at least three pathways are used for repair, and pathway choice varies across different positions. Additionally, we find that absence of homologous recombination (HR) enhances half-maximum distances at the *DAFCs*, revealing that repair of DSBs by HR inhibits re-replication fork progression.

It therefore seems that DSB repair pathway choice during re-replication is a complicated process influenced by genomic position, repair kinetics and developmental timing. Additionally, the preferred repair mechanism may not be universal across all re-replication systems. We have not tested the role of all possible repair pathways at the *DAFCs*, and it is likely that others are involved. Our current approach limits us to testing pathways that have unique components. Global examination of mechanisms for re-replication DSB repair will require deep sequencing of repair junctions in amplifying follicle cells. To be confident that observed junctions are the result of re-replication induced damage, sequences need to be compared to follicle cells isolated from the same female just prior to amplification initiation. Although a variety of repair pathways could be active, only the most efficient will generate detectable junctions. Therefore deep sequencing in mutants shown to be required for repair, such as *ligIV*, *mus308* and *ligIV; mus308*,

is necessary to increase the frequency of rare repair events. This approach also will provide valuable insight into the role of primary sequence in pathways choice, not just in the context of re-replication but for general DSB repair. As we learn more about the components and signatures of other DSB repair pathways, this dataset could be revisited and complimented with new mutant analysis. These experiments would provide a comprehensive picture of the factors influencing DSB repair mechanisms during re-replication and the consequences on genome integrity.

Repair of Re-replication Double-Strand Breaks by Break-Induced Replication

We have not tested the role of break-induced replication (BIR) in repairing re-replication forks during follicle cell amplification. The fork collision model (Davidson *et al.* 2006) predicts that collapsed re-replication forks generate single-sided DSBs (ssDSBs) when a fork meets an unligated Okazaki fragment on the lagging strand of the fork in front of it (Fig. 1) (Abbas & Dutta 2013). Studies of BIR at defined DSBs show that this pathway is used when there is homology to only one side of the break and establishes a single replication fork (Malkova *et al.* 1996, 2005, Signon *et al.* 2001). Therefore BIR is predicted to be the preferred pathway for repair of ssDSB (Kraus *et al.* 2001, Abbas & Dutta 2013). However, the BIR pathway lacks unique genetic determinants, making it difficult to elucidate the role of BIR repair by measuring fork progression in repair mutants. Although we have found that mutants in the BIR components *pol32* and *pif1* significantly reduce fork progression, both of these factors play a role in other aspects of fork progression (Chapter 4) (Burgers & Gerik 1998, Lydeard *et al.* 2007, Sanders 2010, Paeschke *et al.* 2011, Sabouri *et al.* 2012, Wilson 2013 *et al.*, Saini *et al.* 2013, Sabouri *et al.* 2014, Vasianovich *et al.* 2014). Therefore, we currently cannot attribute the measured effects to loss of BIR repair.

Figure 1. Re-replication is predicted to generate single-sided DSBs where the leading strand meets an unligated Okazaki fragment

(Top) A single origin initiation on the parental DNA (black) generates two bi-directional forks replication forks and two daughter strands (blue). The leading strands are shown as one continuous arrow, the Okazaki fragments of the lagging strands are shown as short head-to-tail arrows.

(Middle) A second initiation from the same origin generates four replication forks that replicate along both the parental (black) and newly copied (blue) templates. Daughter strands from the second round of replication are shown in red. Ligated Okazaki fragments are shown as joint head-to-tail arrows.

(Bottom) Forks generated on the right side of the origin are shown. As the leading strand from the second origin firing (red, continuous arrow) meets the first replication fork, it encounters an unligated Okazaki fragment on the lagging strand it is using as a template (blue, short arrows). Replication to the end of this unligated Okazaki fragment generates a DSB at the site of fork collision (gray circle).

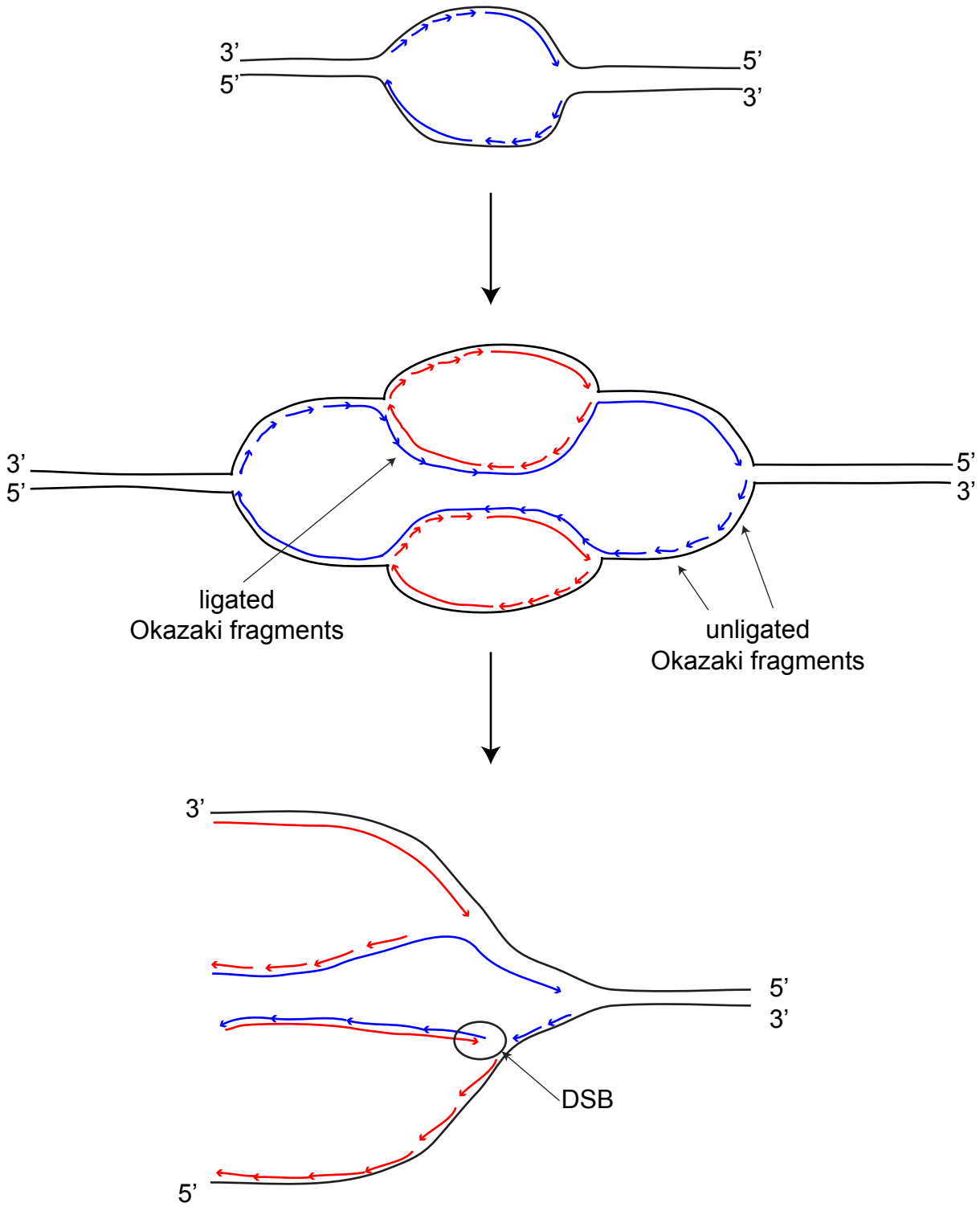
3’
5’
5’
3’
3’
5’
5’
3’
ligated
Okazaki fragments
unligated
Okazaki fragments
3’
5’
3’
DSB
5’

BIR does not rely on the pre-RC components ORC or Cdc6, but does require Cdt1 and Mcm2-7 helicase to establish new BIR forks in the absence of a replication origin (Lydeard *et al.* 2010). During canonical origin firing, Cdt1 is removed from the origin by targeted degradation in S-Phase. In Drosophila, removal of the Cdt1 homolog DUP is mediated by CyclinE/CDK2 phosphorylation (Thomer *et al.* 2004) and the DUP PIP- box domain (Lee *et al.* 2010). However, at the *DAFCs* DUP escapes degradation and travels with replication forks for the duration of amplification (Claycomb *et al.* 2002). During origin firing in stage 10B and 11, BrdU forms a single focus where it is incorporated at the origin and surrounding forks (Calvi *et al.* 1998, Claycomb *et al.* 2002). By stages 12 and 13, the *DAFC-66D* origin no longer fires, but existing replication forks continue to travel; this results in the resolution of two adjacent BrdU foci around the *DAFC-66D* origin, called the double-bar structure (Claycomb *et al.* 2002). Likewise, DUP resolves into a double-bar structure in stages 12 and 13, coincident with BrdU incorporation (Claycomb *et al.* 2002). Conversely, ORC is present only at the origin of replication and is removed once origin firing is complete (Claycomb *et al.* 2002). It was suggested that DUP may be required to stabilize Mcm2-7 at these slow moving re-replication forks (Claycomb *et al.* 2002). In the light of more recent data on the requirement for Cdt1 in BIR, an alternative explanation is that fork-associated DUP at the *DAFCs* is involved in the establishment of origin-independent replication forks via BIR repair. This would suggest that DUP is not travelling with elongating forks, but is being recruited as re-replication forks collapse.

The idea that BIR might be utilized during follicle cell amplification was first proposed upon the characterization of ORC-independent amplification at *DAFC-34B* (Kim & Orr-Weaver 2011). This site undergoes two separated rounds of origin firing. In stage 10B copy number

increases around three-fold and the pre-RC components ORC and Mcm2-7 localize to the origin. At stage 13, copy number increases another two-fold and Mcm2-7 is loaded; however, ORC cannot be detected by ChIP-chip or ChIP-qPCR after stage 10B. It therefore appears the second origin firing at *DAFC-34B* is ORC-independent (Kim & Orr-Weaver 2011). The authors proposed that collapsed forks generated during stage 10B may increase copy number at stage 13 via a BIR mechanism (Kim & Orr-Weaver 2011). We have since shown that DSBs are generated throughout all six *DAFCs* in both stage 10B and 13 (Alexander *et al.* 2015). Additionally, the DSB marker γH2Av exhibits the highest enrichment levels at *DAFC-34B* in stage 13, as measured by ChIP-seq (Alexander *et al.* 2015). The enrichment levels are even greater than those at the highly amplified sites *DAFC-66D* and *DAFC-7F*, which should theoretically experience more fork collision events simply due to the increased number of adjacent forks. This suggests that forks at *DAFC-34B* are highly susceptible to fork collapse, and potentially generate more substrates for BIR repair than the other sites. It would be interesting to measure γH2Av enrichment profiles from stage 11 and stage 12 follicle cells to determine if the rate of DSB generation is accelerated at *DAFC-34B* compared to the other *DAFCs*.

It is also interesting that fork progression is most strongly affected at *DAFC-34B* is *pif1* follicle cells. The half-maximum distance at *DAFC-34B* is reduced by 50% in *pif1* compared to wild-type, whereas the other *DAFCs* exhibit only a 20-30% reduction (Chapter 4). No other mutants analyzed thus far reduce fork progression more than 30% at any site (Alexander *et al.* 2015, Chapter 4). This reveals that *DAFC-34B* is especially sensitive to loss of the Pif1 helicase. It is an interesting possibility that Pif1 may facilitate fork progression independently of BIR at all *DAFCs*, while only *DAFC-34B* requires Pif1 for both replication and BIR. Alternatively, Pif1 may be involved in BIR at all re-replication positions, but the increased amount of DSBs (as

indicated by γH2Av intensity) may make *DAFC-34B* more sensitive to loss of BIR components. However, absence of the essential BIR factor Pol32 had no additional effect on fork progression at *DAFC-34B* compared to the other sites, suggesting Pif1 is functioning independently of BIR at *DAFC-34B*.

A combination of conditional alleles could be used to test whether the second round of origin firing at *DAFC-34B* occurs by a BIR mechanism. Induced degradation of ORC between stages 10B and 13 would reveal if the second round of origin firing is indeed ORC-independent. This system must be sensitive enough to degrade ORC in the 2.5 hour window between stages 10B and 13, so that all stage 10B origin firing events occur normally. To determine if DSBs generated during stage 10B are essential for amplification in stage 13, reciprocal experiments would be done in stage 10B to abolish early origin firing and measure copy number later in stage 13. Additionally, the requirement for Cdt1 in the establishment of BIR forks (Lydeard *et al.* 2010) predicts that degradation of DUP after stage 10B would block the second round of amplification at *DAFC-34B*. A requirement for DUP, but not ORC, would strongly support a model in which stage 13 amplification at *DAFC-34B* occurs by BIR.

Several systems have been developed for targeted degradation of proteins in Drosophila. GFP fusion proteins can be targeted for degradation using the deGradFP system. Co-expression of a GFP single-chain antibody fused to the F-box protein Slmb (NSlmb-vhhGFP) will bind to the GFP fusion protein and target it to the SCF for polyubiquitination and subsequent degradation (Caussinus *et al.* 2012). NSlmb-vhhGFP expression is under UAS control and thus can be combined with a variety of GAL4 drivers (Caussinus *et al.* 2012). Although a functional ORC2-GFP fusion is available (Caussinus *et al.* 2012), there are currently are no drivers that specifically turn on after stage 10B. Therefore NSlmb-vhhGFP would have to be driven by a heat

shock promoter, and conditions optimized to drive expression rapidly. Another recently published system is auxin-inducible degradation, whereby addition of the plant hormone auxin drives association of proteins containing an auxin-degron to the SCF (Trost *et al.* 2016). This system provided a rapid and potentially reversible means for degradation, making it ideal to target proteins between short developmental stages in the follicle cells.

Targeted degradation of pre-RC components would also be highly informative to test the role of BIR repair at the other *DAFCs*. If DSBs are repaired by continued establishment of BIR forks, degradation of DUP after origin firing would reduce the *DAFC* half-maximum distances. It is important to note that these measurements would not be informative at *-62D* or *DAFC-34B*, which undergo origin firing events in stage 13 that recruit DUP (Brian Hua, unpublished data). If fork progression is reduced at the other four *DAFCs*, this result could also be explained by a requirement for DUP in maintaining Mcm2-7 at amplification forks, as was previously suggested (Claycomb *et al.* 2002). However, this model has two major predictions that differ from a BIR mechanism: 1) immunofluorescence experiments looking at Mcm2-7 localization to *DAFC* replication forks will reveal if Mcm2-7 is reduced after DUP degradation, and 2) fork progression is expected to be abolished in the absence of Mcm2-7 on all elongating forks. Conversely, absence of BIR is predicted to affect only a subset of forks that collide and collapse. This would result in a 20-30% decrease in the half-maximum distance, as seen for other DNA damage response and repair mutants (Alexander *et al.* 2015, Chapter 4) rather than a complete block to fork progression. Comparisons to half-maximum distances after targeted degradation of an essential fork component, such as PCNA or Mcm2-7, would establish a baseline for expected distances when fork progression is abolished.

However, the slow kinetics of BIR makes it unlikely to be the preferred mechanism of repair

at all the *DAFCs*. Kinetic studies from defined DSBs found that initiation of BIR takes approximately 2.5 hours longer than HR (Malkova *et al.* 2005), and the first repair products are seen 6-9 hours after the break is generated (Lydeard *et al.* 2010). Based on our results in HR mutants, it seems unlikely that BIR would be a productive repair mechanism in the follicle cells. These studies did find that once BIR forks are established, they progress at speeds comparable to canonical replication forks (Malkova *et al.* 2005). Therefore BIR events initiating in early stage 10B could result in productive fork progression by stage 13. It is interesting to speculate that the delay in origin firing at *DAFC-34B* is simply the result of BIR initiation kinetics rather than developmental regulation.

Recent studies demonstrated that fork elongation during BIR occurs via bubble migration, which is visible by electron microscopy (EM) of replicating DNA and 2D-gel analysis (Saini *et al.* 2013, Wilson *et al.* 2013). The 2D-gel studies found bubble arcs after the initiation of BIR when only elongating forks are expected to be present, which the authors propose is indicative of bubble migration (Saini *et al.* 2013). 2D-gel analysis of replication products within *DAFC-66D* found strong bubble arcs within the region known to contain the origin (Heck and Spradling 1990). However, the authors also found faint bubbles outside of the origin region, which they suggest reflects less efficient usage of other origins during amplification (Heck and Spradling 1990). It is possible these faint bubble arcs are actually BIR bubbles like those seen by Saini and colleagues. Confirmation of migrating bubbles would require 2D-gel analysis of fragments further out from the origin in stage 12-13 follicle cells, after *DAFC-66D* origin firing. EM of studies of the follicle cell amplicons did not report migrating bubble structures (Osheim & Miller, 1983, Osheim *et al.* 1988). However, these studies were done with restriction fragments near the *DAFC-66D* and *-7F* origins and localized origin locations by the presence of elongating

chorion gene transcripts (Osheim & Miller, 1983, Osheim *et al.* 1988). Additionally, the authors note that the complex amplification structures made it difficult to obtain spreads for EM (Osheim *et al.* 1988). Visualization of the lower copy number amplicons at positions outside of the origin region could reveal whether migrating bubbles are generated during follicle cell amplification.

Re-replication fork repair by Nonhomologous End Joining (NHEJ)

Our results demonstrate the NHEJ is required for efficient repair of DSBs generated by re-replication (Alexander *et al.* 2015, Chapter 4). A recent study in yeast also found that NHEJ is utilized for repair of re-replication DSBs (Hanlon & Li 2015). Mutations in the DNA-PK catalytic subunit, required for NHEJ, render Chinese hamster cells sensitive to prolonged exposure to hydroxyurea, suggesting NHEJ helps repair DSBs at collapsed forks (Lundin *et al.* 2002). However, collapsed replication forks are predicted to generate ssDSBs, and therefore a single collapsed fork cannot be repaired by NHEJ. Lundin *et al.* propose that NHEJ repair joins two nearby forks, since hydroxyurea is expected to cause extensive fork collapse (Lundin *et al.* 2002). During S-phase, joining forks in this way would potentially generate large deletions and chromosome re-arrangements, making use of NHEJ repair toxic to the cell. Truong and colleagues propose a model by which re-replication bubbles are removed by nuclease processing and blunt ends on either side are joined by NHEJ (Truong *et al.* 2014). However, maintenance of copy number at the *DAFCs* after origin firing is completed suggests this is not the case (Spradling & Mahowald 1980, Claycomb *et al.* 2002, Kim & Orr-Weaver 2011). Additionally, EM studies show that forks are maintained in an onion skin structure at the amplicons (Osheim & Miller, 1983, Osheim *et al.* 1988).

It is possible that numerous adjacent broken forks generated at the *DAFCs* provide adequate

substrate for NHEJ repair. Potential rearrangements within the *DAFCs* may not be problematic in the follicle cells, which are terminally differentiated and undergo programmed cell death soon after amplification ends. However, the resolution of BrdU/EdU thymidine analogs into clear double-bar structures after origin firing is completed suggests DSB ends are not joined to breaks across the origin. It is possible that nuclease processing of collapsed forks generates compatible DSB ends for NHEJ repair. Sequencing repair junctions in wild-type and *ligIV* follicle cells will provide important insight into how these breaks are processed and repaired by NHEJ.

References

Abbas, T., Keaton, M.A., Dutta, A. (2013). Genomic instability in cancer. Cold Spring Harb. Perspect Biol. *5*, a012914.

Alexander, J.L., Barrasa, I.M., Orr-Weaver, T.L. (2015). Replication fork progression during re-replication requires the DNA damage checkpoint and double-strand break repair. Curr. Biol. *25*, 1654-1660.

Burgers, P. M., and Gerik, K. J. (1998) Structure and processivity of two forms of Saccharomyces cerevisiae DNA polymerase delta. J. Biol. Chem. *273*, 19756–19762.

Calvi, B. R., Lilly, M.A., Spradling, A.C. (1998). Cell cycle control of chorion gene amplification. Genes Dev. *12*, 734-744.

Caussinus, E., Kanca, O., Affolter, M. (2012). Fluorescent fusion protein knockout mediated by anti-GFP nanobody. Nat. Struct. Mol. Biol. 19, 117-121.

Claycomb, J.M., MacAlpine, D.M., Evans, J.G., Bell, S.P., Orr-Weaver, T.L. (2002). Visualization of replication initiation and elongation in *Drosophila*. J. Cell Biol. *159*, 225-236.

Davidson, I.F., Anatoily, L., Blow, J.J. (2006). Deregulated replication licensing causes DNA fragmentation consistent with head-to-tail fork collision. Mol. Cell *24*, 433-443.

Hanlon, S.L., Li, J.J. (2015). Re-replication of a centromere induces chromosomal instability and aneuploidy. PLoS Genet. *4*, e1005039.

Heck, M.M.S., Spradling, A.C. (1990). Multiple Replication Origins Are Used during *Drosophila* Chorion Gene Amplification. J. Cell Biol. *110*, 903-914.

Kim, J.C., Orr-Weaver, T.L. (2011). Analysis of a *Drosophila* amplicon in follicle cells highlights the diversity of metazoan replication origins. Proc. Natl. Acad. Sci. USA 108, 16681-16686.

Kraus, E., Leung, W., Haber, J.E. (2001). Break-induced replication: A review and an example in budding yeast. Proc. Natl. Acad. Sci. USA 98, 8255-8262.

Lee, H.O., Zacharek, S.J., Xiong, Y., Duronio, R.J. (2010). Cell Type – dependent Requirement for PIP Box – regulated Cdt1 Destruction During S Phase. Mol. Biol. Cell. 21, 3639-3653.

Lundin, C., Erixon, K., Arnaudeau, C., Schultz, N., Jenssen, D., Meuth, M., Helleday, T. (2002). Different Roles for Nonhomologous End Joining and Homologous Recombination following Replication Arrest in Mammalian Cells. Mol. Cell. Biol. *22*, 5869-5878.

Lydeard, J.R., Jain, S., Yamaguchi, M., Haber, J.E. (2007). Break-induced replication and telomerase-independent telomere maintenance require Pol32. Nature *448*, 820-823.

Lydeard, J.R., Lipkin-Moore, Z., Sheu, Y., Stillman, B., Burgers, P.M., Haber, J.E. (2010). Break-induced replication requires all essential DNA replication factors except those specific for pre-RC assembly. Genes Dev. *24*, 1133-1144.

Malkova, A., Ivanov, E.L., Haber, J.E. (1996). Double-strand break repair in the absence of RAD51 in yeast: a possible role for break-induced DNA replication. Proc. Natl. Acad. Sci. USA *93*, 7131-7136.

Malkova, A., Naylor, M.L., Yamaguchi, M., Ira, G., Haber, J.E. (2005). RAD51-Dependent Break-Induced Replication Differs in Kinetics and Checkpoint Responses from RAD51-Mediated Gene Conversion. Mol. Cell. Biol. *25*, 933-944.

Osheim, Y.N., Miller, O.L. (1983). Novel amplification and transcriptional activity of chorion genes in *Drosophila melanogaster* follicle cells. Cell *33*, 543-553.

Osheim, Y.N., Miller, O.L., Beyer, A.L. (1988). Visualization of *Drosophila melanogaster* Chorion Genes Undergoing Amplification. Mol. Cell. Biol. *8*, 2811-2821.

Paeschke, K., Capra, J.A., Zakian, V.A. (2011). DNA replication through G-quadruplex motifs is promoted by the *Saccharomyces cerevisiae* Pif1 DNA helicase. Cell *145*, 678-691.

Sabouri, N., McDonald, K.R., Webb, C.J., Cristea, I.M., Zakian, V.A. (2012). DNA replication through hard-to-replicate sites, including both highly transcribed RNA Pol II and Pol III genes, requires the S. pombe Pfh1 helicase. Genes Dev. *26*, 581–593.

Sabouri, N., Capra, J.A., Zakian, V.A. (2014). The essential *Schizosaccharomyces pombe* Pfh1 DNA helicase promotes fork movement past G-quadruplex motifs to prevent DNA damage. BMC Biol. *12*, 101.

Saini, N., Ramakrishnan, S., Elango, R., Ayyar, S., Zhang, Y., Deem, A., Ira, G., Haber, J.E., Lobachev, K.S., Malkova, A. (2013). Migrating bubble during break-induced replication drives conservative DNA synthesis. Nature *502*, 389-392.

Sanders, C.M. (2010). Human Pif1 helicase is a G-quadruplex DNA-binding protein with G-quadruplex DNA-unwinding activity. Biochem. J. *430*, 119–128.

Signon, L., Malkova, A., Naylor, M.L., Klein, H., Haber, J.E. (2001). Genetic Requirements for *RAD51* - and *RAD54* -Independent Break-Induced Replication Repair of a Chromosomal Double-Strand Break. Mol. Biol. Cell *21*, 2048-2056.

Spradling, A.C., Mahowald, A.P. (1980). Amplification of genes for chorion proteins during oogenesis in *Drosophila melanogaster*. Proc. Natl. Acad. Sci. USA *77*, 1096-1100.

Thomer, M., May, N.R., Aggarwal, B.D., Kwok, G., Calvi, B.R. (2004). *Drosophila double-parked* is sufficient to induce re-replication during development and is regulated by cyclin E/CDK2. Development *131*, 4807-4818.

Trost, M., Blattner, A.C., Lehner, C.F. (2016). Regulated protein depletion by the auxin-inducible degradation system in *Drosophila melanogaster*. Fly (Austin). [Epub ahead of print].

Truong, L.N., Li, Y., Sun, E., Ang, K., Hwang, P.Y.H., Wu, X. (2014). Homologous recombination is a primary pathway to repair DNA double-strand breaks generated during DNA rereplication. J. Biol. Chem. *289*, 28910-28923.

Vasianovich, Y., Harrington, L.A., Makovets, S. (2014). Break-Induced Replication Requires DNA Damage-Induced Phosphorylation of Pif1 and Leads to Telomere Lengthening. PLoS Genet. *10*, e1004679.

Wilson, M.A., Kwon, Y., Xu, Y., Chung, W.H., Chi, P., Niu, H., Mayle, R., Chen, X., Malkova, A., Sung, P., Ira, G. (2013). Pif1 helicase and Polδ promote recombination-coupled DNA synthesis via bubble migration. Nature *502*, 393-396.